

ISTANBUL TECHNICAL UNIVERSITY ★ GRADUATE SCHOOL

**HIGH-RESOLUTION GRAVIMETRIC GEOID MODELING
IN THE ERA OF SATELLITE AND AIRBORNE GRAVIMETRY**

Ph.D. THESIS

Mustafa Serkan IŞIK

Department of Geomatics Engineering

Geomatics Engineering Programme

OCTOBER 2022

ISTANBUL TECHNICAL UNIVERSITY ★ GRADUATE SCHOOL

**HIGH-RESOLUTION GRAVIMETRIC GEOID MODELING
IN THE ERA OF SATELLITE AND AIRBORNE GRAVIMETRY**

Ph.D. THESIS

**Mustafa Serkan IŞIK
(501162607)**

Department of Geomatics Engineering

Geomatics Engineering Programme

Thesis Advisor: Assoc. Prof. Dr. Bihter EROL

OCTOBER 2022

İSTANBUL TEKNİK ÜNİVERSİTESİ ★ LİSANSÜSTÜ EĞİTİM ENSTİTÜSÜ

**UYDU VE HAVA GRAVİMETRİSİ ÇAĞINDA
YÜKSEK ÇÖZÜNÜRLÜKLÜ GRAVİMETRİK GEOİT MODELLEME**

DOKTORA TEZİ

**Mustafa Serkan IŞIK
(501162607)**

Geomatik Mühendisliği Anabilim Dalı

Geomatik Mühendisliği Programı

Tez Danışmanı: Doç. Dr. Bihter EROL

EKİM 2022

Mustafa Serkan IŞIK, a Ph.D. student of ITU Graduate School student ID 501162607 successfully defended the thesis entitled “HIGH-RESOLUTION GRAVIMETRIC GEOID MODELING IN THE ERA OF SATELLITE AND AIRBORNE GRAVIMETRY”, which he prepared after fulfilling the requirements specified in the associated legislations, before the jury whose signatures are below.

Thesis Advisor : **Assoc. Prof. Dr. Bihter EROL**
Istanbul Technical University

Jury Members : **Prof. Dr. Nebiye MUSAOĞLU**
Istanbul Technical University

Prof. Dr. Doğan Uğur ŞANLI
Yıldız Technical University

Prof. Dr. Reha Metin ALKAN
Istanbul Technical University

Prof. Dr. Uğur DOĞAN
Yıldız Technical University

Date of Submission : **8 September 2022**
Date of Defense : **6 October 2022**

*To Ömer Akin,
A friend to be remembered.*

FOREWORD

First of all, I would like to thank my supervisor, Assoc. Prof. Dr. Bihter EROL, for her guidance and constant support throughout my Ph.D. studies and my academic life. A special thanks to Prof. Dr. Serdar EROL for his support anytime I needed. I would also like to thank my committee members, Prof. Dr. Nebiye MUSAOĞLU and Prof. Dr. Uğur ŞANLI, for their contributions through these years.

A joy to work with a friend, and it is another pleasure to work side by side with strong figures in science. I will always be indebted to Mehmet Furkan ÇELİK, Ozan ÖZTÜRK, and Fatma Feyza SAKİL for their endless support in my personal and academic life. I would like to express my deepest gratitude to them for their invaluable advice, continuous support, and patience.

I am grateful to have the pleasure of working with my two dearest friends, Muhammed Raşit ÇEVİKALP and Bilal MUTLU. They were always willing and enthusiastic to assist in any way they could throughout our studies.

It is important to be surrounded by people who not only put up with you during these challenging times but also appreciate your presence in their life. And for that, I would like to extend my sincere thanks to my dear friends Gizem SOYDAN, Fatma Duygu CEYLAN, Nabil ADRAR, Gizem ÇATALKAYA, and Hakan ALAKOCA. I wish to thank my loving and supportive friends Elif Rüya ÖZTÜRK, Volkan ÖZBEY, Batuhan SARITÜRK, Ali TUNC, Öykü KOÇ, and Zeren ŞENYILDIZ PİROĞLU.

Last but not least, I would like to express my gratitude to my parents Vicdan Işık and Hasan IŞIK, my sister Begüm HOMBROUCKX, my brother-in-law Niek HOMBROUCKX and my cousin Işılay IŞIK. Without their tremendous understanding and encouragement in the past few years, it would be impossible for me to complete my study.

The US National Geodetic Survey (NGS) is acknowledged for providing the data set for "Colorado 1 cm Geoid Experiment" under IAG Joint Working Group 2.2.2. The funding provided by the Scientific and Technological Council of Turkey (TÜBİTAK) Grant No:114Y581 is gratefully acknowledged. The GNSS/leveling and tide-gauge data in Turkey are provided by Istanbul Technical University General Research Project with Protocol no. MGA-2018-41592. The gravity anomaly dataset in Turkey was used from the ITU Gravity Research Group (ITU-GRG) database.

October 2022

Mustafa Serkan IŞIK
(Geomatics Engineer, M.Sc.)

TABLE OF CONTENTS

	<u>Page</u>
FOREWORD	ix
TABLE OF CONTENTS	xii
ABBREVIATIONS	xiii
SYMBOLS	xv
LIST OF TABLES	xix
LIST OF FIGURES	xxiv
SUMMARY	xxv
ÖZET	xxix
1. INTRODUCTION	1
2. HIGH-RESOLUTION GEOID MODELING USING LEAST SQUARES MODIFICATION OF STOKES AND HOTINE FORMULAS IN COLORADO	9
2.1 Introduction	9
2.2 Methodology	13
2.2.1 Downward continuation of airborne gravity data	13
2.2.2 Geoid Modeling by the Least Squares Modification of Stokes and Hotine Integrals	15
2.2.2.1 Additive corrections	17
2.3 Data description	19
2.3.1 Terrestrial and airborne gravity data	20
2.3.2 Global geopotential model	22
2.3.3 Digital elevation model	22
2.3.4 GPS/leveling data	23
2.4 Results	24
2.4.1 Downward continuation of airborne gravity	24
2.4.2 Comparison of the resulting geoid models	28
2.4.3 Validation using GPS/leveling data	30
2.4.3.1 GSVS17 comparisons	30
2.4.4 Area comparison of geoid grids	33
2.5 Conclusions and discussion	34
3. INVESTIGATION OF THE GEOID MODEL ACCURACY IMPROVEMENT IN TURKEY	39
3.1 Introduction	39
3.2 Study Area and the Used Data	44
3.2.1 Gravity data and preliminary preparation	44
3.2.2 Validation datasets	51
3.3 Geoid Modelling	54
3.3.1 Least squares modification of Stokes integral with additive corrections (LSMSA) method	54
3.3.2 Numerical test results	57
3.4 Conclusion and Discussions	68
4. GEOID MODELING WITH LEAST SQUARES MODIFICATION OF HOTINE'S INTEGRAL USING GRAVITY DISTURBANCES IN TURKEY	73
4.1 Introduction	73
4.2 Method and Material	76
4.2.1 Least squares modification of Hotine's integral with additive corrections method	76
4.2.2 Dataset and pre-processing	80
4.2.2.1 Terrestrial gravity data	80
4.2.2.2 GNSS/leveling data	84
4.3 Gravimetric Geoid Modelling	84

4.4	Conclusions	95
5.	IMPROVEMENT OF GOCE-BASED GLOBAL GEOPOTENTIAL MODELS FOR GRAVIMETRIC GEOID MODELING IN TURKEY ...	99
5.1	Introduction	99
5.2	Methodology	102
5.2.1	Spectral enhancement method	102
5.2.2	Gravimetric geoid modeling	104
5.3	Study Area and Data Set.....	106
5.3.1	Global geopotential models.....	106
5.3.2	Residual terrain model	109
5.3.3	Gravity data	109
5.3.4	Validation data set.....	110
5.4	Results and Discussions	112
5.4.1	Evaluation of global geopotential models.....	112
5.4.2	Evaluation of gravimetric geoid models	114
5.5	Conclusions	118
6.	CONCLUSIONS	121
REFERENCES		125
CURRICULUM VITAE		143

ABBREVIATIONS

AGC	: Atmospheric Gravity Correction
CHAMP	: Challenging Minisatellite Payload
DIR	: Direct
DTU	: Denmark Technical University
EGM2008	: Earth Gravitational Model 2008
ERTM2160	: Earth Residual Terrain Modelled-gravity field 2160
expGeoid	: Experimental Geoid Model
FA	: Free Air Correction
FFT	: Fast Fourier Transform
GDM	: The General Directorate of Mapping
GDMRE	: The General Directorate of Mineral Research and Exploration
GGM	: Global Geopotential Model
GNSS	: Global Navigation Satellite System
GOCE	: Gravity field and steady-state Ocean Circulation Explorer
GOCO	: Global Observation Combination
GPS	: Global Positioning System
GRS67	: Geodetic Reference System 1967
GRS80	: Geodetic Reference System 1980
GRACE	: Gravity Recovery and Climate Experiment
GRAV-D	: Gravity for the Redefinition of the American Vertical Datum
GSVS17	: Geoid Slope Validation Survey 2017
HGM	: Harita Genel Müdürlüğü
HPF	: High Processing Facility
IAG	: International Association of Geodesy
IGSN71	: International Gravity Standardization Net 1971
IHRS	: International Height Reference System
ITRF	: International Terrestrial Reference Frame
ITU-GRG	: Istanbul Technical University Gravity Research Group
IzJRS	: Izmir Geodetic Reference System
JWG	: Joint Working Group
LSC	: Least Squares Collocation
LSMHA	: Least Squares Modification of Hotine's Integral with Additive corrections
LSMSA	: Least Squares Modification of Stokes' Integral with Additive corrections
LVD	: Local Vertical Datum
MSL	: Mean Sea Level
MSS	: Mean Sea Surface
MTA	: The General Directorate of Mineral Research and Exploration
NAVD88	: North American Vertical Datum 1988
NGA	: National Geospatial-Intelligence Agency
NGS	: National Geodetic Survey

NOAA	: National Oceanic and Atmospheric Administration
NVD	: National Vertical Datum
PTC	: Planar Terrain Correction
RTE	: Residual Terrain Effect
RTM	: Residual Terrain Model
SEM	: Spectral Enhancement Method
SGG	: Satellite Gravity Gradiometry
SLR	: Satellite Laser Ranging
SPW	: Space-wise
SRTM	: Shuttle Radar Topography Mission
SST	: Satellite to Satellite Tracking
SVD	: Singular Value Decomposition
TC	: Terrain correction
TG	: Tide-gauge
TIM	: Time-wise
TPAO	: Türkiye Petrolleri Anonim Ortaklığı
TUDES	: Turkish National Sea Level Monitoring Network
TUDKA	: Turkey National Vertical Control Network
TUTGA	: Turkish National Fundamental GPS Network
TÜBİTAK	: The Scientific and Technological Research Institution of Turkey
XGM2016	: Experimental Gravity Field Model 2016
XGM2019e	: Experimental Gravity Field Model 2019

SYMBOLS

\hat{s}	: Signal to be predicted
\mathbf{x}	: Observation vector
\mathbf{C}_{sx}	: Signal cross-covariance matrix
\mathbf{C}_{ss}	: Signal auto-covariance matrix
\mathbf{D}	: Noise-covariance matrix
\mathbf{C}_h	: Covariance of gravity anomalies at flight altitude
D	: Short-wavelength attenuation parameters
T	: Long-wavelength attenuation parameters
l	: Planar distance
x, y, z	: Planar coordinates
\hat{N}	: Estimated geoid height
\tilde{N}	: Approximate geoid height
ζ	: Height anomaly
δN_{COMB}	: Combined topographic correction
δN_{DWC}	: Combined downward continuation correction
δN_{ATM}	: Combined atmospheric correction
δN_{ELL}	: Combined ellipsoidal correction
$S(\psi)$: Stokes' function
$S^L(\psi)$: Modified Stokes' function
ψ	: Spherical distance
Δg	: Surface gravity anomaly
$d\sigma$: Surface element
s_n	: Modification parameter
Q_n^L	: Truncation coefficient
Q_n	: Molodensky truncation coefficient
e_{nk}	: Paul's coefficient
Δg_n^{GGM}	: Laplace harmonics of degree n
M	: Maximum expansion of the global geopotential model
L	: Degree of modification
σ_0	: Integration cap
P_n	: Unnormalized Legendre polynomials
C_{nm}	: Coefficients of global geopotential model
$Y_{nm}(\theta, \lambda)$: Fully normalized surface spherical harmonics
θ, λ, r	: Co-latitude, longitude and geocentric radius
$H(\psi)$: Hotine's function
$H^L(\psi)$: Modified Hotine's function
δg	: Surface gravity disturbance
δg_n^{GGM}	: Laplace harmonics of gravity disturbance of degree n
ρ	: Topographic mass density
ρ_A	: Atmospheric mass density

H	: Orthometric height
$\partial \Delta g / \partial r$: Vertical gradient of gravity anomaly
$\partial \delta g / \partial r$: Vertical gradient of gravity disturbance
\mathbf{H}_n	: Laplace harmonics of topographic heights
\mathbf{H}_{nm}	: Fully normalized spherical harmonic coefficients of heights
G_M	: Gravitational constant for the Earth
$G_{M_{GRS80}}$: Gravitational constant for the GRS80 ellipsoid
$G_{M_{GGM}}$: Gravitational constant for Global geopotential model
W_0	: Conventional value of potential
U_0	: Potential value of reference ellipsoid
R	: Mean Earth radius
a, b	: Semi-major and semi-minor radius of reference ellipsoid
E_{nm}, F_{nm}, G_{nm}	: Coefficients for the ellipsoidal correction
N_o	: Zero-degree term geoid height
N_{dir}	: Direct topographic effect on geoid height
N_{ing}	: Indirect topographic effect on geoid height
Δg_{FA}	: Free-air gravity anomaly
Δg_P^{FA}	: Free-air gravity anomaly computed using planar approach
Δg_S^{FA}	: Free-air gravity anomaly computed using spherical approach
Δg_{CPB}	: Planar complete Bouguer gravity anomaly
Δg_{CSB}	: Spherical complete Bouguer gravity anomaly
δg_{BP}	: Bouguer plate
δg_{TC}	: Terrain correction
δg_{PTC}	: Planar terrain correction
γ	: Normal gravity
γ_e	: Normal gravity at the Equator
γ_p	: Normal gravity at the pole
$\partial \gamma / \partial h$: Vertical gradient of normal gravity
N_{Model}	: Geoid height from gravimetric geoid
$N_{GNSS/lev}$: Geoid height from GNSS and leveling measurements
ΔN	: Residual geoid height
$M(t)$: Monthly sea level time series
t_0	: Reference epoch
$M(t_0)$: Mean sea level at epoch t_0
v	: Linear trend of time series
A_k	: Amplitude
ω_k	: Angular frequency
φ	: Phase of annual and semi-annual signals of the time series
$\varepsilon(t)$: Un-modeled components of time series
N_{TG}^{GG}	: Geoid undulation at tide gauge station
N_{TG}^{GG}	: Geoid undulation at tide gauge station calculated from gravimetric geoid
$N_{TG}^{MSS/MSL}$: Geoid undulation at tide gauge station calculated from MSS and MSL
MSS_A^{DTU}	: Mean sea surface interpolated for the altimetry point
MSL_{TG}^{NVD}	: Mean sea level at the tide gauge station
δN	: Datum shift between the gravimetric geoid and the national vertical datum

$\Delta\bar{C}_{nm}, \bar{S}_{nm}$: Spherical harmonic coefficients of disturbing potential
\bar{C}_{nm}^W	: Spherical harmonic coefficients of gravity potential
\bar{C}_{nm}^U	: Spherical harmonic coefficients of normal potential
\bar{P}_{nm}	: Fully normalized associated Legendre function
T	: Disturbing potential
$\bar{\gamma}$: Mean normal gravity along the normal of telluroid
$H_{tidefree}$: Tide free (non-tidal) orthometric heights
$H_{meantide}$: Mean tide orthometric heights

LIST OF TABLES

	<u>Page</u>
Table 2.1 : Statistics of residual gravity anomalies [unit: mGal].....	26
Table 2.2 : Statistics of airborne and terrestrial combined gravity anomalies and gravity disturbances [unit: mGal].	28
Table 2.3 : Statistics of the final geoid models [unit: m].	30
Table 2.4 : External validation results of the models using historical GPS/leveling data ($\Delta N = N_{\text{Model}} - N_{\text{GPS/lev}}$) [unit: cm].	33
Table 2.5 : External validation results of the models using the GPS/leveling data at the GSVS17 profile ($\Delta N = N_{\text{Model}} - N_{\text{GPS/lev}}$) [unit: cm].	33
Table 2.6 : Statistics of the geoid height differences between the ITU-GRG solutions and the mean of all institutions ($\Delta N = N_{\text{Model}} - N_{\text{Mean}}$) at the GSVS17 profile [unit: cm].	34
Table 2.7 : Statistics of differences between the individual geoid models and the mean geoid model in a $1' \times 1'$ -grid, [unit: cm].	36
Table 3.1 : Statistics of gravity anomaly datasets (only Turkey land area) [unit: mGal].	51
Table 3.2 : Turkish National Sea Level Monitoring Network tide gauge stations.	52
Table 3.3 : The statistics of the residual geoid heights at GPS/leveling stations (cm).	60
Table 3.4 : The validation results of the models at the tide gauge (TG) stations. .	66
Table 3.5 : The statistics of the residual geoid heights at GPS/leveling stations after seven-parameter surface fitting (cm).	68
Table 3.6 : The statistics of the $N_S^{1\min}$ geoid model components and additive corrections in LSMSA algorithm.....	68
Table 4.1 : The statistics of the geoid height differences at 100 TUTGA GNSS/leveling stations ($N_{(\text{GNSS/Leveling})} - N_{\text{Model}}$) [unit: cm].....	90
Table 4.2 : The statistics of the misclosure values for baselines of 100 TUTGA GNSS/leveling benchmarks, which are categorized based on the orthometric height difference for all baseline combinations [unit: cm].	93
Table 4.3 : The statistics of the geoid height differences at 100 TUTGA GNSS/leveling stations ($N_{(\text{GNSS/Leveling})} - N_{\text{Model}}$) [unit: cm].....	93
Table 4.4 : The statistics of the misclosure values for all baseline combinations of 301 IZJRS GNSS/leveling benchmarks categorized based on the orthometric height difference [unit: cm].	96
Table 5.1 : Tested global geopotential models and their data content.	108
Table 5.2 : Statistics of gravimetric geoid model accuracy computed using TIM R6 and EGM2008 models. [unit: cm].....	117

LIST OF FIGURES

	<u>Page</u>
Figure 2.1 : Gravity datasets: Terrestrial gravity measurements (blue), duplicated measurements (red) and airborne gravity measurements (orange), target geoid area for terrestrial-only and combined solutions (solid black line), and target geoid area for airborne-only solutions (dashed black line).	20
Figure 2.2 : (a) Surface gravity anomalies and (b) airborne gravity anomalies at flight level.	22
Figure 2.3 : GPS/leveling benchmarks on the topography of SRTM v4.1 (3" resolution) in the Colorado area. Black triangles indicate the historical GPS/leveling data, and red triangles indicate the GSVS17 GPS/leveling data. Target geoid area for the terrestrial-only and combined solutions (solid black line), and target geoid area for the airborne-only solutions (dashed blue line)..	24
Figure 2.4 : (a) Terrestrial residual gravity anomalies and (b) airborne residual gravity anomalies before downward continuation ($\Delta g_{FA} - \Delta g_{GGM} - \Delta g_{RTM}$).....	26
Figure 2.5 : Covariance model and empirical covariance of the residual gravity anomalies.....	27
Figure 2.6 : (a) Airborne (after downward continuation) and terrestrial residual gravity anomalies on Earth's surface and (b) gridded residual gravity anomalies in the contour map.....	27
Figure 2.7 : Gridded and restored combined (airborne and terrestrial): (a) gravity anomalies and (b) gravity disturbances.....	28
Figure 2.8 : (a) Stokes combined (solution S.C) and (b) Hotine combined (solution H.C) solutions. (c) Difference between the Stokes and Hotine combined solutions ($\hat{N}_{Hotine} - \hat{N}_{Stokes}$).....	29
Figure 2.9 : Accuracies of the models according to the standard deviations of geoid height differences at the GPS/leveling benchmarks of the GSVS17 profile [unit: cm].	31
Figure 2.10 : Geoid height differences ($\Delta N = N_{Model} - N_{GPS/lev}$) at the GPS/leveling benchmarks of the GSVS17 profile: (a) Stokes integral and (b) Hotine integral.....	32
Figure 2.11 : Geoid differences between the presented solutions and mean of all institutions ($\Delta N = N_{Model} - N_{Mean}$) at the GSVS17 profile: (a) Stokes integral and (b) Hotine integral.	35
Figure 2.12 : Differences between the computed geoid models and the validation model at a $1' \times 1'$ -grid for the (a) official geoid solution, (b) Stokes combined (S.C) solution, and (c) Hotine combined (H.C) solution. .	36

Figure 3.1 : Study area: distribution of GPS/leveling benchmarks (triangles)and tide gauge stations (circles) on the SRTM topography of Turkey. (Data from Jarvis et al., 2008).	45
Figure 3.2 : Complete Bouguer anomalies in Turkey (original 5' resolution grid dataset shifted to IGSN71 gravity datum) (minimum = -205.07 mGal, maximum = 74.94 mGal, mean = -69.00 mGal, standard deviation = 55.45 mGal).....	45
Figure 3.3 : Flowchart of the preparation of gravity anomaly datasets.	46
Figure 3.4 : Planar terrain corrections (δg_{PTC}) on gravity (unit: mGal) (minimum = 0.00 mGal, maximum = 168.82 mGal, mean = 2.34 mGal,standard deviation = 3.28 mGal.	48
Figure 3.5 : SRTM2gravity full signal model ($\delta g_{SRTM2Gravity}$) (unit: mGal) (minimum = 17.65 mGal, maximum = 448.81 mGal, mean = 155.76 mGal, standard deviation = 72.60 mGal) (Data from Hirt et al., 2019).....	49
Figure 3.6 : Residual gravity signal from SRTM2gravity model (unit: mGal) (minimum = -206.190 mGal, maximum = 109.010 mGal, mean = -1.847 mGal, standard deviation = 14.675 mGal). (Data from Hirt et al., 2019).....	51
Figure 3.7 : Free-air gravity anomalies using: (a) the planar approximation $\Delta g_P^{(FA,1min)}$, (b) the spherical approximation $\Delta g_S^{(FA,1min)}$, (c) The difference map of gravity anomalies ($\Delta g_P^{(FA,1min)} - \Delta g_S^{(FA,1min)}$).	53
Figure 3.8 : Validation of geoid models at tide gauge stations.	55
Figure 3.9 : Standard deviation of the residual geoid heights at GPS/Levelling stations for the varying computation (a) 5' resolution planar approximation (ΔN_P^5 min); (b) 1' resolution planar approximation parameters for: (ΔN_P^1 min); (c) the 1' resolution spherical approximation (ΔN_S^1 min) (units: cm).....	59
Figure 3.10 : The validation results at the GPS/levelling (triangles) and tide gauge (circles) stations (unit: cm): (a) distribution of the geoid height residuals at stations for the N_P^{5min} model; (b) distribution of the geoid height residuals at stations for the N_P^{1min} model; (c) distribution of the geoid height residuals at stations for the N_S^{1min} model; (d) correlations between the geoid height residuals and the heights of the GPS/levelling benchmarks for the N_P^{5min} model; (e) correlations between the geoid height residuals and the heights of the GPS/levelling benchmarks for the N_P^{1min} model; and (f) correlations between the geoid height residuals and the heights of the GPS/levelling benchmarks for the N_S^{1min} model.....	62
Figure 3.11 : The interpolation error associated with the DTU13MSS model along the coastlines of Turkey (unit: cm). The tide gauge stations are shown with white circles.	64

Figure 3.12 : (a) Differences between the two 1' resolution geoid models, $N_P^{1\text{ min}} - N_S^{1\text{ min}}$ (minimum = -0.234 m, maximum = 0.593 m, mean = 0.003 m, standard deviation = 0.018 m); and (b) distribution of these differences with respect to their orthometric heights (unit: centimeters).	65
Figure 3.13 : $N_S^{1\text{ min}}$ geoid model: (a) approximate geoid heights (\tilde{N}); (b) combined topographic correction (δN_{TOMB}^{COM}); (c) combined downward continuation correction (δN_{DWC}^{COMB}); (d) combined atmospheric correction (δN_{ATM}^{COMB})); (e) combined ellipsoidal correction (δN_{ELL}^{COMB}); and (f) final geoid model (\hat{N}).	71
Figure 4.1 : The computation steps of the least squares modification of Hotine's integral with additive corrections (LSMHA) method.	80
Figure 4.2 : (a) The location of the gravity observation points by the General Directorate of Mineral Research and Exploration with their complete Bouguer anomaly values [unit: mGal]. Please note that the complete Bouguer anomaly values at these locations were re-generated from the 1-arcminute grid given in (b) since the original point-wise gravity measurements are not available for this study.	82
Figure 4.3 : (a) Gravity anomaly and, (b) gravity disturbance grids in Turkey....	83
Figure 4.4 : The distribution of: (a) 100 TUTGA GNSS/leveling benchmarks in Turkey and, (b) 301 IzJRS GNSS/leveling benchmarks in Izmir province shown over the topography of Turkey.	85
Figure 4.5 : $N_S^{1\text{ min}}$ geoid model: (a) approximate geoid heights (\tilde{N}); (b) combined topographic correction (δN_{TOMB}^{COM}); (c) combined downward continuation correction (δN_{DWC}^{COMB}); (d) combined atmospheric correction (δN_{ATM}^{COMB})); (e) combined ellipsoidal correction (δN_{ELL}^{COMB}); and (f) final geoid model (\hat{N}).	87
Figure 4.6 : Residual geoid heights (after 1-parameter fitting, which removes only a shift) at 100 TUTGA GNSS/leveling stations for Hotine (a) and Stokes (b) geoid solutions [unit: meters].....	91
Figure 4.7 : Relative accuracies and misclosures for Stokes and Hotine geoid models according to 100 TUTGA GNSS/leveling benchmarks [unit: meters]: (a) the change in the relative accuracy of Stokes and Hotine geoid models with respect to increasing baseline length after 1-parameter and 7-parameter surface fitting; (b) and (c) the misclosure values for Stokes's and Hotine's solutions, respectively, along the baselines. The circular markers with the lighter tone of colors represent misclosures after 1-parameter fitting. The cross markers with the darker tone of colors represent misclosures after 7-parameter fitting. The black line represents the error tolerance limit of the 3 _{rd} order leveling network for backward and forward leveling.	92

Figure 4.8 : Residual geoid heights (after 1-parameter fitting) at 301 IzJRS GNSS/leveling stations for Hotine (a) and Stokes (b) geoid solutions [unit: meters]. (c) and (d) show the distribution of the residual geoid heights w.r.t. the orthometric heights of the benchmarks.....	94
Figure 4.9 : Relative accuracies and misclosures for Stokes and Hotine geoid models according to 301 IzJRS GNSS/leveling benchmarks [unit: meters]: (a) the change in the relative accuracy of Stokes and Hotine geoid models with respect to increasing baseline length after 1-parameter and 7-parameter surface fitting; (b) and (c) the misclosure values for Stokes's and Hotine's solutions, respectively, along the baselines. The circular markers with the lighter tone of colors represent misclosures after 1-parameter fitting. The cross markers with the darker tone of colors represent misclosures after 7-parameter fitting. The black line represents the error tolerance limit of the 3 _{rd} order leveling network for backward and forward leveling.	95
Figure 5.1 : Residual terrain effects on geoid from ERTM2160 model (<i>Minimum</i> = -0.168 m, <i>Maximum</i> = 0.184 m, <i>Mean</i> = 0.000 m, <i>SD</i> = 0.025 m).	110
Figure 5.2 : Location of gravity measurements (blue points) and GPS/leveling benchmarks (red triangles) on topography of Turkey.	111
Figure 5.3 : Free-air anomaly grid used in this study (<i>Min</i> = -236.2 mGal, <i>Max</i> = 300.8 mGal, <i>Mean</i> = 35.1 mGal, <i>STD</i> = 55.6 mGal).	111
Figure 5.4 : Standard deviations of spectrally enhanced GOCE models at each expansion degree: (a) DIR models, (b) TIM models, (c) SPW models, and (d) GOCO models.	113
Figure 5.5 : The standard deviation (colored bars) of spectrally enhanced GOCE models at optimum expansion degree and their mean values (black bars).	114
Figure 5.6 : Residual geoid heights of (a) gravimetric geoid model computed with EGM2008 (expGeoid-3) at GPS/leveling stations and (b) gravimetric geoid model computed with TIM-R6/EGM2008 mixed global geopotential model (expGeoid-4) at GPS/leveling stations. The long wavelength geoid height differences computed using TIM-R6 and EGM2008 GGMs at 205 degree/order are given in (c) where the statistics are: <i>Minimum</i> = -49.8 cm, <i>Maximum</i> = 25.0 cm, <i>Mean</i> = -1.6 cm, <i>SD</i> = 9.3 cm. Differences between expGeoid-3 and expGeoid-4 (<i>N_{expGeoid-4}</i> - <i>N_{expGeoid-3}</i>) are given in (d) where the statistics are: <i>Minimum</i> = -67.0 cm, <i>Maximum</i> = 47.7 cm, <i>Mean</i> = -1.0 cm, <i>SD</i> = 13.9 cm.	118
Figure 5.7 : Experimental gravimetric geoid model calculated with mixed global geopotential model as reference model (expGeoid-4; <i>Minimum</i> = 8.827 m, <i>Maximum</i> = 41.778 m, <i>Mean</i> = 30.793 m, <i>SD</i> = 6.781 m).	119

HIGH-RESOLUTION GRAVIMETRIC GEOID MODELING IN THE ERA OF SATELLITE AND AIRBORNE GRAVIMETRY

SUMMARY

With the advances in positioning and inertial navigation systems, the accuracy obtained from the airborne gravimetry technique has reached very important levels that aid high-resolution gravity field modeling. The data obtained from the airborne gravimetry is of great importance in complementing the deficiencies of terrestrial data in mountainous areas and land-sea transitions in coastal areas where modeling the geoid are most troublesome.

In this thesis, high-resolution regional gravimetric geoid modeling was investigated in light of the recent advancements in the field of gravimetry, more specifically satellite and airborne gravimetry. With recently developed GOCE-based global geopotential models and advanced stochastic techniques to model the regional gravity field as a solution of the geodetic boundary value problem, it is possible to achieve a high-resolution geoid model which can alter the traditional vertical reference system realization. In this regard, four studies are carried out in two test regions: Colorado, the USA, and Turkey.

The first study focused on the contribution of airborne gravity measurements to gravimetric geoid modeling in a high topography, Colorado, USA, via the least squares modification of Stokes (LSMSA) and Hotine (LSMHA) integrals with additive corrections techniques. The study included filtering the high-frequency airborne gravimeter data with minimum loss of signal and downward continuing it to the Earth's surface by Least Squares Collocation method with a planar logarithmic covariance model. The reduced data was optimally combined with the satellite data from the global geopotential model and terrestrial gravity data to calculate a high-accuracy gravimetric geoid model. In this combination, the error variance of each data set was taken into account to stochastically determine the variance of input gravity anomaly/disturbance data set for Stokes and Hotine integrals. To clarify the importance of airborne gravity data to the study, three gravity data sets were created: terrestrial-only, airborne-only, and combined. The computed gravimetric geoid models were tested with highly accurate GPS/leveling benchmarks collected for the validation of models along a profile passing through the rough topography of the Colorado mountains. The results indicated the contribution of airborne gravity data over the mountainous regions, clearly. In conclusion, we obtained two gravimetric geoid models calculated using combined data set via LSMSA and LSMHA methodologies whose absolute accuracies are 2.69 cm and 2.87 cm , respectively.

In the rest of the thesis, we focused on improving the accuracy of the gravimetric geoid model in Turkey. The first study that concerns the geoid model of Turkey dealt

with the downscaling of low-resolution gravity anomaly data set, which originally has $\sim 9\text{ km}$ resolution, to a spatial resolution of $\sim 2\text{ km}$. This task was achieved via the proper modeling of the topographic attraction on gravity using planar and spherical approaches for Bouguer gravity anomalies. While the planar approach was implemented for the computation of complete Bouguer gravity anomalies using classical terrain correction based on the mass-prism technique, the spherical approach was applied using a global model for the topographic attraction that is SRTM2Gravity. Based on these two approaches, the low-resolution complete Bouguer anomalies were enriched to higher-resolution data set, and consequently, surface gravity anomalies were calculated from planar and spherical complete Bouguer anomalies. Three gravimetric geoid models were calculated via the LSMSA technique, a low-resolution reference geoid with a planar approach, and two high-resolution geoids via planar and spherical approaches. Based on the accuracy assessment at 100 homogeneously distributed GPS/leveling benchmarks, the accuracy of the best-performing geoid was found as 8.6 cm using spherical approximation. The performance of gravimetric geoid models using the down-scaled surface gravity anomalies was significantly better compared to the low-resolution solution, the spherical approach being slightly better than the planar one. Hence, the success of the down-scaling was proven in terms of the accuracy achieved by the high-resolution gravimetric geoid models.

Following the improvements brought by the 1-arcmin resolution gravity data set, we conducted another study that investigates the performance of Hotine's integral for the gravimetric geoid modeling using gravity disturbances, in comparison to Stokes' counterpart. Hotine's integral, as opposed to Stokes', uses gravity disturbances which require no orthometric height information of the stations that must be obtained via traditional geometric leveling. Hence, it provides a promising new strategy for gravimetric geoid modeling studies in the era of GNSS technologies. In this context, we computed a gravimetric geoid model of Turkey using LSMHA methodology and tested both Hotine and Stokes geoid models using 100 GPS/leveling benchmarks over Turkey and 301 local GPS/leveling stations located in the western part of Turkey. The assessment of the geoid models was conducted in both absolute and relative manners for country-wide and local tests. The results indicate the performance of Hotine's integral for gravimetric geoid modeling using gravity disturbances gives promising results. The accuracy of the Hotine geoid was found as 8.8 cm while its Stokes counterpart had 8.6 cm accuracy against 100 GPS/leveling data set, after the systematic differences between the geoid surface and local vertical datum were modeled via a 7-parameter model. In the local assessment of the geoid models, both techniques showed $\sim 4\text{ cm}$ agreement with 301 GPS/leveling data set. This study showed that the availability of ellipsoidal height information for newly collected gravity data set in Turkey, being collected within the scope of height system modernization efforts, will facilitate the use of Hotine's integral in the near future.

In the final part of this thesis, we investigated the contribution of long-wavelength geoid signals by exploiting the global gravity field models computed with Gravity Field and Steady-State Ocean Circulation Explorer (GOCE) satellite mission data. Prior to the geoid modeling, we first analyzed the global model series calculated with direct (DIR), time-wise (TIM), and space-wise (SPW) approaches, together with the GOCO model series. We assessed the performance of all releases of the model

series using the Spectral Enhancement Method (SEM). As a result, the sixth release of DIR, TIM, and GOCO models with an expansion degree of 205 was found as the optimum combination to retrieve long-wavelength signals of the gravity field. Out of these three models, we enhanced the TIM-R6 model by combining its coefficients with an ultra-high resolution model EGM2008 via linear blending technique to achieve a model up to 360 degree and order. The blended model was used as a reference for high-resolution gravimetric geoid modeling via the LSMHA technique. The evaluation of the performance of the computed model at 100 GPS/leveling benchmarks revealed $\sim 23\%$ improvement in the standard deviation over EGM2008 based gravimetric geoid model. By showing a *7.8 cm* agreement (after-fit) against the validation data set, this model outperforms the former LSMSA and LSMHA geoid models computed with XGM2019e global geopotential models. In conclusion, this study conclusively showed how important the choice of global geopotential model and its degree of expansion for the gravimetric geoid modeling studies.

UYDU VE HAVA GRAVİMETRİSİ ÇAĞINDA YÜKSEK ÇÖZÜNÜRLÜKLÜ GRAVİMETRİK GEOİT MODELLEME

ÖZET

Topografik kütlelerin düzensiz yapısı gravite alanının modellenip geoidin yüksek doğrulukta hesaplanması için gereken gravite ölçmelerinin yeterli doğruluğa ve dağılıma sahip olmasını zorlaştırmaktadır. Dağlık alanlarda yersel verinin yeterli sıklıkta elde edilmesi çok büyük bir maliyet ve zaman gerektirmektedir. Denizlerde yapılan ölçmelerde ise özellikle açık denizler ve okyanuslarda istenilen homojenlikte ölçmelerin elde edilmesi mümkün değildir. Bu kapsamda uydu gravimetre yöntemi önemli bir veri kaynağıdır. Ancak yörunge yüksekliği sebebiyle uydudan elde edilen gravite verileri uzun dalga boylu sinyalleri modellemeye yardımcı olmaktadır. Orta ve kısa dalga boylu bileşenler denizlerde altimetre uydularından ve karalarda ise yersel ölçmelerden sağlanmak zorundadır. Bununla birlikte, kıyılara yaklaşıkça altimetre uydularının sinyallerinin geri saçılımlarındaki gürültü oranının artması, geoidin kıyı kesimlerde doğruluğunun önemli ölçüde kötüleşmesine sebep olmaktadır.

Konum belirleme ve ataletsel navigasyon sistemlerindeki teknolojik gelişmeler ile birlikte uçak/hava gravimetre yönteminden elde edilen doğruluk çok önemli seviyelere gelmiştir. Bu yöntem, hem dağlık alanlarda yersel verideki eksiklikleri tamamlamada hem de kıyı kesimlerde kara-deniz geçişlerindeki veri eksikliğinin kapatılmasında önemli bir yere sahiptir. Ancak, hava gravimetre yöntemiyle elde edilen veriler, türbülanslı fiziksel bir ortamda gürültülü GNSS konum vektörünün türevleri ile gürültülü ataletsel sensör (ivmeölçer, dönüpölçer) verileriyle elde edilebildiğinden yüksek frekanslı gürültüye sahiptir. Verinin uygun yöntemler kullanılarak filtrelenmesi ve gürültüsünün azaltılması gerekmektedir. Bunun yanı sıra, uçuş yüksekliğinde elde edilen bu verilerin geoit modellemede kullanılabilmesi için aşağı uzanım (downward continuation) yöntemleri kullanılarak yeryüzüne veya geoit yüzeyine indirgenmesi gerekmektedir.

Bu tez kapsamında, hava gravimetri yönteminden elde edilen gravite verilerinin işlenmesi ve dağlık alanda geoit modeli doğruluğuna katkısının incelenmesi amacıyla Amerika Birleşik Devletleri Colorado eyaletinde gravimetrik geoit modelleme çalışması yapılmıştır. Colorado geoit deneyi, 2017 yılında Uluslararası Jeodezi Birliği'nin (IAG) Ortak Çalışma Grubu (JWG) 2.2.2 (1 cm geoit deneyi) tarafından ortak bir çalışma olarak başlatılarak organize edilmiş ve farklı kurum ve araştırma grupları katkıda bulunmuştur. Yapılan ilk çalışmanın amacı, aynı girdi veri seti ile hesaplanan farklı geoid belirleme yaklaşımlarından elde edilen gravite potansiyellerinin Uluslararası Yükseklik Referans Sistemi (IHRSS) kapsamında tekrarlanabilirliğini görmek ve farklı yaklaşımlarda elde edilen gravimetrik geoitlerin performanslarının kıyaslanmasıdır. Veri seti, Colorado, ABD'de yaklaşık $550\text{ km} \times 730\text{ km}$ 'lık bir dağlık alana ait yersel gravimetri ve hava gravimetri ölçmelerini, sayısal

arazi modelini, XGM2016 global jeopotansiyel modelini ve model doğrulamaları için GPS/nivelman verilerini içermektedir. Veri seti Ulusal Jeodezi Araştırması (NGS) departmanı tarafından sağlanmıştır. Bu çerçevede, yapılan ilk çalışma, İstanbul Teknik Üniversitesi - Gravite Araştırma Grubu (ITU-GRG) tarafından elde edilen deneysel sonuçlar üzerinden Colorado geoidinin modellemesi üzerine bir karşılaştırma sunmayı amaçlamaktadır. Bu çalışmada, Stokes ve Hotine integral formüllerinin en küçük kareler modifikasyonları yöntemlerini ITU-GRG tarafından yazılan yazılımı kullanarak Colorado geoidini modellemeye odaklanıldı. Her iki yöntem ile sadece yersel gravite, sadece hava gravite ve bütünsel gravite veri setlerine dayalı gravimetrik geoit modeller hesaplandı. Daha sonra, hesaplanan deneysel geoit modelleri, tarihsel ve yakın zamanda profil şeklinde ölçülen GPS/nivelman veri setleri kullanılarak doğruluk analizi yapıldı ve ayrıca IAG JWG 2.2.2'nin "1 cm geoit deneyi" için farklı kurumlar tarafından sunulan çözümlerle karşılaştırıldı. Tüm doğrulama sonuçları için, Hotine ve Stokes integral formülleri, geoit doğruluğu açısından benzer performanslar verdi. Bununla birlikte, bütünsel veri seti kullanılarak hesaplanan modeller, sadece yersel gravite ve sadece hava gravite tabanlı geoit çözümlerinden daha iyi doğruluğa sahip olduğu tespit edildi. Bütünsel verileri kullanan geoid model çözümlerinin doğruluğu, GSVS17 (Geoid Slope Validation Survey 2017) profilinin GPS/nivelman verileri kullanılarak yapılan test sonuçlarında Hotine yöntemi için 2.69 cm ve Stokes yöntemi için 2.87 cm olarak raporlanmıştır. Amerikan Düşey Datumun Yeniden Tanımlanması için Gravite (GRAV-D) projesinden elde edilen havadan gravimetri verileri, özellikle bölgenin dağlık kısımlarında geoit modelinin geliştirilmesine önemli ölçüde katkıda bulunmuştur.

İkinci çalışma, Stokes integralinin en küçük kareler modifikasyonu ve ek düzeltmeler (LSMSA) yöntemiyle sıklaştırılmış gravite anomalileri gridlerini kullanarak Türkiye'deki gravimetrik geoit modelinin doğruluğunun iyileştirmesini araştırmaktadır. Geoit modellerinin LSMSA hesaplamalarında, topografik kitlelerin ileri modellenmesiyle (forward modeling) tamamlanmış Bouguer anomali grid veri setinden elde edilen yüzey gravite anomalileri kullanılmıştır. Hesaplamalarda orijinal $5'$ yay dakikası ($\sim 9\text{ km}$) çözümürlükteki Bouguer anomali veri setine ek olarak, $1'$ yay dakikası ($\sim 2\text{ km}$) çözümürlüğe artırılmış versiyonları da kullanılmıştır. Gravite gridlerinin çözümürlüklerinin artırılmasında, hem düzlemsel (planar) hem de küresel (spherical) yaklaşımda tamamlanmış Bouguer anomalileri kullanılmıştır. Böylece gravite gridlemede hem gravite grid yoğunlaştırmasının hem de Bouguer indirgeme işlemi için uygulanan yaklaşımın geoit model doğrulukları üzerindeki etkileri incelenmiştir. Bouguer gravite indirgemeleri, düzlemsel yaklaşım için klasik formüller kullanılarak gerçekleştirilirken, sayısal testlerde küresel yaklaşım için yüksek çözümürlüklü SRTM2Gravity global modelinden elde edilen gravimetrik arazi düzeltmeleri kullanılmıştır. Hesaplanan geoit modelleri, ülke genelinde homojen olarak dağılmış 100 GPS/nivelman veri seti ile karşılaştırılarak doğrulanmıştır. Ayrıca, modellerden elde edilen geoit yükseklikleri kıyı şeridi boyunca altı mareograf istasyonlarında karşılaştırılmıştır. Böylece, modellerin kıyılardaki uyuşumunun değerlendirilmesi için ek bir kontrol sağlanmıştır. Sonuç olarak, Türkiye'deki küresel tamamlanmış Bouguer anomalilerinden hesaplanan $1'$ yay dakikası çözümürlüklü yüzey gravite anomalileri kullanılarak elde edilen geoit modeli çözümünün doğruluğu

GPS/nivelman noktalarındaki geoit yüksekliği farklarının standart sapmasıyla 8.6 cm olarak bulunmuştur.

Üçüncü çalışma, Türkiye'de Hotine integrali yönteminin en küçük kareler modifikasyonu ve ek düzeltmelerini (LSMHA) kullanarak bölgesel gravimetrik geoit modelleme doğruluk performansını araştırmayı amaçlamaktadır. Gravimetrik geoit modeli, tamamlanmış Bouguer anomali gridinden hesaplanan $1' \times 1'$ çözünürlüklü gravite bozuklukları kullanılarak hesaplanmıştır. Ülke genelinde 100 adet homojen dağılımdaki GPS/nivelman veri seti ile yerel olarak homojen dağılıma sahip 301 adet hassas GNSS/nivelman veri seti kullanılarak mutlak ve göreceli olarak geoit doğruluğu belirlenmiştir. Gravimetrik geoit modeli ile bölgesel düşey datum arasındaki sistematik farklılıkların kaldırılmasından önce (before-fit) ve sonra (after-fit) için doğruluk istatistikleri ayrıca belirtilmiştir. LSMHA ile hesaplanan geoid modelinden elde edilen doğruluk, yaygın olarak kullanılan Stokes integralinin en küçük kareler modifikasyonu (LSMSA) yöntemi ile hesaplanan en uygun geoid modeli ile karşılaştırılmıştır. Sonuçlar, Hotine çözümünün doğruluğunu, tüm ülkedeki Stokes muadilinden elde edilen 8.6 cm mutlak doğruluğu ile karşılaştırıldığında, 8.8 cm olduğunu ortaya koymaktadır. Türkiye'nin batısındaki yerel değerlendirmeye dayalı olarak, modeller yerel 301 GPS/nivelman kriterlerinde ülke çapındaki doğrulama sonuçlarından çok daha iyi uyum performansı göstermektedir. Hotine ve Stokes çözümlerinin yerel GPS/nivelman veri setindeki doğrulukları sırasıyla 4.4 ve $4.3\text{ cm}'dir$. Sonuç olarak, gravite bozukluğu kullanılarak bölgesel gravimetrik geoit modelleme yapan LSMHA yönteminin LSMSA yöntemine yakın ve kıyaslanabilir bir sonuç verdiği ortaya konmuştur.

Dördüncü çalışmanın amacı, Türkiye'de homojen olarak dağıtılmış 100 adet GPS/nivelman istasyonları kullanılarak son yayınlanan GOCE tabanlı sadece uydu verilerine dayalı hesaplanmış global jeopotansiyel modellerin performansını değerlendirmektir. Doğrudan (Direct, DIR), zamana dayalı (time-wise, TIM), mekana dayalı (space-wise, SPW) ve GOCO model serileri, GPS/nivelman veri seti ile spektral olarak karşılaştırılabilir hale getirmek için spektral iyileştirme yöntemi (spectral enhancement method, SEM) kullanılarak doğrulukları analiz edilmiştir. Küresel harmonik açılımlar kullanılarak GOCE modellerinden geoit yüksekliklerinin hesaplanması, gravite alanı sinyalinin kısa dalga boylu bileşenleri, ultra yüksek çözünürlüklü global jeopotansiyel model EGM2008 ve artık arazi etkisinden tamamlanmıştır. GOCE modellerinin performansları, EGM2008 modelinin maksimum açının derecesinde elde edilen doğruluğuna göre değerlendirilmiştir. En iyi performansı gösteren modeller, 9.3 cm standart sapma ile DIR, TIM ve GOCO modellerinin altıncı sürümü olarak bulunmuştur. Stokes integralinin en küçük kareler modifikasyonu ve ek düzeltmeleri yöntemi ile gravimetrik geoit modelinin hesaplanmasında 205 derece/mertebe açılıma kadar TIM-R6 modeli referans model olarak kullanılmıştır. Gravimetrik geoit için referans model, lineer birleştirme (linear blending) tekniği kullanılarak TIM-R6 ve EGM2008 modellerinin katsayılarının birleştirilmesiyle oluşturulmuştur. Spektral olarak birleştirilen global jeopotansiyel model ile hesaplanan gravimetrik geoit modeli EGM2008 modelinin 360 derece/mertebeye kadar açılımı ile hesaplanan gravimetrik geoit modeline göre $\sim\%23$ daha yüksek doğruluk sağlanmıştır. Bu çalışma ile GOCE uydusunun Türkiye'de gravite alanı spektrumunun orta dalga boyundaki kısımlarına katkısı ortaya konmuştur.

1. INTRODUCTION

Height system modernization to re-define the current vertical datum, which is conventionally based on mean sea level, as a gravimetric geoid requires a highly accurate geoid model to transform the ellipsoidal height into orthometric height. This task needs a special attention in certain areas where the geoid modeling is problematic, such as coastal and mountainous areas. In such topographies, the irregular structure of the topographic masses makes it difficult for the gravity measurements to have sufficient accuracy and distribution for modeling the geoid with high accuracy. Obtaining terrestrial data with sufficient distribution in mountain areas requires a great cost and time. In the measurements made in water bodies, it is not possible to obtain the measurements with desired homogeneity, especially in open seas and oceans. In this context, the satellite gravimeter method is an important data source. However, due to the orbital height, the gravity data obtained from the satellite techniques is used to model long wavelength signals properly. Medium and short wavelength components can be obtained from altimeter satellites in seas and from terrestrial measurements on land. Nonetheless, the increase in the noise of the radar backscatter of altimeter satellites, as they approach the coasts, causes the accuracy of the geoid in coastal areas deteriorate significantly.

Airborne gravimetry is a valuable method for fast data collection to cover large areas. It is used to obtain gravity data, especially in areas where the terrain is rough, difficult to access or dangerous, such as mountainous areas, coastal areas, etc. where the gravity field modeling is relatively a difficult task. It has been reported by researchers that airborne gravimetry data, which can complement the deficiencies of satellite gravimetry, altimeter and terrestrial gravity data, provides significant improvements in the modeling of the gravity field (Hwang et al., 2006; Zhao et al., 2018; Wu et al., 2019; Isik et al., 2021; Wang et al., 2021).

The data obtained from the airborne gravimeter has a high frequency signal structure. This is caused by the turbulence during the flight, and noisy GNSS position, its first (velocity) and second derivatives (acceleration), and also noisy inertial sensor data. The data should be filtered using appropriate methods and its noise level should be reduced via low-pass filters, such as Gaussian, Butterworth filters (Hwang et al., 2006; Olesen, 2003). In order to filter the effect of noise with a minimum signal loss, the parameters of the low-pass filter must be selected appropriately. Moreover, to be able to combine the airborne gravity with the terrestrial gravimetry measurements, the gravity values at flight height must be reduced to the Earth's surface or geoid surface by using appropriate ill-posed downward continuation methods.

The Colorado geoid experiment was initiated and organized as a joint study by the Joint Working Group (JWG) 2.2.2 (1-cm geoid experiment) of the International Association of Geodesy (IAG) in 2017, and different institutions and research groups contributed to this study. To outline the contribution of airborne gravimetry to the accuracy of regional geoid modeling, as ITU-GRG team, we conducted a research to investigate the modeling of high accuracy gravimetric geoid model of Colorado using Least Squares Modification of Stokes and Hotine Integrals with additive corrections (LSMSA) (Isik et al., 2021). After the Joint Working Group successfully finalize the methodological research for the assessment of different geoid modeling techniques and downward continuation algorithms, the working group summarized the findings in an overview paper that combines the solutions of each group (Wang et al., 2021). This working group now left its place to another one named "*JWG 2.2.1: Error assessment of the 1 cm geoid experiment*". In this working, each group focuses on the validation of their own existing solution against extended Geoid Slope Validation Survey 2017 data provided by National Geodetic Survey (NGS), US to investigate the possible error sources that may stem from data collection, data preparation and manipulation, downward continuation and gravimetric geoid modeling.

In the first part of this thesis (Isik et al., 2021), we reported our contribution to the 1 cm Colorado Experiment conducted within the scope of JWG 2.2.2. The aim of this experimentation was to clarify the repeatability of gravity potential values as International Height Reference System (IHRS) coordinates from different geoid

determination approaches carried out with the same input dataset. The dataset included the terrestrial and airborne gravity observations, a digital terrain model, the XGM2016 global geopotential model and GPS/leveling data for model validations belonging to a mountainous area of approximately $550\text{ km} \times 730\text{ km}$ in Colorado, US. The dataset was provided by National Geodetic Survey (NGS) department. In this frame, this article aims providing a discussion on Colorado geoid modeling through individual experimental results obtained by Istanbul Technical University-Gravity Research Group (ITU-GRG). This contribution mainly focused on modeling the Colorado geoid using the least squares modifications of Stokes and Hotine integral formulas with additive corrections. The computations using each formula were carried out using ITU-GRG software, including the solution variants based on terrestrial-only, airborne-only and combined gravity datasets. Then, the calculated experimental geoid models were validated using historical and recently measured profile-based GPS/leveling datasets, and they were also compared with the official solutions submitted by different institutions for the “1-cm geoid experiment” of IAG JWG 2.2.2. For all validation results, the Hotine and Stokes integral formulas yielded similar performances in terms of geoid accuracy; however, the models computed using the combined data had better accuracy than those using the terrestrial-only and airborne-only solutions. The geoid model solutions using the combined data had an accuracy of 2.69 cm for the Hotine method and 2.87 cm for the Stokes method in the test results using GPS/leveling data of the GSVS17 (Geoid Slope Validation Survey 2017) profile. Airborne data from the Gravity for the Redefinition of the American Vertical Datum (GRAV-D) project contributed significantly towards improving the geoid model, especially in the mountainous parts of the area.

As challenging it is to model an accurate gravimetric geoid model in topographically challenging area such as the case of Colorado with high quality gravity data set, it is much more rival task to improve the performance of the geoid model in places where the gravity data set has lower quality and resolution. The geoid modeling studies in Turkey were initiated with the astro-geodetic geoid modeling and doppler derived geoid heights (Ayan, 1976, 1978; Gürkan, 1978) has left their place to the gravimetric geoid modeling studies with Turkey Geoid 1991 (TG-91), the first gravimetric geoid

(Ayhan, 1993). The precise geoid modeling studies in Turkey were accelerated after the establishment of the Turkish National Fundamental GPS Network in 1999, with the requirement of a practical transformation model between the GNSS ellipsoidal heights and the orthometric heights in regional vertical datum. Through these years, significant amount of geoid studies have been conducted using modernized techniques and improved solutions for long-wavelength gravity signal provided by state-of-art (by the time being of course) global geopotential models (Kılıçoglu et al., 2005; Ayhan et al., 2002; Yıldız et al., 2006; Kılıçoglu et al., 2011). Through these efforts to improve the accuracy of geoid model via different approaches and global geopotential models, one thing was certain, and it was the necessity to replace the existing gravity measurement with more accurate ones.

In 2015, the height system modernization efforts were accelerated with the joint efforts of the General Directorate of Mapping (GDM), the General Directorate of Mineral Research and Exploration (GDMRE), the Turkish Petroleum Corporation (TPAO), Marmara Research Center (MAM) and National Metrology Institute (UME). together with the Scientific and Technological Research Council of Turkey (TÜBİTAK). Within the context of this modernization project, the terrestrial gravity measurements were collected with $\sim 9\text{ km}$ (5-arcmin) intervals, covering the entire country in a grid-wise form. In topographically challenging areas, such as mountains and large water bodies, it is planned to make airborne gravity surveys. Airborne surveys are still on-going and will be extended to cover the coastlines, inland water bodies and regions not accessible by land in Turkey.

With the CHAMP, GRACE and GOCE satellite gravity missions, significant improvements have been achieved in the degrees of expansion (resolutions) and accuracy of the global geopotential models. Specifically the contribution of GOCE satellite to the static gravity field is significant in term of achieving 1-cm geoid goal that can replace the traditional mean sea level based vertical datum. However, satellite data alone is not sufficient to model the gravity field with the desired accuracy. In this context, geoid can be modeled with high accuracy by combining the global geopotential models obtained with satellite gravity data and other gravity measurement techniques made at regional/local scale. This can be achieved efficiently

with the stochastic modifications of Stokes/Hotine integrals by combining the global geopotential model and surface gravity anomalies using their a-priori variance information. This way, the drawback of the surface gravity anomalies can be compensated in a certain level.

The second part of this thesis, which covers the chapters 3, 4, and 5, includes the efforts to improve the accuracy of gravimetric geoid model of Turkey with the aid of recent satellite gravimetry contribution made by GOCE, and stochastic kernel modification of Stokes and Hotine integrals in a least squares sense. First, we attempted to increase the spatial resolution of surface gravity anomaly grid from 5-arcmin ($5'$) resolution to 1-arcmin ($1'$) resolution by exploiting the forward modeling of short-scale topographic signals on gravity. After successfully achieving this goal, we calculated the densified gravity disturbance data set to model the gravimetric geoid via LSMHA technique for the first time in Turkey and showed how accurate this approach can model the geoid compared to its Stokes' counterpart. Finally, we assessed the performance of GOCE-based satellite only global geopotential models in Turkey to show the improvements made by GOCE observations to the long-wavelength signals of gravity spectrum. In this way, we clarified the best fitting global geopotential models as well as their optimum degree of expansion. In the last step, the best fitting model was linearly blended with Earth Gravity Model 2008 - EGM2008 (Pavlis et al., 2012) to achieve more accurate spherical harmonic coefficients set. This linearly blended model was used as a reference model for gravimetric geoid modeling, and the performance of the output model was compared with the former experimental geoid models.

The second study (Isik et al., 2022b) investigated the accuracy improvement of the gravimetric geoid model in Turkey using densified grids of the gravity anomalies with the least-squares modification of the Stokes integral with additive corrections (LSMSA) method. In LSMSA computations of the geoid models, the surface gravity anomalies, which were derived from the complete Bouguer anomaly grid data set by forward modeling the topographic masses, were used. In the computations, in addition to the original $5'$ -resolution ($\sim 9\ km$) Bouguer anomaly data set, its densified versions to $1'$ -resolution ($\sim 2\ km$) also were used. The densification of the gravity grids was carried out using both planar-and spherical-type complete Bouguer anomalies. Thus,

the effects of both gravity grid densification and the applied approximation for the Bouguer reduction process in gravity gridding on the geoid model accuracies were examined in order. The Bouguer gravity reductions were carried out using classical formulas for the planar approximation, whereas the gravimetric terrain corrections from the high-resolution SRTM2gravity global model were employed for the spherical approximation in numerical tests. The calculated geoid models were validated at 100 homogeneously distributed GPS/leveling benchmarks over the country. In the tests, the geoid undulations derived from the models also were compared with the observations at six tide gauge stations along the coastlines. The latter provided an additional check for the assessment of the models' compatibility at the coastal boundaries. In conclusion, the accuracy of the best geoid model solution (8.6 cm by means of the standard deviation of geoid undulation differences at GPS/leveling benchmarks) was achieved using 1'-resolution gravity anomalies restored from the spherical complete Bouguer anomalies in Turkey.

The third study (Isik et al., 2022a) aims to investigate the regional gravimetric geoid modeling accuracy performance using least squares modification of Hotine's integral with additive corrections (LSMHA) method in Turkey. The gravimetric geoid model is computed using $1' \times 1'$ resolution gravity disturbances calculated from the complete Bouguer anomaly grid. It is validated in absolute and relative manners using the countrywide and locally distributed precise GNSS/leveling dataset having 100 and 301 benchmarks, respectively. The validation statistics are generated before and after removing the systematic differences between the geoid model and the local vertical datum. The obtained accuracy of the calculated geoid model with LSMHA is compared with the best-fitting geoid model computed via commonly used least squares modification of Stokes's integral (LSMSA) method. The results reveal that the accuracy of the Hotine's solution is 8.8 cm, compared to the 8.6 cm achieved from the Stokes counterpart in the whole country. Based on the local assessment in the western part of Turkey, the models show much better fitting performance at the local 301 GNSS/leveling benchmarks than the countrywide validation results. The accuracies of the Hotine's and Stokes's solutions at the local GNSS/leveling dataset are 4.4 and 4.3 cm, respectively. As a result, it is revealed that the LSMHA method

using gravity disturbance gives a competitive result to the LSMSA method in regional gravimetric geoid modeling.

The aim of the fourth, and final study (Isik et al., 2022c), is to evaluate the performance of the recent GOCE-based satellite-only global geopotential models using 100 homogeneously distributed GPS/leveling stations in Turkey. Direct (DIR), time-wise (TIM), space-wise (SPW), and GOCO satellite-only model series were validated using the spectral enhancement method in order to make the models spectrally comparable with the GNSS/leveling data set. In the computation of geoid heights from GOCE models using spherical harmonic expansions, the short wavelength components of the gravity field signal were completed from ultra high-resolution global geopotential model EGM2008 and residual terrain effect. The performances of GOCE models were evaluated with respect to the accuracy of EGM2008 at the maximum degree of expansion. The best performing models were found as the sixth release of DIR, TIM, and GOCO models with 9.3 cm standard deviation. TIM-R6 up to 205 degree/order expansion was used as a reference model for the computation of gravimetric geoid model via least squares modification of Stokes integral with additive corrections method. The reference model for the gravimetric geoid was created by combining the coefficients of TIM-R6 and EGM2008 models using the linear blending technique. The spectrally mixed global geopotential model improved the accuracy of the gravimetric geoid model $\sim 23\%$ with respect to the gravimetric geoid model calculated with EGM2008 up to 360 degrees. The contribution of the GOCE satellite in medium wavelength parts of the gravity field spectrum was clarified in Turkey.

After this introduction chapter, the chapters 2, 3, 4 and 5 of this thesis is organized based on the four papers mentioned above. The last chapter (Chapter 6) finalizes the thesis with conclusions and discussions of the papers. Some of the chapters of this thesis are published/under review in journals indexed by SCI-Expanded as,

- Chapter 2 is published as a paper entitled "*High-resolution geoid modeling using least squares modification of Stokes and Hotine formulas in Colorado*" in *Journal of Geodesy*.

- Chapter 3 is published as a paper entitled "*Investigation of the Geoid Model Accuracy Improvement in Turkey*" in *Journal of Surveying Engineering*.
- Chapter 4 is published as a paper entitled "*Geoid modeling with least squares modification of Hotine's integral using gravity disturbances in Turkey*" in *Earth Science Informatics*.
- Chapter 5 is submitted as a paper entitled "*Improvement of GOCE-based Global Geopotential Models for Gravimetric Geoid Modeling in Turkey*" to *Geosciences*.

2. HIGH-RESOLUTION GEOID MODELING USING LEAST SQUARES MODIFICATION OF STOKES AND HOTINE FORMULAS IN COLORADO¹

2.1 Introduction

The 1-cm Colorado geoid experiment was initiated and performed as a joint research project by IAG JWG 2.2.2, and it plays an important role in international height system realization (IHRs) studies. Calculating a high-accuracy geoid model is a key issue for geoid-based vertical datum definition and regional datum unification to define a global physical height system. The main goal of the 1-cm geoid experiment in the Colorado region was to provide comparative results on the differences between the geoid modeling approaches using terrestrial, airborne and combined gravity datasets via precise validation results. In this manner, fourteen institutions from thirteen countries contributed to the joint research project, in which they computed the height anomalies, the geoid undulations, and the potential values in the area. Comprehensive explanations and results for this experiment are given in Wang et al. (2021).

As an equipotential surface of Earth's gravity field, the geoid is considered a datum for defining physical height systems, and the data and formulas for its modeling vary (Hofmann-Wellenhof and Moritz, 2006). In spherical approximation, the geoid can be modeled by the integration of gravity-derived quantities, such as gravity anomalies and/or gravity disturbances. The well-known Stokes (1849) formula proposes an integration that requires global coverage of gravity anomalies, and the Hotine (1969) integral formula uses gravity disturbances. Since globally distributed gravity observations are unavailable, these integral formulas have to be computed in a limited data coverage area with an introduced integration cap. However, this limitation leads to a loss of the gravity signal because of the effect of masses lying outside of the integration cap. Therefore, Molodensky et al. (1962) proposed a modification

¹This chapter is based on : Isik, M. S., Erol, B., Erol, S., & Sakil, F. F. (2021). High-resolution geoid modeling using least squares modification of Stokes and Hotine formulas in Colorado. Journal of Geodesy, 95(5), 49. <https://doi.org/10.1007/s00190-021-01501-z>

of the Stokes integral that enables the combination of available gravity anomaly data collected around the target area and modeled gravity anomaly data obtained via global geopotential model (GGM) coefficients. Additionally, a number of modifications of the Stokes integral are presented in the literature, including deterministic modifications, such as by Wong and Gore (1969), Meissl (1971), and Evans and Featherstone (2000); and stochastic modifications, such as by Sjöberg (1980, 2003a) and Wenzel (1982).

Sjöberg (2003a) formulated a stochastic modification of the Stokes integral called the least squares modification of the Stokes formula with additive corrections (LSMSA), and it adopts a kernel modification to minimize the expected global mean square error of the geoid model using stochastic information for the gravity data and global geopotential model coefficients. Ellmann (2005a) developed a MATLAB program for calculating the modification parameters for the Stokes integral in the least squares sense. In this contribution, the suggested method uses surface gravity anomalies instead of geoid surface anomalies as the input for the Stokes function. Downward continuation, topographic, atmospheric, and ellipsoidal effects are restored onto the geoid heights as additive corrections. Although modifications of the Stokes formula are more common in the literature, Hotine modifications have also been performed by Jekeli (1979, 1980) and Zelin and Yecai (1991). One advantage of using the Hotine integral is the easy derivation of the input gravity disturbances using ellipsoidal height information. Analogous to the LSMSA by Sjöberg (2003a) and Märdla et al. (2018) proposed the least squares modification of the Hotine formula with additive corrections (LSMHA).

As a participating group of the "1-cm Geoid Experiment in Colorado", we submitted a geoid model for the study area calculated by the least squares modification of the Stokes integral using terrestrial-airborne combined data. This model is presented in Wang et al. (2021) along with fourteen models submitted by other participating institutions. For the sake of clarity, the previously submitted model will be named the "official solution" in this paper; moreover, six additional experimental geoid models and their comparisons calculated by using the least squares modification of the Stokes (S) and Hotine (H) integral formulas with additive corrections are presented. For each method, the optimum combination of gravity observations with the global geopotential

model (GGM) was investigated. Hence, terrestrial-only (T), airborne-only (A), and combined (C) data solutions are presented separately in the article. Compared with the official solution, the harmonic correction term was included in the residual terrain correction during the downward continuation of the airborne gravity data. Thus, the Stokes model with the combined gravity data (S.C) solution led to improved results from the geoid model that it was previously submitted as the official solution in Wang et al. (2021). The validation results of the so-called official and the new solutions calculated in this study are given in detail in Sect. 2.4.

Airborne gravity measurements cannot be used directly in combination with terrestrial gravity measurements in geoid calculations because they refer to gravity values at different altitudes from the mean sea level and/or the geoid surface. Therefore, downward continuation of airborne gravity observations to the Earth's surface using an appropriate strategy is necessary for employing these observed along with terrestrial gravity data in geoid computations. In the literature, a number of methods are available for the downward continuation process of gravity values (see Wang, 1988; Vaníček et al., 1996; Tscherning et al., 1998; Huang et al., 2003; Alberts and Klees, 2004; Hwang et al., 2007; Zhao et al., 2018), and the primary methods include the least squares collocation (LSC) (see Tscherning et al., 1998; Alberts and Klees, 2004; Hwang et al., 2007; Zhao et al., 2018), Poisson integral (see Wang, 1988; Vaníček et al., 1996; Huang et al., 2003), and Fast Fourier Transform (FFT) (see Wang, 1988; Hwang et al., 2007) techniques, and the cited works also include comparative results of these techniques for geoid modeling applications. These studies showed that the LSC method has superior performance and advantages compared to the other methods. Therefore, in this study, we adopted and successfully applied the LSC approach with the planar logarithmic covariance model of Forsberg (1987) in the downward continuation of airborne gravity data to calculate geoid models with the combined data.

In the validation of the calculated geoid models, two GPS/leveling datasets were used that include historical data distributed over the Colorado area and the recently released GSVS17 (Geoid Slope Validation Survey 2017) profile data (Wang et al., 2021; van Westrum et al., 2021). Both datasets were provided by the NGS/NOAA

(US National Geodetic Survey/National Oceanic and Atmospheric Administration). Although the estimated accuracy of the historical dataset is not as high as that of the GSVS17 profile data and may be considered insufficient because detailed inference is observed for geoid model accuracies, these data provided an area-based evaluation of the geoid model performance and an opportunity for comparative assessments of the geoid solutions in the area (Wang et al., 2021). Moreover, the GSVS17 profile (van Westrum et al., 2021) includes more accurate GPS/leveling data and was also used to validate our geoid model solutions, including the official model, and calculated statistics were considered in the assessments. In addition to the validations using the GPS/leveling datasets, the models computed in this paper (Wang et al., 2021) were also compared with the mean of the submitted models of the participating institutions (including ours) at the GSVS17 benchmarks. In these comparisons, the validation model was altered for each investigated experimental model; therefore, each model was individually applied to derive the mean of the models. In addition to the comparisons made for the GSVS17 locations, whole geoid grids (at a 1' resolution) were compared to the mean of all submitted models to assess the model performances over the entire area. The results showed that the geoid model solutions derived using the Hotine and Stokes integral formulas had almost the same accuracies. The airborne gravity data made a significant contribution to improving the geoid model accuracy, especially for rugged terrain. The accuracies of the geoid model solutions using the combined data are 2.69 cm for the Hotine method and 2.87 cm for the Stokes method based on the standard deviations of geoid height differences at the GPS/leveling benchmarks of the GSVS17 profile. The combined geoid model solutions were compared with the mean of the submitted geoid models by different institutions to the “1-cm geoid experiment” of IAG JWG 2.2.2 (Wang et al., 2021), and the results had standard deviations of 1.09 cm for the Hotine method and 1.13 cm for the Stokes methods using the GSVS17 profile.

This paper consists of five sections. In Sect. 2.1, the background and objectives of the study are given. In Sect. 2.2, the theory of the downward continuation of airborne gravity data and the geoid modeling methodology using the least squares modifications of the Stokes and Hotine integrals are presented. In Sect. 2.3, the gravity

datasets utilized in this study are introduced. In Sect. 2.4, the numerical results of the downward continuation of the gravity data, the combination of the terrestrial and airborne gravity datasets, and the statistics of validation and comparisons of the geoid model solutions derived using the Stokes and Hotine integrals are presented. In Sect. 2.5, the conclusions and a discussion of the findings are given.

2.2 Methodology

In this section, the methodology for the preparation of airborne gravity data as an input for geoid computation followed by the geoid modeling methodology with least squares modification of the Stokes and Hotine formulas is explained.

2.2.1 Downward continuation of airborne gravity data

With advancements in the field of GNSS positioning, especially kinematic positioning, the accuracy of airborne gravimetry has been significantly enhanced. This technique can be used in areas where gravity data are difficult to obtain, such as water bodies, mountainous areas, or polar regions. The continuation of the geoid along coastal areas can be achieved successfully by using airborne gravity measurements (Wu et al., 2019). Some of the prominent methods used in the downward continuation of airborne gravity data are least squares collocation (Forsberg, 1987; Alberts and Klees, 2004; Zhao et al., 2018), Fast Fourier Transform (Hwang et al., 2006), and Poisson integral (Huang et al., 2003).

In this study, we used the LSC method with a planar logarithmic covariance model (Forsberg, 1987) based on a consideration of the reported superior performance of the LSC technique. Tscherning et al. (1998) applied the LSC method to optimally combine ground gravity data with airborne data in Greenland and concluded that the downward continuation of gravity using the LSC method brought a number of advantages. Alberts and Klees (2004) numerically compared the performance of the planar approximation of LSC method using the attenuated planar logarithmic covariance model and the Poisson integral formula in calculations with airborne gravity data and a synthetic gravity field model, and they found that the LSC method was superior to the Poisson integral formula. Hwang et al. (2007) carried out a study in Taiwan and used the FFT

and LSC as two downward continuation methods in preparing airborne gravity data for geoid modeling, and they concluded that the LSC method was superior. Zhao et al. (2018) investigated the performance of downward continuation methods, including the Poisson integral formula, the semiparametric method combined with regularization (SPR), and LSC with the planar logarithmic covariance model using synthetic data in the Tibetan Plateau, and they reported that the LSC approach generated the best results in terms of the RMS of the downward continuation errors; moreover, based on the outputs of the tests in the Tibetan Plateau, the LSC with a terrain correction was applied for the downward continuation of airborne gravity data in Taiwan as well (see Zhao et al., 2018).

Thus, these comparative studies provided us with insights into the performances of commonly applied downward continuation approaches, and since the LSC with the planar logarithmic covariance model (Alberts and Klees, 2004; Zhao et al., 2018) was shown to achieve acceptable results in practice, we implemented this method for computing the gravity anomalies and disturbances on Earth's surface from airborne observations. In this method, the gravity anomaly signal, represented by \hat{s} at sea level (or the geoid), is estimated using a vector of observations containing surface gravity (at sea level) and airborne gravity data (at flight level). The general formula of the least squares collocation is given in Moritz (1980) as follows:

$$\hat{s} = \mathbf{C}_{sx} [\mathbf{C}_{ss} + \mathbf{D}]^{-1} \mathbf{x} \quad (2.1)$$

where \hat{s} is the signal to be predicted, \mathbf{x} is the observation vector, \mathbf{C}_{sx} is the signal cross-covariance matrix, \mathbf{C}_{ss} is the signal autocovariance matrix, and \mathbf{D} is the noise-covariance matrix.

Auto-covariance \mathbf{C}_{ss} and cross-covariance \mathbf{C}_{sx} matrices are calculated using an analytical covariance model. As stated above, in this study, the planar logarithmic covariance model proposed by Forsberg (1987) for airborne gravimetry was adopted. Based on the model, the covariance between the two points P and Q is given as follows:

$$\begin{aligned} C(x_P - x_Q, y_P - y_Q, z_P + z_Q) \\ = \frac{C_h}{\sum_{i=0}^3 \alpha_i \log(2D_i + 4h)} \sum_{i=0}^3 \alpha_i \log \left(z_i + \sqrt{l_i^2 + D_i^2} \right) \end{aligned} \quad (2.2)$$

where C_h represents the covariance of gravity anomalies at flight altitude h . The remaining parameters are given as follows:

$$\begin{aligned}\alpha_0 &= 1, \alpha_1 = -3, \alpha_2 = 3, \alpha_3 = -1 \\ z_i &= z_P + z_Q + D_i \\ D_i &= D + iT \\ l_i &= \sqrt{(x_P - x_Q)^2 + (y_P - y_Q)^2}\end{aligned}\tag{2.3}$$

where x, y , and z are north, east and up planar coordinates, respectively, D is the short-wavelength attenuation parameter, T is a long-wavelength attenuation parameter, which is the compensation depth, and l_i is the planar distance between points P and Q . Details on the theory of the least squares collocation method for the downward continuation of airborne gravity data can be found in Forsberg (1987).

2.2.2 Geoid Modeling by the Least Squares Modification of Stokes and Hotine Integrals

The geoid modeling methodologies adopted in this study (Sjöberg, 2003b; Märdla et al., 2018) for the Stokes and Hotine integrals were based on the following assumptions: there is a homogeneous distribution of gravity data over the whole integration area, the integration area is a sphere, and there are no topographic masses over the sphere of the integration. The first assumption is treated by introducing the modification parameters, which enable us to limit the integration area in a spherical cap. The latter is treated by restoring the direct and indirect effects of the masses onto the geoid afterward. The estimated geoid model \hat{N} is computed by adding these so-called additive corrections to the approximate geoid height as follows:

$$\hat{N} = \tilde{N} + \delta N_{\text{COMB}} + \delta N_{\text{DWC}} + \delta N_{\text{ATM}} + \delta N_{\text{ELL}}\tag{2.4}$$

where \tilde{N} is the approximate geoid height calculated using the modified integral (near-zone contribution) and Laplace harmonics of the gravity anomalies (far-zone contribution), δN_{COMB} is the combined topographic correction, δN_{DWC} is the combined downward continuation correction, δN_{ATM} is the combined atmospheric correction and δN_{ELL} is the combined ellipsoidal correction.

The approximate geoid height \tilde{N} for the Stokes formula is computed as follows:

$$\tilde{N} = \frac{R}{4\pi\gamma} \iint_{\sigma_0} S^L(\psi) \Delta g \, d\sigma + \frac{R}{2\gamma} \sum_{n=2}^M (s_n + Q_n^L) \Delta g_n^{\text{GGM}} \quad (2.5)$$

where σ_0 is the spherical cap, $S^L(\psi)$ is the modified Stokes' function of spherical distance ψ between the computation point and the integration points, Δg is the surface gravity anomalies, s_n is the modification parameter, Q_n^L is the truncation coefficient by Paul (1973), Δg_n^{GGM} is the Laplace harmonics of degree n calculated from the global geopotential model, M is the maximum expansion of the global geopotential model and L is the degree of modification. s_n is calculated in a least squares sense so that the estimated global mean square error of the modification would be minimized and unbiased modification parameters are used (Ellmann, 2005a,b).

The first term in Eq. 2.5 is the near zone component calculated using gravity observations within the integration cap σ_0 . The second term constitutes the far zone component of the geoid and presents a relatively lower frequency signal.

The modified Stokes' function is given as follows:

$$S^L(\psi) = S(\psi) - \sum_{n=2}^L \frac{2n+1}{2} s_n P_n(\cos \psi) \quad (2.6)$$

where the first term on the right-hand side of the equation is the closed form of the original Stokes function in spectral form and P_n represents the unnormalized Legendre polynomials.

The Laplace harmonics of the gravity anomaly of degree n can be calculated as follows (Hofmann-Wellenhof and Moritz, 2006, Eq. 9-18):

$$\Delta g_n^{\text{GGM}} = \frac{GM}{a^2} \left(\frac{a}{r} \right)^{n+2} (n-1) \sum_{m=-n}^M C_{nm} Y_{nm}(\theta, \lambda) \quad (2.7)$$

where a is the equatorial radius of the reference ellipsoid, r is the geocentric radius, C_{nm} is the global geopotential model coefficient, $Y_{nm}(\theta, \lambda)$ is the fully normalized surface spherical harmonics, and θ and λ are the co-latitude and longitude, respectively.

The modification for the Hotine integral is performed analogously to Eq. 2.5 as follows (Märdla et al., 2018):

$$\tilde{N} = \frac{R}{4\pi\gamma} \iint_{\sigma_0} H^L(\psi) \delta g \, d\sigma + \frac{R}{2\gamma} \sum_{n=0}^M (s_n + Q_n^L) \delta g_n^{\text{GGM}} \quad (2.8)$$

$$H^L(\psi) = H(\psi) - \sum_{n=0}^L \frac{2n+1}{2} s_n P_n(\cos \psi) \quad (2.9)$$

$$\delta g_n^{\text{GGM}} = \frac{GM}{a^2} \left(\frac{a}{r} \right)^{n+2} (n+1) \sum_{m=-n}^M C_{nm} Y_{nm} \quad (2.10)$$

In Eq. 2.8, δg is the surface gravity disturbance, Q_n^L is the truncation coefficient by Jekeli (1979), and δg_n^{GGM} is the Laplace harmonics of the gravity disturbance of degree M calculated from the global geopotential model, and these parameters are different from that in Eq. 2.5. It should be noted that the degree of the modification of the kernel L and the maximum expansion degree of the geopotential model M start from zero in the Hotine integration. Additionally, the numerical values of s_n also differ due to the different parameters considered in the linear system of equation (Märdla et al., 2018, Sec. 2.4).

2.2.2.1 Additive corrections

In this section, computational formulas for the additive corrections for the least squares modified Stokes formula are given based on Sjöberg (2003a). For the Hotine counterpart, computations are performed using the methodology proposed by Märdla et al. (2018), although they are not explained in detail here because of space limitations. Readers should refer to Märdla (2017) and Sakil (2018, Chapter 2.6.1) for additional details.

Combined topographic correction

The combined topographic effect involves both direct and indirect topographic effects and is computed as follows (Kiahmehr, 2006):

$$\delta N_{\text{comb}}^{\text{Topo}} = \delta N_{\text{dir}} + \delta N_{\text{ind}} \approx -\frac{2\pi G\rho}{\gamma} \left(\tilde{H}^2 + \frac{2\tilde{H}^3}{3R} \right) \quad (2.11)$$

where the mean topographic mass density ρ is taken as 2670 kg/m^3 and \tilde{H} represents the Laplace surface harmonics of the topographic heights (H_n). These harmonics are calculated using fully normalized spherical harmonic coefficients (H_{nm}) of the heights as follows (Sneeuw, 1994):

$$H_n(P) = \sum_{m=-n}^n H_{nm} Y_{nm} \quad (2.12)$$

Downward continuation correction

Downward continuation correction is applied for the analytical continuation of gravity anomalies to the geoid. In classical geoid determination approaches, the downward continuation correction is applied directly to the surface gravity anomalies. Sjöberg (2003c) proposed a formula that computes the downward continuation effect over the geoid as follows (see also Agren, 2004, Sec. 5.4.1 and Sec. 9.5.3):

$$\delta N_{\text{DWC}}(P) = \delta N_{\text{DWC}}^1(P) + \delta N_{\text{DWC}}^{L1,\text{Far}}(P) + \delta N_{\text{DWC}}^{L2}(P) \quad (2.13)$$

where

$$\delta N_{\text{DWC}}^1(P) = \frac{\Delta g(P)}{\gamma} H_P + 3 \frac{N_P^0}{r_P} H_P \quad (2.14)$$

and

$$\delta N_{\text{DWC}}^{L1,\text{Far}}(P) = \frac{R}{2\gamma} \sum_{n=2}^M (s_n^* + Q_n^L) \left[\left(\frac{R}{r_P} \right)^{n+2} - 1 \right] \Delta g_n(P) \quad (2.15)$$

and

$$\delta N_{\text{DWC}}^{L2}(P) = \frac{R}{4\pi\gamma} \iint_{\sigma_0} S^L(\psi) \left(\frac{\partial \Delta g}{\partial r} \Big|_P \right) (H_P - H_Q) \quad (2.16)$$

where N_P^0 is the approximate geoid height and $r_P = R + H_P$. The vertical gradient of the gravity anomaly at computation point $P \frac{\partial \Delta g}{\partial r} \Big|_P$ is calculated as follows (Hofmann-Wellenhof and Moritz 2006, Eqs. 2-391):

$$\frac{\partial \Delta g}{\partial r} = \frac{R^2}{2\pi} \iint_{\sigma} \frac{\Delta g_Q - \Delta g_P}{l_0^3} d\sigma_0 - \frac{2}{R} \Delta g_P \quad (2.17)$$

where l_0 is the spatial distance between computation point P and running point Q ; this distance is computed as follows:

$$l_0 = 2R \sin \frac{\Psi_{PQ}}{2} \quad (2.18)$$

Atmospheric correction

The atmospheric mass outside of the surface of the geoid needs to be considered since the determination of the geoid using Stokes' formula requires that all masses outside the geoid be removed. The effect of the atmospheric masses over the geoid to be restored is computed as follows (Kiahmehr, 2006):

$$\begin{aligned} \delta N_{\text{comb}}^{\text{ATM}}(P) = & -\frac{2\pi R \rho_0}{\gamma} H_n(P) \left(\sum_{n=2}^M \frac{2}{n-1} - s_n - Q_n^L \right) H_n(P) \\ & - \sum_{n=M+1}^{\infty} \left(\frac{2}{n-1} - \frac{n+1}{2n+1} Q_n^L \right) \end{aligned} \quad (2.19)$$

where ρ_0 is the atmospheric density at sea level and H_n is the Laplace surface harmonics of the topographic height.

Ellipsoidal correction

The ellipsoidal correction is applied for the spherical approximation of the geoid in the computation of the Stokes integral. The formulation of ellipsoidal correction in the LSMSA method is given in Sjöberg (2004b) as follows:

$$\delta N_{\text{ell}} = \frac{R}{2\gamma} \sum_{n=2}^{\infty} \left(\frac{2}{n-1} - s_n - Q_n^L \right) \left(\frac{a-R}{R} \Delta g_n^{\text{GGM}}(P) + \frac{a}{R} (\delta g_e)_n \right) \quad (2.20)$$

In the equation, $(\delta g_e)_n$ is formulated as follows:

$$(\delta g_e)_n = GM \frac{e^2}{2a^2} \sum_{m=-n}^n \{ [2 - (n+2)F_{nm}] C_{nm} \\ - (n+1)G_{nm}C_{n-2,m} \\ - (n+7)E_{nm}C_{n+2,m}Y_{nm} \} \quad (2.21)$$

where E_{nm} , F_{nm} and G_{nm} are the related coefficients for the ellipsoidal correction (Sjöberg, 2004b, Appendix).

2.3 Data description

The datasets used in this study were provided by the US National Geodetic Survey (NGS). These datasets include terrestrial gravity data from the US National Geospatial Intelligence Agency (NGA) and NGS, GRAV-D airborne gravity data, digital elevation model, and GPS/leveling data in an area of approximately 550 km by 730 km in Colorado, US (between latitudes 35°N to 40°N and longitudes 110°W to 102°W). The topography of the study area is rough, which makes it challenging to compute the (quasi-) geoid accurately in the area. The geoid computations were carried out within 1° inside the data coverage area (between 36°N – 39° N and 109°W – 103°W, see Figure 2.1), which is consistent with the Colorado experiment (please see Wang et al., 2021, Appendix I). In this section, the specifications of the dataset and preprocessing are detailed.

2.3.1 Terrestrial and airborne gravity data

The terrestrial gravity dataset includes 59,303 gravity observations from the National Geospatial Intelligence Agency (NGA) and National Geodetic Survey (NGS) databases. In Figure 2.1, the distribution of the terrestrial gravity measurements is shown. The terrestrial gravity measurements are dense in the northern and southwestern parts, whereas the data are sparsely distributed in the central and eastern parts of the study area. The dataset was checked for duplicated points, and points with the same location but different observation values were detected. If the points sharing the same location had a height difference of more than 1 m or a gravity difference of 1mGal ($1\text{mGal} = 10^{-5} \text{ m/s}^2$), then they were both removed. Hence, 1092 points in total were excluded from the dataset.

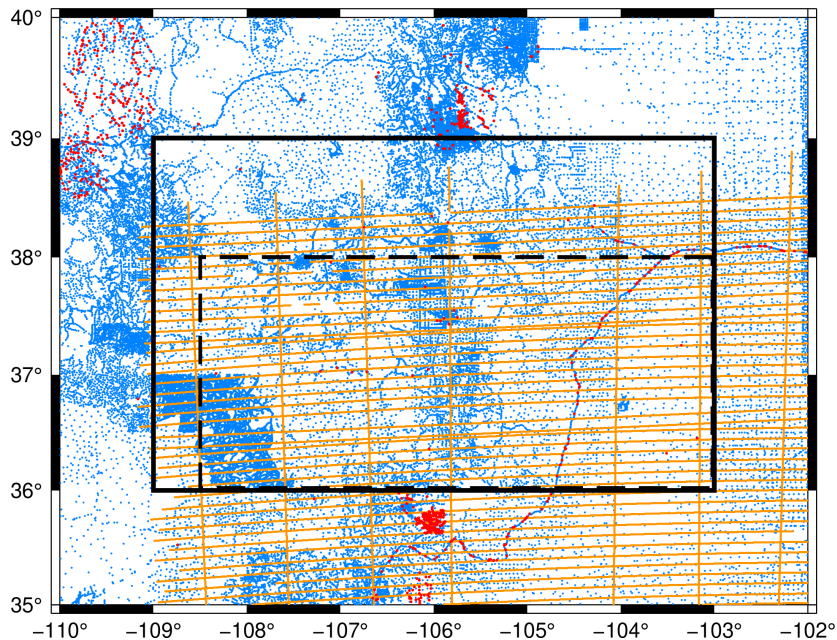


Figure 2.1 : Gravity datasets: Terrestrial gravity measurements (blue), duplicated measurements (red) and airborne gravity measurements (orange), target geoid area for terrestrial-only and combined solutions (solid black line), and target geoid area for airborne-only solutions (dashed black line).

Originally, the airborne gravity dataset (MS05 block) included 2,440,466 gravity measurements in the east-west direction. Additionally, 118,020 cross-track gravity measurements along the north-south direction to perform a crossover error analysis.

The spacing between the east and west tracks is 10 km, while that between the north and south cross tracks is approximately 80 km. The mean flight altitude is approximately 6200 m. The data were filtered 3 times with the Gaussian 6-sigma filter (Wang et al., 2021). The GRAV-D Team (2018) reported that the data have a bias between different tracks. To overcome this problem, the NGS provided another dataset, which was debiased and downsampled to a 1 Hz frequency from 20 Hz (283,716 gravity measurements). However, since these data still contain a high-frequency signal, they were filtered with a Gaussian low-pass filter. To ease the computation, the given airborne dataset was downsampled to an approximately 1 km interval (25,624 gravity points). This sampling interval was selected since it provided an areawise point density, which was reasonable for computing a geoid model with $1' \times 1'$ grid spacing, which was the required spatial resolution in the study (see Figure 2.1 for gravity dataset in the study area).

Free-air gravity anomalies for the airborne dataset were calculated as follows:

$$\Delta g = g_{\text{obs}} - \gamma_0 + \delta_{\text{FAC}} \quad (2.22)$$

where Δg is the free-air gravity anomaly at the flight level, g_{obs} is the gravity measurement at the flight level, γ_0 is the normal gravity on the reference ellipsoid calculated using the Somigliana-Pizzetti formula (Hofmann-Wellenhof and Moritz, 2006, Eq. 2-146) and δ_{FAC} is the free-air correction. The free-air correction term was calculated with the 2nd order gravity gradient formula as follows:

$$\delta_{\text{FAC}} = \frac{2\gamma_e}{a} \left(1 + \frac{(a-b)}{a} + \frac{\omega^2 a^2 b}{GM} - 2 \frac{(a-b)}{a} \sin^2 \phi \right) H - \frac{3\gamma_e}{a^2} H^2 \quad (2.23)$$

where orthometric heights H are computed by subtracting the geoid heights (N) calculated from the EGM2008 gravity field model (Pavlis et al., 2012) up to 2190 degree/ order from the ellipsoidal heights (h) of airborne gravity. To maintain consistency with airborne data, free-air corrections for surface gravity anomalies were also computed with the 2nd-order gravity gradient formula. Additionally, the atmospheric gravity correction was computed according to Eq. 2.24 and added to the surface gravity anomalies (Wenzel, 1985).

$$\delta_{\text{AGC}} = 0.874 - 9.9 \times 10^{-5} H + 3.5625 \times 10^{-9} H^2 \quad (2.24)$$

The free-air gravity anomalies for both terrestrial and airborne gravity data are shown in Figure 2.2. The terrestrial free-air anomalies at the terrain level vary between -114 and 210 mGal, whereas airborne free-air anomalies at flight altitudes change from -41 to 126 mGal (see Table 2.1).

2.3.2 Global geopotential model

In this study, the Experimental Gravity Field Model 2016 (XGM2016) (see Pail et al. (2016, 2018) for details) as a combined model up to 719 degree/order was used to model the low-frequency signal of gravity anomalies in the remove-restore procedure before the downward continuation of airborne gravity. This geopotential model was also used as a reference model for regional geoid model computations.

The XGM2016 model has been given in the zero tide system. To maintain consistency with the basic agreements for the computations, which are given in Appendix I of Wang et al. (2021), the model was converted to a tide-free permanent tide system as follows (Rapp et al., 1991):

$$C_{2,0}^{TF} = C_{2,0}^{ZT} + 3.11080 \cdot 10^{-8} \times \frac{0.3}{\sqrt{5}} \quad (2.25)$$

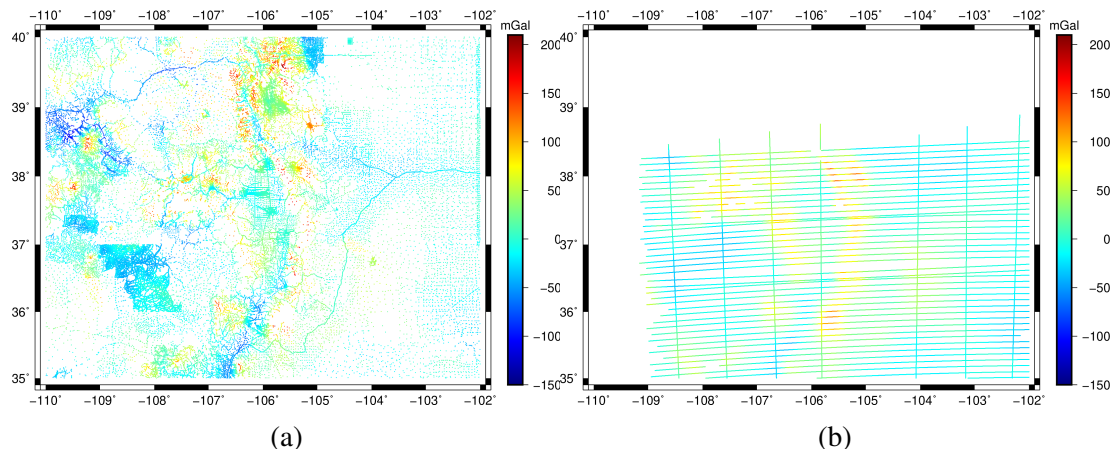


Figure 2.2 : (a) Surface gravity anomalies and (b) airborne gravity anomalies at flight level.

2.3.3 Digital elevation model

The SRTM v4.1 data (Jarvis et al., 2008) were provided to the contributing groups of the "1-cm Geoid experiment" in a 3 arc-second (90 m) resolution model throughout

the region (Wang et al. 2021, this issue). Consecutive cells that had a height difference greater than 500 m were flagged and fixed for errors and voids (Ahlgren et al., 2018; Li et al., 2019)(Ahlgren et al. 2018; Li et al. 2019). The topography of the study area is shown in Figure 2.3. The provided digital elevation model was expanded by 1° for the forward modeling of gravity via residual terrain model computation. The elevations have a mean of 1860 m and a standard deviation of 621 m in the study area. The topographic heights vary between 636 and 4385 m.

2.3.4 GPS/leveling data

Two GPS/leveling datasets were used within the study area to validate the calculated geoid models. In the first dataset, there were 509 historical GPS/leveling benchmarks: 467 were taken from the NGS Integrated Database and the remaining 42 benchmarks were taken from the NGS OPUS-Share Tool (<https://www.ngs.noaa.gov/OPUS/>). The orthometric heights of these GPS/leveling data are in the NAVD88 (North American Vertical Datum of 1988) vertical datum, and the gravimetric corrections on topographic heights were calculated according to the Helmert orthometric height hypothesis. Although the accuracy of the historical GPS/leveling data is not exactly known, Wang et al. (2021) (see in Sect. 4) estimated the accuracy of the dataset to be approximately 3 – 5 cm.

Additionally, the accuracy of the geoid models was evaluated using the GPS/leveling data at 223 benchmarks of the GSVS17 profile. These benchmarks were collected by the NGS along a 360 km line in the rugged terrain of southern Colorado (Figure 2.3) that ranged in elevation from 1900 to 3300 m, with a station spacing of approximately 1.6 km (van Westrum et al., 2021). The reported GPS position and orthometric height accuracies of the GSVS17 benchmarks are ~ 1 cm (Wang et al., 2021; van Westrum et al., 2021).

The distribution of the historical GPS/leveling and the GSVS17 points are shown in Figure 2.3. Historical data have a sparse distribution throughout the study area because of the rough topography. Only 194 of the 509 historical points are located inside the geoid computation area, which is 1° inside the data coverage. Since the airborne-only geoid solutions were limited to $36^{\circ}\text{N}/38^{\circ}\text{N}$ latitudes and $108.5^{\circ}\text{W}/103^{\circ}\text{W}$ longitudes

due to the smaller coverage of the airborne data, 75 GPS/leveling points located inside the target area were utilized for the validations.

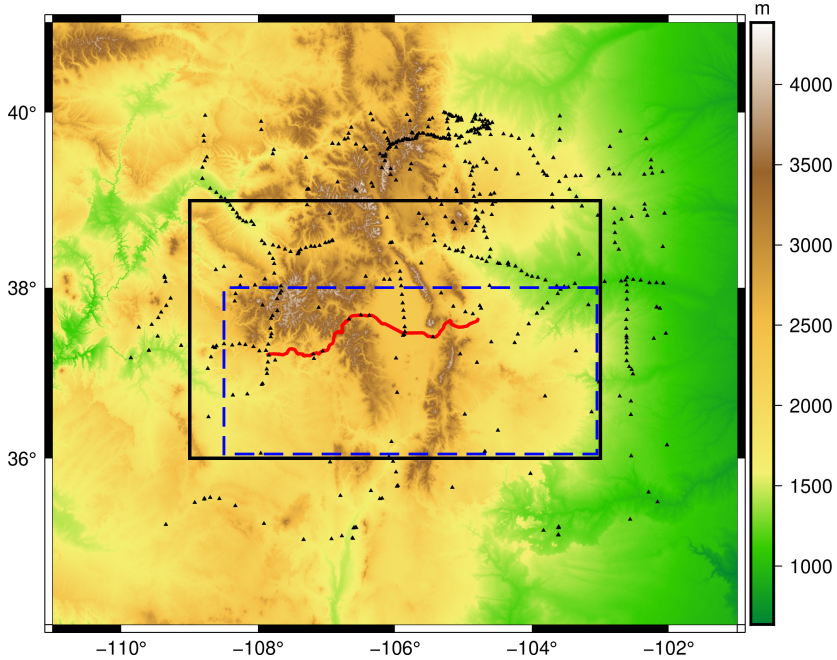


Figure 2.3 : GPS/leveling benchmarks on the topography of SRTM v4.1 (3" resolution) in the Colorado area. Black triangles indicate the historical GPS/leveling data, and red triangles indicate the GSVS17 GPS/leveling data. Target geoid area for the terrestrial-only and combined solutions (solid black line), and target geoid area for the airborne-only solutions (dashed blue line).

2.4 Results

2.4.1 Downward continuation of airborne gravity

In the downward continuation of airborne gravity anomalies, the well-known remove-restore schema was followed to reduce the computational errors (Forsberg, 1984; Forsberg and Tscherning, 1981). In the remove-restore method, the low-frequency gravity information was modeled using a global geopotential model (GGM) and then subtracted from the observed gravity values. Since the reference gravity by the GGM was removed from the observed gravity, the remaining part of the airborne gravity observations corresponds to discrete samples of the band-limited gravity values only. This band limitation has a positive contribution towards stabilizing the numerical evaluation of the downward continuation problem and hence

achieving improved results (Novák and Heck, 2002). In the standard practice of the remove-restore method, both the long-wavelength gravity component and the topographic gravity effect were removed from the gravity observations to obtain the residual gravity anomalies. The topographic gravity effect was attributed to the short-wavelength component and evaluated using the attraction of the masses between the actual height of the computation point and a mean surface; this reduction process is called the "residual terrain model" (RTM) (Forsberg, 1984).

In this study, the residual gravity anomalies were calculated by subtracting the long-wavelength signal computed from the XGM2016 global geopotential model up to 719 degree/order and the short-wavelength signal, which was modeled by the RTM according to Forsberg (1984). The RTM method is commonly applied for terrain reduction in the downward continuation process and uses numerical integration of mass prisms to remove the topographic mass above the reference surface and fill up the mass deficit below the reference surface (Forsberg and Tscherning, 1981). The reference surface was a mean elevation surface generated from the SRTM elevation model by applying a moving average low-pass filter using the TCGRID module of the GRAVSOFT package (Forsberg and Tscherning, 2008). The kernel size of the low pass filter was chosen in accordance with the maximum degree of expansion of the global geopotential model; therefore, the short-wavelength parts of the gravity anomaly signal omitted by the spherical harmonic expansion could be modeled. Since the maximum degree of expansion was chosen as 719, the resolution of the low-pass filter was set to 27.75 km to represent the signals above the 720 degree/order of the spectrum. It should be mentioned that the RTM correction for the airborne gravity anomalies was smoothed by the Gaussian 6-sigma filter because it was applied to the airborne gravity anomalies along track. The statistics of the remove steps for both the airborne and terrestrial gravity datasets are given in Table 2.1. The distribution of the residual gravity anomalies for terrestrial and airborne data is shown in Figure 2.4.

The covariance model parameters explained in Sect. 2.1 were computed by fitting the logarithmic function to the empirical covariance model formed by variance $C_h = 62.6$ mGal² of the residual gravity anomalies at flight altitude (see Figure 2.5). The Bjerhammar sphere depth (D) and compensation depth (T) were estimated from the

Table 2.1 : Statistics of residual gravity anomalies [unit: mGal].

	Min	Max	Mean	STD
Terrestrial				
Δg_{FA}	-113.446	209.729	4.688	37.828
$\Delta g_{\text{FA}} - \Delta g_{\text{GGM}}$	-131.918	134.792	-6.898	22.369
$\Delta g_{\text{FA}} - \Delta g_{\text{GGM}} - \Delta g_{\text{RTM}}$	-74.020	89.256	-0.723	14.728
Airborne				
Δg_{FA}	-41.084	126.321	8.946	29.020
$\Delta g_{\text{FA}} - \Delta g_{\text{GGM}}$	-43.198	66.772	-2.872	7.907
$\Delta g_{\text{FA}} - \Delta g_{\text{GGM}} - \Delta g_{\text{RTM}}$	-43.042	52.254	-2.627	7.229

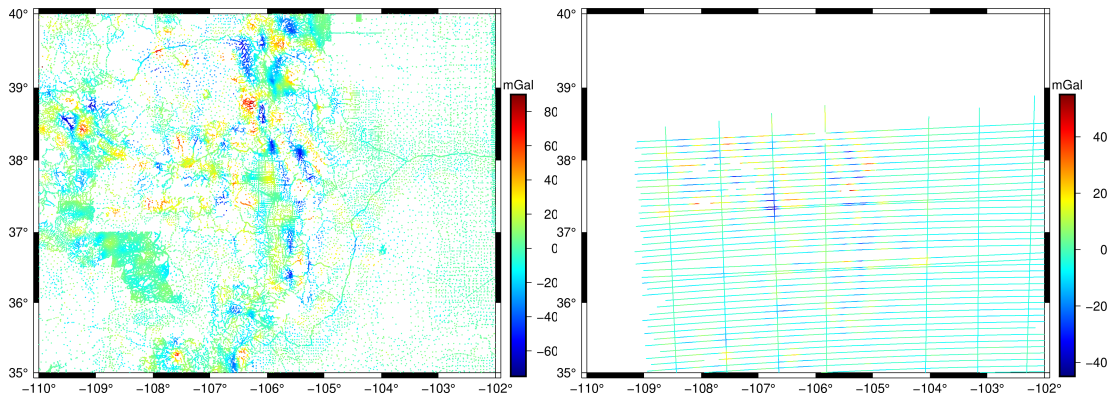


Figure 2.4 : (a) Terrestrial residual gravity anomalies and (b) airborne residual gravity anomalies before downward continuation ($\Delta g_{\text{FA}} - \Delta g_{\text{GGM}} - \Delta g_{\text{RTM}}$).

fitted model as 6 km and 16 km, respectively. A priori errors of the airborne and terrestrial datasets were considered 2 mGal and 1 mGal, respectively. The LSC with planar approximation was performed in Python 3 programming language. However, the solution of collocation equations was carried out using Cholesky Decomposition in the Linear Algebra Package (LAPACK) Fortran Library (LAPACK–Linear Algebra Package, 2000). To reduce the computational load, downward continuation was performed within $1^\circ \times 1^\circ$ blocks with $0.5^\circ \times 0.5^\circ$ overlaps. In each block, the airborne gravity anomaly residuals continued downward to the terrain altitude.

Downward-continued residual gravity anomalies and the terrestrial residual gravity anomalies (see Figure 2.6a) were gridded using the GEOGRID module of the GRAVSOFT package (see Figure 2.6b) (Forsberg and Tscherning, 2008). The long-wavelength and the short-wavelength components were restored to the residual gravity anomaly grid to calculate the combined surface gravity anomalies

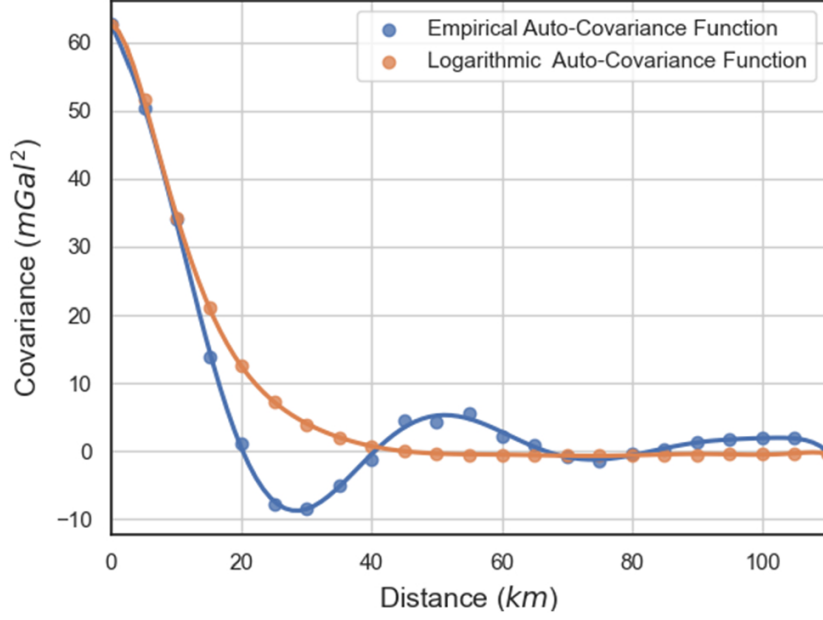


Figure 2.5 : Covariance model and empirical covariance of the residual gravity anomalies.

(Figure 2.7a). The merged dataset has a spatial resolution of approximately 2 km ($1' \times 1'$). The gravity disturbances (Figure 2.7b) were generated from gravity anomalies using an existing geoid model (EGM2008 gravity field model up to 2190 d/o) according to Eq. 2.26. Table 2.2 gives the statistics of the gravity anomaly and disturbance datasets for the geoid computations.

$$\delta g - \Delta g = \frac{2T}{R} \approx 0.3086N \quad (2.26)$$

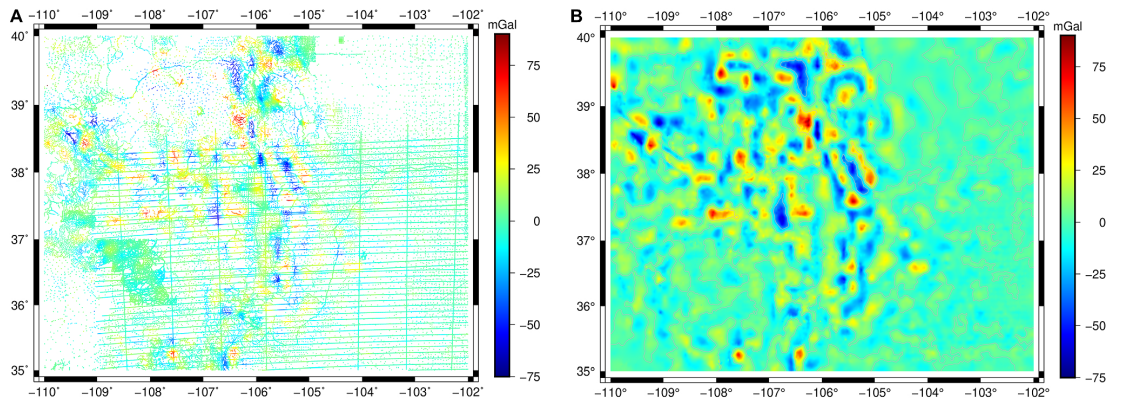


Figure 2.6 : (a) Airborne (after downward continuation) and terrestrial residual gravity anomalies on Earth's surface and (b) gridded residual gravity anomalies in the contour map.

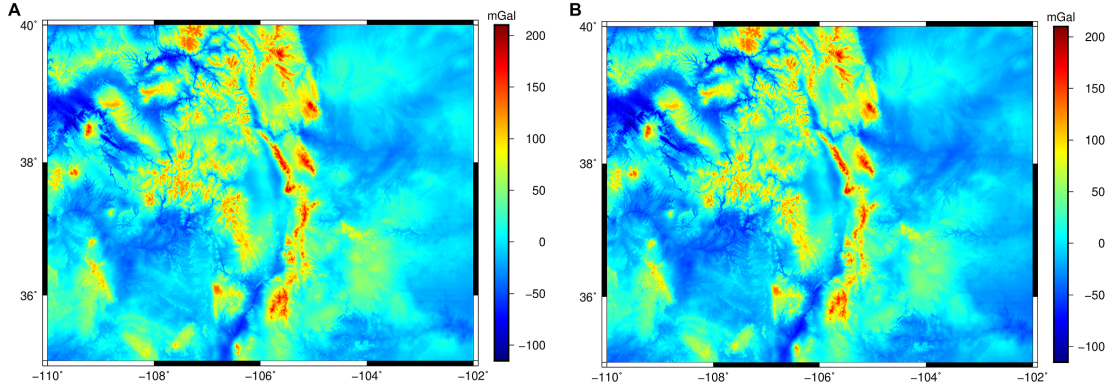


Figure 2.7 : Gridded and restored combined (airborne and terrestrial): (a) gravity anomalies and (b) gravity disturbances.

Table 2.2 : Statistics of airborne and terrestrial combined gravity anomalies and gravity disturbances [unit: mGal].

	Min	Max	Mean	STD
Δg	-110.302	203.221	12.441	37.062
δg	-116.731	198.562	6.435	37.609

2.4.2 Comparison of the resulting geoid models

The geoid models were computed following the methodology described in Sect. 2.2.2. In the computations, GRS80 has been adopted as a reference ellipsoid (Moritz, 2000), the geoid models were computed in the tide-free system, and zero-degree term geoid height N_0 was included according to Sánchez and Sideris (2017).

$$N_0 = \frac{(GM_{GGM} - GM_{GRSR0})}{r_{P_0} \gamma_{Q_0}} - \frac{W_0 - U_0}{\gamma_{Q_0}} \quad (2.27)$$

In this equation, the first term on the right-hand side is the zero-degree term caused by the difference between the Earth gravity constants of the geopotential model used in the geoid computation and the reference ellipsoid and the second term represents the difference between the conventional value of potential W_0 , adopted by IAG (Sánchez et al., 2016), and the potential value on the reference ellipsoid (U_0). The value of the zero-degree term, considering the XGM2016 geopotential model and GRS80 reference ellipsoid, is approximately -0.1781 m in the study area.

The modification parameters s_n for Stokes (Eq. 2.5) and Hotine (Eq. 2.8) integrals were estimated based on the unbiased solution of the least squares method using singular value decomposition (SVD). The error degree variance of the gravity

anomalies was constructed using a bandlimited white noise model, where the standard deviation was taken as 3 mGal. In the Stokes integration, we tested 0.5° and 1° integration radii and expansion degrees between 360 and 719 (with 40 degree intervals) for the global geopotential model. The integration radius ψ_0 was chosen as 0.5° , and the maximum expansion degree of the XGM2016 model and the modification degree of the kernel were set as 719 for both the Stokes and Hotine integration because this value yielded the best standard deviation in the Stokes and Hotine kernels.

Based on the parameters given above, the statistics of the computed geoid models are given in Table 2.3. Additionally, models that employ combined data (C) with the Stokes (S.C) and Hotine (H.C) functions are presented in Figure 2.8a and Figure 2.6b, respectively. The results indicated that the difference in the estimated geoid heights

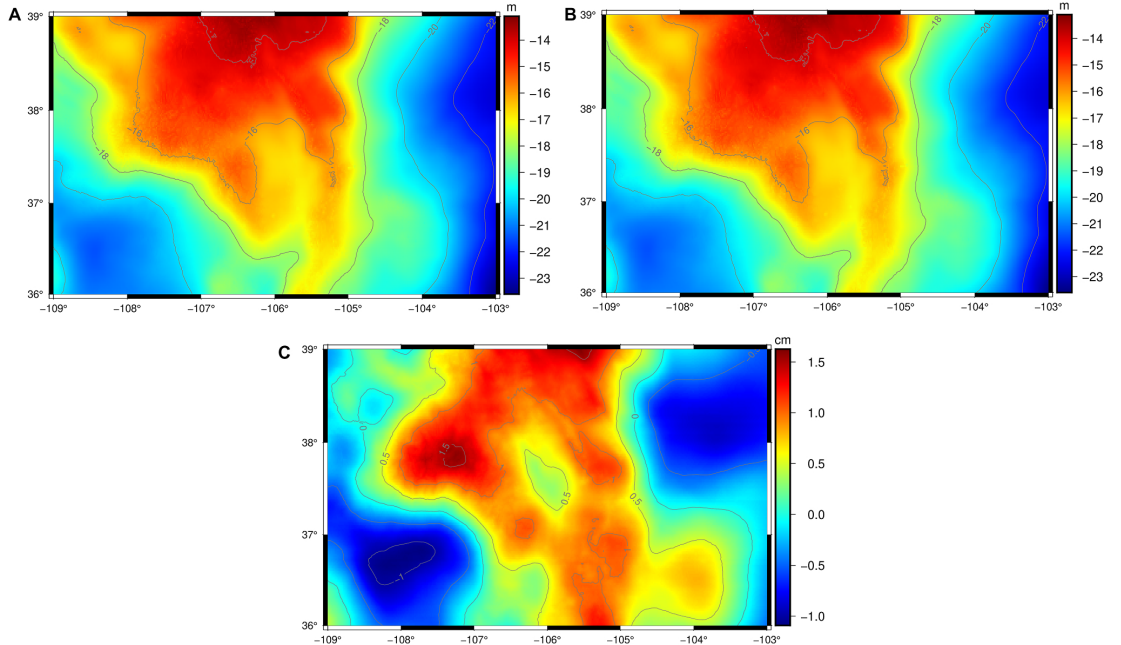


Figure 2.8 : (a) Stokes combined (solution S.C) and (b) Hotine combined (solution H.C) solutions. (c) Difference between the Stokes and Hotine combined solutions ($\hat{N}_{\text{Hotine}} - \hat{N}_{\text{Stokes}}$).

\hat{N} between the combined solutions (S.C) and (H.C) varies from -1.09 to 1.62 cm, whereas the mean value and the standard deviation of the differences are 0.27 cm and 0.67 cm, respectively (see Figure 2.8c). The numerical differences in the additive corrections on geoid models are mainly caused by the combined downward

continuation effect δN_{DWC} , with a maximum value of -2 mm dominated by the δN_{DWC}^1 component. Overall, the differences vary by ± 2 cm.

As mentioned in Sect. 1, the residual terrain model parameters used in the downward continuation of the airborne gravity data for the official solution were different from those of the newly computed models. The harmonic correction was employed in the newly computed models, whereas it was ignored in the official solution. Therefore, although the geoid determination method and the datasets used were the same for the official solution in Wang et al. (2021) and the S.C solution, the models yielded different accuracies.

2.4.3 Validation using GPS/leveling data

External validation statistics using 75 historical GPS/leveling measurements indicated that the accuracies of the estimated geoid models are between 6.5 and 7.0 cm for both the Stokes and Hotine integrations. Table 2.4 gives the performances of the geoid models in the area covered by all solutions (see Figure 2.3, blue dashed box). The official (combined) solution submitted to the Colorado experiment (please see Wang et al. (2021)) performed worse than the newly computed geoid models. However, it should be noted that the estimated observational accuracy of the historical dataset was 3-5 cm (Wang et al., 2021).

Table 2.3 : Statistics of the final geoid models [unit: m].

Method	Data	Min	Max	Mean	STD
Stokes	Combined	-23.578	-13.294	-18.226	2.360
	Terrestrial-only (S.T)	-23.583	-13.928	-18.262	2.245
	Airborne-only (S.A)*	-23.584	-14.654	-18.531	2.003
Hotine	Combined (S.C)	-23.763	-13.366	-18.257	2.383
	Terrestrial-only (H.T)	-23.587	-13.163	-18.074	2.386
	Airborne-only (H.A)*	-23.589	-14.644	-18.528	2.008
	Combined (H.C)	-23.592	-13.178	-18.078	2.389

*Airborne-only solutions cover less area than the rest of the models

2.4.3.1 GSVS17 comparisons

A more rigorous assessment of the accuracies of the calculated geoid models was provided in the validation results with the GSVS 17 profile dataset. Table 2.5 shows

the statistics of the geoid height differences between the models and observations at the 223 GPS/leveling benchmarks of the GSVS17 profile. Considering the statistics in the table, the best performing model is the H.C solution, with a standard deviation of 2.69 cm. The graphic shown in Figure 2.9 visualizes the accuracies of the models via the standard deviations; hence, it provides a better illustration of the model accuracies. The geoid height differences ($\Delta N = N_{\text{Model}} - N_{\text{GPS/lev}}$) at the benchmarks along the 360 kmGSVS17 profile are shown in Figure 2.10a for the Stokes method and Figure 2.10b for the Hotine method. In these figures, considering the geoid height differences at the benchmarks on the high topography (please see the GSVS points with IDs ranging from 1075-1100 and 1175-1200), we can recognize the improvements in the combined models (blue line in the graphics) that include airborne gravity data. A comparison of the official model (Wang et al., 2021) (yellow line graphics) with the combined model calculated in this study (blue line graphics) shows that the latter fits the GPS/leveling values better along the profile.

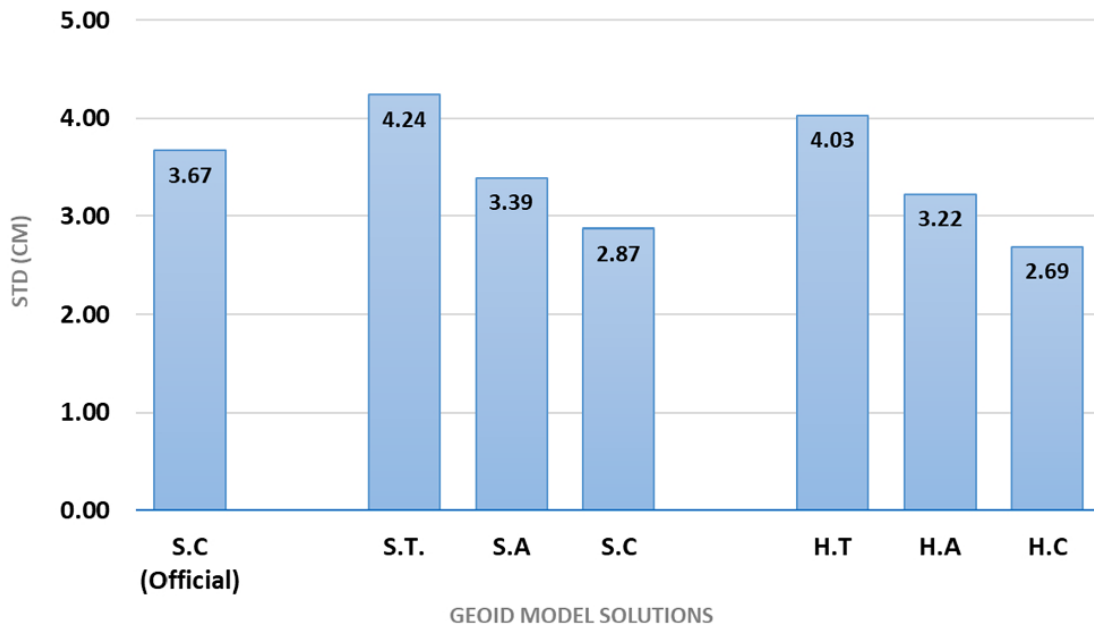


Figure 2.9 : Accuracies of the models according to the standard deviations of geoid height differences at the GPS/leveling benchmarks of the GSVS17 profile [unit: cm].

The geoid models calculated in this research by the Stokes and Hotine integral formulas using the terrestrial-only, airborne-only, and combined datasets were also validated in relative manner at the GSVS17 profile using the mean of the fourteen geoid models, which have already been submitted to the Colorado experiment. The mean

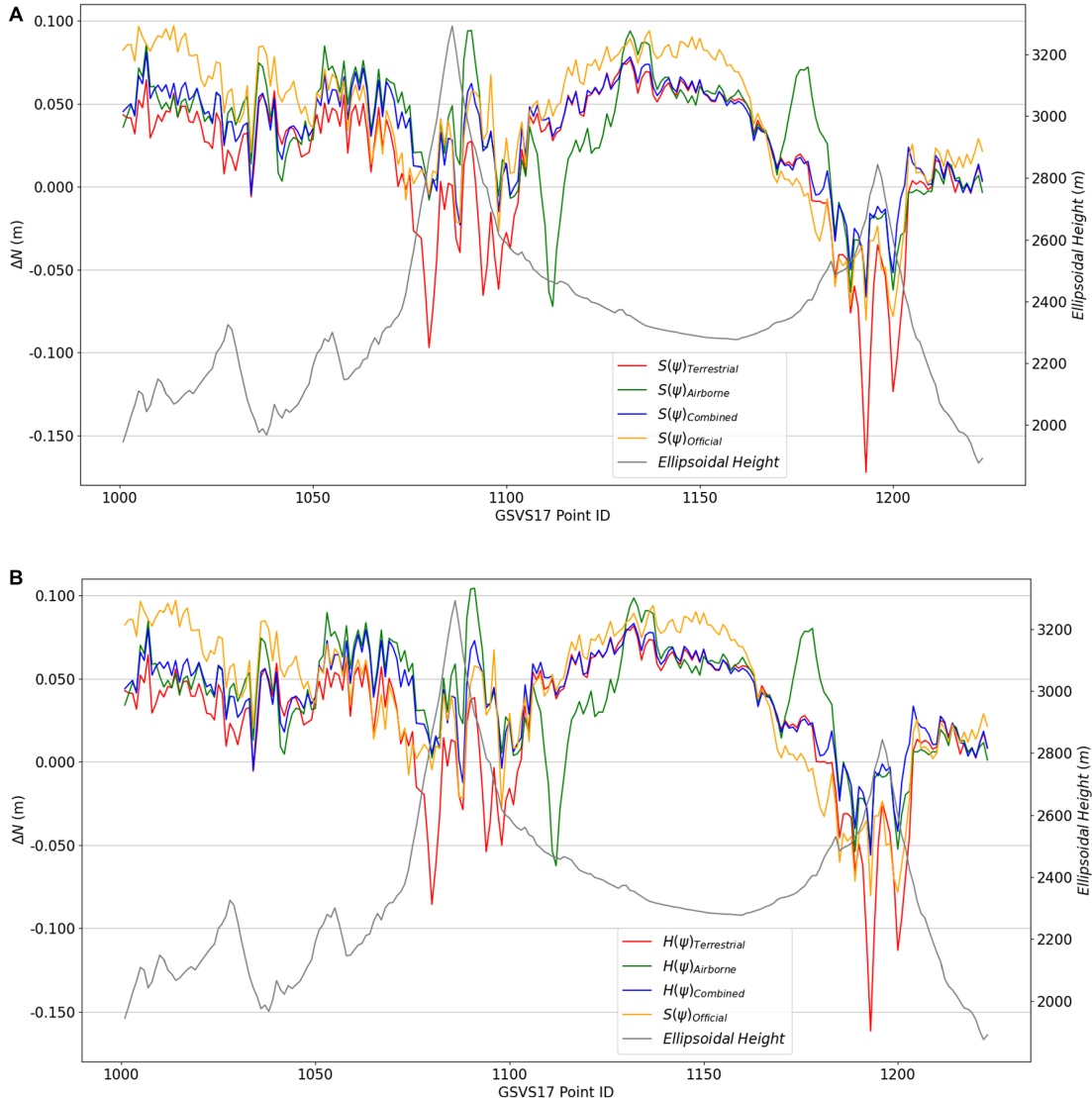


Figure 2.10 : Geoid height differences ($\Delta N = N_{\text{Model}} - N_{\text{GPS/lev}}$) at the GPS/leveling benchmarks of the GSVS17 profile: (a) Stokes integral and (b) Hotine integral.

validation model changed for each geoid solution since the individual models were used to calculate the mean geoid. Table 2.6 shows that the geoid models computed by the Stokes and Hotine integrals presented similar results for the same type of input data. The final accuracy of the models computed with the Hotine integral is slightly better than that computed with the Stokes integral. The highest standard deviations were observed for the geoid models computed with terrestrial-only datasets. The models computed with combined datasets showed better agreement with the mean validation model. The lowest standard deviation of 1.09 cm was achieved with the Hotine integral and the combined dataset. The new combined solutions showed better agreement with

the mean geoid compared to the official solution, which had a standard deviation of 2.08 cm. Figure 2.11 shows the geoid height differences between the presented solutions and the mean validation model at the GSVS17 profile. The large deviations in the terrestrial-only geoid model correspond to locations with high topography, whereas the combined geoid models performed better in these areas, which showed that including the airborne measurements improved the accuracy of the geoid models. It is also worth mentioning that the mean accuracy of all submitted combined models from all institutions was 1.93 cm (Wang et al., 2021).

Table 2.4 : External validation results of the models using historical GPS/leveling data ($\Delta N = N_{\text{Model}} - N_{\text{GPS/lev}}$) [unit: cm].

Method	Data	Min	Max	Mean	Range	STD
Stokes	Official (combined)	-23.46	14.75	1.97	38.21	7.19
	Terrestrial-only (S.T)	-19.38	20.86	4.08	40.24	6.92
	Airborne-only (S.A)	-18.17	19.91	3.52	38.08	6.80
Hotine	Combined (S.C)	-16.73	20.06	3.85	36.79	6.68
	Terrestrial-only (H.T)	-17.98	21.22	4.08	39.20	6.73
	Airborne-only (H.A)	-16.84	20.21	3.76	37.05	6.66
	Combined (H.C)	-15.37	20.39	4.12	35.76	6.53

Table 2.5 : External validation results of the models using the GPS/leveling data at the GSVS17 profile ($\Delta N = N_{\text{Model}} - N_{\text{GPS/lev}}$) [unit: cm].

Method	Data	Min	Max	Mean	Range	STD
Stokes	Official (combined)	-6.80	9.90	3.89	16.70	3.67
	Terrestrial-only (S.T)	-17.24	7.66	1.77	24.90	4.24
	Airborne-only (S.A)	-7.22	9.41	3.25	16.63	3.39
Hotine	Combined (S.C)	-6.65	8.11	3.27	14.76	2.87
	Terrestrial-only (H.T)	-16.16	8.17	2.43	24.33	4.03
	Airborne-only (H.A)	-6.25	10.43	3.83	16.68	3.22
	Combined (H.C)	-5.61	8.32	3.89	13.93	2.69

2.4.4 Area comparison of geoid grids

The $1' \times 1'$ grids of all the combined geoid solutions presented in this paper were compared with the means of the models submitted to the Colorado experiment by other institutions, and the statistics are presented in Table 2.7. The official solution of the ITU-GRG, which is presented in Wang et al. (2021), has the worst standard deviation and presents a range of the geoid height differences that exceeds 60 cm.

The new solutions that are computed by both the Stokes and Hotine functions with the combined dataset in this study show better agreement with the mean geoid grid. The range of the differences is significantly low compared to the official solution. The official geoid solution (Figure 2.12a) shows that the differences from the mean model are highly correlated with the topography while the newly computed models show significantly lower differences in mountainous regions (Figure 2.12b and Figure 2.12c). An improvement in the accuracy of the newly computed models compared to the official solution can be seen in Table 2.7, whereas the mean accuracy of the area differences of all institutions is 3.1 cm.

Table 2.6 : Statistics of the geoid height differences between the ITU-GRG solutions and the mean of all institutions ($\Delta N = N_{\text{Model}} - N_{\text{Mean}}$) at the GSVS17 profile [unit: cm].

Method	Solution	Min	Max	Mean	Range	STD
Stokes (official)	Combined	-4.49	5.22	1.50	9.71	2.08
Stokes	Terrestrial-only (S.T)	-7.83	5.66	2.56	13.49	2.49
	Airborne-only (S.A)	-5.24	9.39	3.95	14.63	2.01
	Combined (S.C)	-0.34	6.35	3.96	6.69	1.13
Hotine	Terrestrial-only (H.T)	-6.83	6.57	3.18	13.40	2.33
	Airborne-only (H.A)	-4.35	10.14	4.49	14.49	1.96
	Combined (H.C)	-0.36	7.23	4.54	7.59	1.09

2.5 Conclusions and discussion

In this study, a geoid model of the Colorado region of the USA was calculated using terrestrial and airborne gravity datasets provided by the NGS. The gravity anomalies computed by the airborne gravity dataset were downward continued to Earth's surface using the planar approximation of the least squares collocation method. To reduce the computational errors in the downward continuation, the remove-restore technique was used. The analytical function, which is a planar logarithmic function, was fitted to the empirical covariance of the residual gravity anomalies created by removing the long-wavelength gravity signal by the GGM and the short-wavelength gravity signal by the RTM to calculate the covariance model parameters. The downward continued residual gravity anomalies were merged with the terrestrial residual gravity anomalies

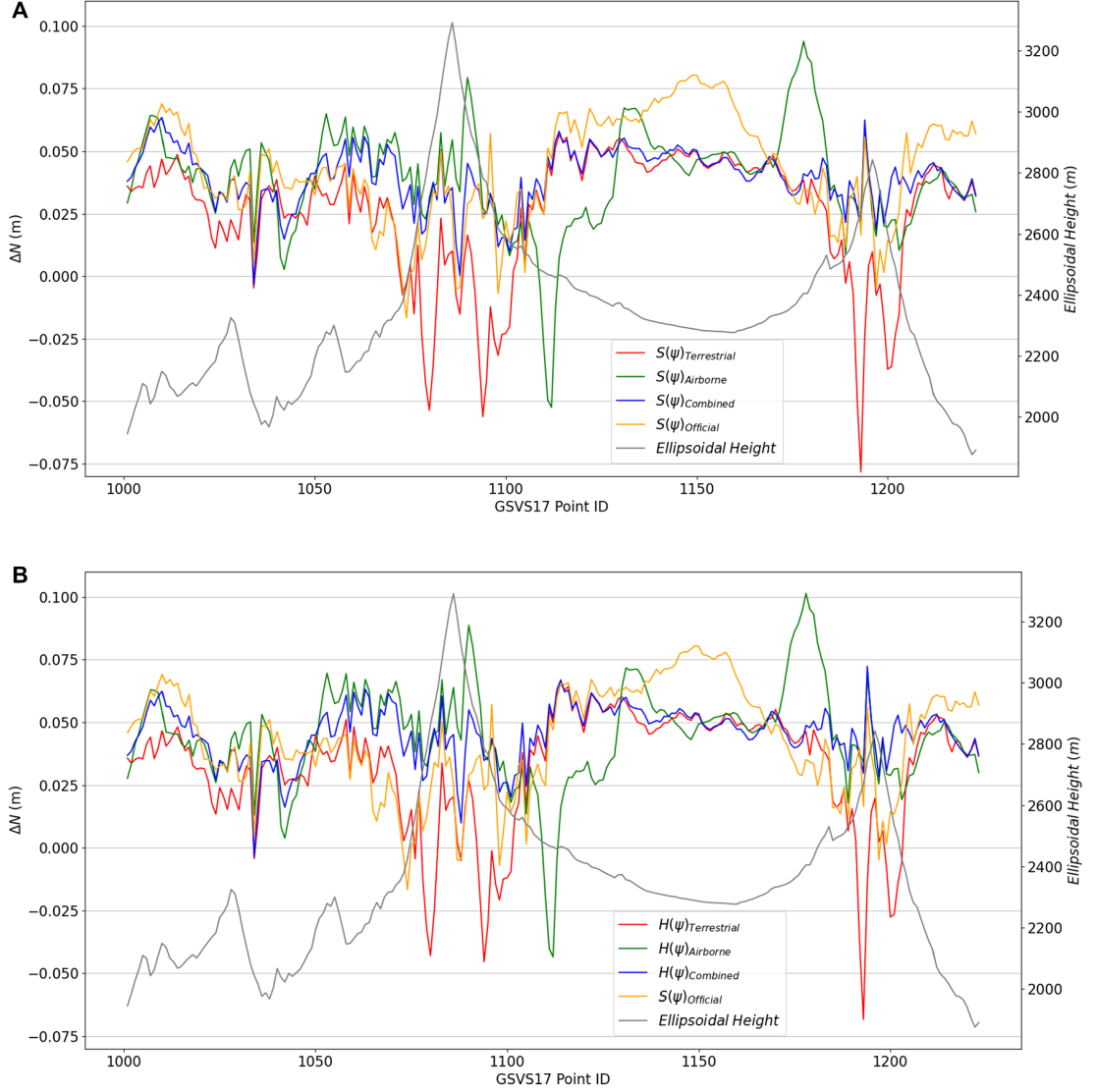


Figure 2.11 : Geoid differences between the presented solutions and mean of all institutions ($\Delta N = N_{\text{Model}} - N_{\text{Mean}}$) at the GSVS17 profile: (a) Stokes integral and (b) Hotine integral.

using the LSC approach, and their accuracies were assumed to be 2 mGal and 1 mGal, respectively. geoid determination together with the terrestrial-only and geoid determination together with the terrestrial-only and airborne-only solutions. The geoid models were calculated and Hotine integral methods.

The accuracies of the models in terms of standard deviations of the geoid height differences were assessed separately using 75 historical GPS/leveling benchmarks distributed in the area and 223 GPS/leveling benchmarks of the GSVS17 profile along the rugged terrain in the southern part of the area. Additionally, the computed

Table 2.7 : Statistics of differences between the individual geoid models and the mean geoid model in a $1' \times 1'$ -grid, [unit: cm].

Method	Data	Min	Max	Mean	Range	STD
Stokes (official)	Combined	-18.51	43.44	0.14	61.95	5.40
Stokes	Combined	-8.48	30.43	2.83	38.91	2.71
Hotine	Combined	-7.67	30.18	3.98	37.85	2.59

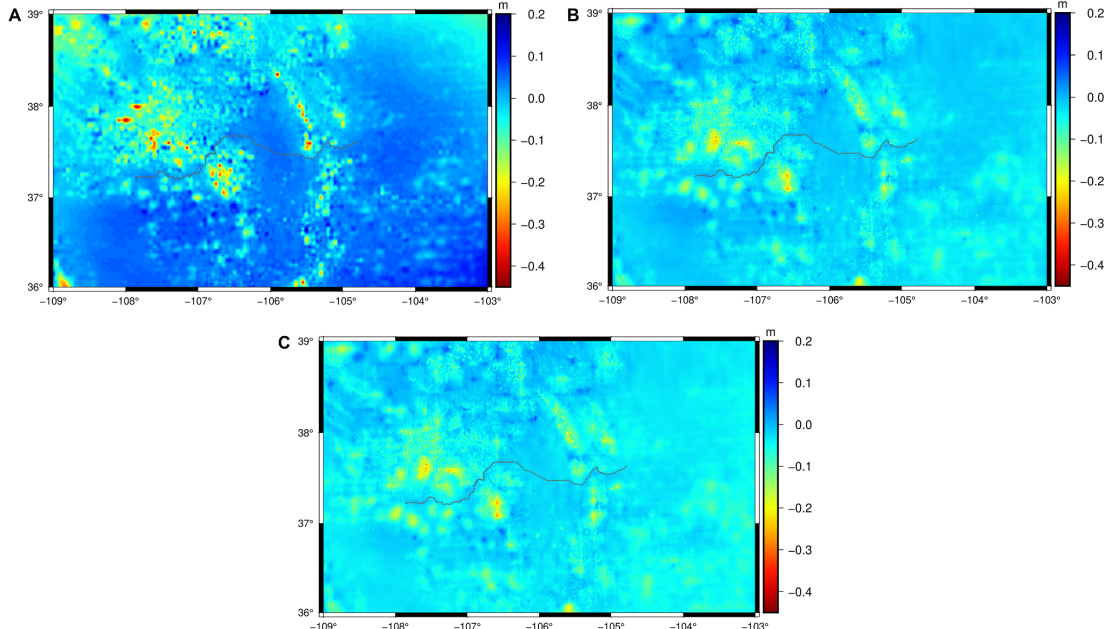


Figure 2.12 : Differences between the computed geoid models and the validation model at a $1' \times 1'$ -grid for the (a) official geoid solution, (b) Stokes combined (S.C) solution, and (c) Hotine combined (H.C) solution.

models were compared with the mean value of the solutions submitted by the fourteen institutions to the Colorado experiment. These comparisons with the mean validation model were carried out at the benchmarks of the GSVS17 profile for all presented geoid models as well as at the $1' \times 1'$ grid nodes of the geoid models that calculated with combined data.

The following findings were derived based on the validation and comparison results:

- In the statistical validation using GPS/leveling data from the GSVS17 profile, the best geoid model accuracy was obtained with the H.C solution and it is 2.69 cm. This accuracy ranks 4th among all models submitted to the Colorado experiment of IAG JWG 2.2.2.

- The validation results using the GPS/leveling data from the GSVS17 profile showed that the contribution of the airborne data improved the geoid solution accuracy by 33% along the entire profile. Considering the validation statistics for the benchmarks in the mountainous parts of the profile (elevations > 2300 m), the improvement rate when including airborne data (terrestrial-only versus combined solutions for both Stokes and Hotine formulas) in the solutions was 40%. However, in the moderate parts of the profile (elevations < 2300 m), the difference between the accuracies of the terrestrial-only and combined models was insignificant.
- Regarding the validation results using GPS/leveling data from the GSVS17 profile, the Stokes combined (S.C) and Hotine combined (H.C) solutions provided a 22% and 27% improvement with respect to the official solution. This improvement was mostly due to a consideration of the harmonic correction term in the residual terrain correction during the downward continuation of the airborne gravity data in the latter solutions. - The comparisons over the benchmarks of the GSVS17 profile revealed that the newly computed models in this study showed better consistency with the mean of the 14 institutions' solutions (the so-called "mean validation model" in the article) than our official solution.
- In these comparison results, the Stokes combined (solution S.C) and Hotine combined (solution H.C) solutions presented a 46% and 48% better fit with the mean validation model than the submitted official model, respectively.
- The validation statistics at the historical GPS/leveling benchmarks also indicated the accuracy improvement of the newly computed models with respect to the official model.
- In the grid comparisons of the newly calculated models with the mean validation models at the 1' resolution grid nodes, both the S.C and H.C solutions showed a 50% improvement compared to the submitted official solution.

In terms of the overall results, the Stokes and Hotine integration methods yielded similar accuracies in the geoid model solutions. For both the Stokes and Hotine integrals, the best geoid model accuracies were achieved when using the combined

dataset. The airborne-only solutions were slightly better than the terrestrial-only solutions. The results also indicated that including airborne gravity data together with terrestrial gravity data significantly improved the accuracy of the geoid models, especially in regions with high topography.

In this article, we provide investigation results for improving the accuracy of the Colorado geoid model using the Stokes and Hotine integral formulas with terrestrial data, airborne data and combined datasets. We also reported on improvements to the new solutions compared to our official solution submitted in Wang et al. (2021). In future studies, we plan to perform further analyses to quantify the remaining error sources in the determination of geoids, including the effect of topographic reductions, geoid-to-quasi-geoid transformations and different approaches for handling airborne data, thereby furthering our contribution to the joint research in IAG JWG 2.2.2.

3. INVESTIGATION OF THE GEOID MODEL ACCURACY IMPROVEMENT IN TURKEY¹

3.1 Introduction

The advancements in the field of global navigation satellite systems (GNSS) and the increase in the number of GNSS constellations and satellites made it possible to accurately determine three-dimensional (3D) point positions on or above the Earth's surface. The height information obtained from the GNSS positioning techniques refers to an analytically defined reference ellipsoid, and these ellipsoidal heights are not practically useful in most engineering and surveying applications because they do not realize the physical reality of the Earth's gravity field. However, the GNSS ellipsoidal heights (h) are transformed to the physically meaningful orthometric heights (H), which correspond to the distances from the geoid surface to the point on topography along the plumb line. The transformation process relies on a simple formulation ($H = h - N$) with the geoid undulation parameter N obtained from a precise geoid model (Hofmann-Wellenhof and Moritz, 2006).

Geoid modeling studies in Turkey were initiated with the determination of the astrogeodetic geoid models in 1976 (Ayan, 1978; Gürkan, 1978). The first gravimetric geoid, Turkey Geoid 1991 (TG-91), was calculated by Ayhan (1993). Precise geoid modeling studies in Turkey were accelerated after the establishment of the Turkish National Fundamental global positioning system (GPS) Network in 1999, with the requirement of a practical transformation model between the GNSS ellipsoidal heights and the orthometric heights in regional vertical datum. Kılıçoğlu (2002) calculated the Turkey Geoid 1999 (TG-99A) hybrid geoid model using the least-squares collocation (LSC) method with fitting at GPS/leveling data benchmarks (Ayhan et al., 2002). With the release of high-degree and order global geopotential models, Turkey Geoid 2003

¹This chapter is based on : Işık, M. S., Erol, S., & Erol, B. (2022). Investigation of the Geoid Model Accuracy Improvement in Turkey. Journal of Surveying Engineering, 148(3). [https://doi.org/10.1061/\(ASCE\)SU.1943-5428.0000397](https://doi.org/10.1061/(ASCE)SU.1943-5428.0000397)

(TG03) was computed using the remove–compute–restore (RCR) method. Kılıçoglu et al. (2005) reported the accuracy of TG03 to be 10 cm. Turkey Geoid 2007 (TG07) was calculated with the fast Fourier transform (FFT) technique using the EGM96 and GGM02S geopotential models. The accuracy of TG07 was reported to be 9 cm (Yıldız et al., 2006). After the release of Earth Gravitational Model 2008 (EGM2008), Turkey Geoid 2009 (TG09) was computed using FFT with an accuracy of 8.4 cm (Kılıçoglu et al., 2011). The accuracy of these geoid models did not improve significantly over the years. The advancements in the field of satellite gravimetry and improved gravimetric geoid modeling techniques, although they can reduce the disadvantages of low-quality terrestrial gravity data, are not enough to model the gravimetric geoid with a required accuracy in the absence of the terrestrial measurements with the required accuracy and spatial resolution. Failure to improve the geoid model accuracies in Turkey further is due to the fact that the terrestrial gravity data in the national database were obtained from different institutions and had heterogeneous accuracies, as well as to the insufficiency of the control data used to validate the accuracy of the calculated geoid models. The terrestrial gravity data used in computations of the released models were measured essentially by three governmental institutions—the General Directorate of Mapping (GDM), the General Directorate of Mineral Research and Exploration (GDMRE), and the Turkish Petroleum Corporation—and detailed information regarding the densities, distribution, and accuracies of these data sets was provided by Erol et al. (2020b). The calculated geoid models were validated at historical GPS/leveling benchmarks, the ellipsoidal coordinates of which were determined with GPS measurements in International Terrestrial Reference Frame (ITRF) datum, and collocated orthometric heights were derived from adjustment of the leveling observations in national vertical datum (NVD). The control GPS/leveling data used to validate the calculated geoid models in this study is also a part of this historical data set. Thus, the validation results of this research are comparable to the released accuracies of the official Turkey geoid models. However, unlike the determination of the official Turkey geoid models, only the available 5' gridded version of gravity measurements conducted by GDMRE (Erol et al., 2020b) and a part of GPS/leveling validation data were used in this research. Considering the data

availability for the research, the purpose of this investigation was to examine the impact of methodologic variations on geoid model determination accuracy rather than to aim for a higher-accuracy geoid model determination for Turkey.

To switch from the classical vertical control network–based vertical datum realization to a geoid model–based vertical datum in a country, the regional geoid model must be determined with $\sim 1 - 2 \text{ cm}$ accuracy. In the current situation, because the Turkey geoid models have not been able to improve to the required accuracy level for the geoid model–based vertical datum realization, a new stage with a project called the Height System Modernization and Redefinition of the Vertical Datum in Turkey was initiated in 2012 by the GDM and Scientific and Technological Research Council of Turkey (TUBITAK). The aim of this collaborative project was to enrich the gravity database with the new terrestrial gravity measurements throughout almost the entire country, and airborne gravity measurements in limited areas such as high mountains, lakes, and coastlines where terrestrial gravimetry is troublesome (Simav, 2020; Simav et al., 2013, 2020). Relying on the preliminary results of this project, the Turkish Geoid Model 2020 (TG-20) was calculated using a combination of historical and new gravity measurements, and it was recently published by Yıldız et al. (2021). The validation results of the new model with the historical GPS/leveling data set showed that the TG-20 and the previously released TG-03 models have similar accuracies of about 9-10 cm. This result emphasized the necessity of quality GPS/leveling data for proper validation of the computed geoid models in Turkey. Yıldız et al. (2021) also provided the validation statistics of the TG-20 model at the newly collected limited number of high-precision GPS/leveling benchmarks which were established and measured along a number of profiles in the country, and reported standard deviations of geoid undulations between 1 and 6 cm. These precise validation data sets are not in public domain; therefore, we were unable to use them to validate the experimental geoid models calculated in this research.

The methodological improvements in the geoid modeling are of great importance, especially when the quality of the terrestrial gravity data is insufficient in an area. The most commonly used technique, remove-compute-restore, has begun to be overtaken by recently developed techniques such as the least-squares modification of the Stokes

integral with additive corrections (LSMSA) technique (Ågren et al., 2009). The methodology developed by the Royal Institute of Technology (KTH) involves the modification of the Stokes kernel in a least-squares sense to minimize the expected global mean square error of geoid estimation by including the errors introduced by the gravity data and the global geopotential model. The technique has been applied successfully in areas with high-quality gravity data sets (Ågren and Sjöberg, 2014; Ellmann et al., 2020; Isik et al., 2021; Sakil et al., 2021; Yıldız et al., 2012). The LSMSA was applied in central Turkey by Abbak et al. (2012a,b), who showed the advantages of the method over the RCR technique. The method was applied by Isik and Erol (2016) to the whole of Turkey, and better agreement was found for the LSMSA technique than for RCR.

This study investigated the effect of the gravity grid densification on the accuracy of geoid model determination with the LSMSA method. The original data set used in the study included 5'-resolution complete Bouguer anomalies, which have been calculated by reducing and gridding the pointwise gravity observations with densities varying between 1.5 and 3.5 km throughout the whole country. Erol et al. (2020b) estimated the accuracy of the complete Bouguer anomalies as $\sim 5 \text{ mGal}$. In the designed experiment, different geoid models were calculated using the free air anomalies calculated from the original 5'-resolution data sets and its 1'-resolution densified versions by restoring the gravitational effect of the topographical masses. In densification of the gravity grids on the reference surface, both planar and spherical complete Bouguer anomalies were considered, and two 1'-resolution dense grids were generated for geoid computations. The classical formulas with digital terrain model data were employed for calculating the Bouguer plate (Heiskanen and Moritz, 1967, Eq. 3-15) and terrain corrections in planar approximation (Forsberg, 1984), whereas the spherical complete Bouguer anomalies were calculated by directly using the complete spherical topographical corrections from the high-resolution SRTM2gravity global model (Hirt et al., 2019). Thus, with densification of the 5'-resolution original grids to 1' resolution, which approximately corresponds to the density of the pointwise observations, the higher frequencies of the gravity field signal were involved in quasi-geoid or geoid model computation using restored free air anomalies with the

LSMSA method. Accordingly, the geoid model solutions using the free air anomalies restored from the 5'-resolution (original data set, i.e., planar complete Bouguer anomalies), 1'-resolution planar, and spherical complete Bouguer anomaly grids were calculated. In addition to area-based (grid-to-grid) comparisons of the calculated geoid models to assess their fit, the external accuracies of the models were estimated using 100 homogeneously distributed GPS/leveling benchmarks in the country. The consistencies of the models along the coastlines also were validated at six tide gauge stations. The numerical test results showed the contribution of the grid densification to the improvement of the geoid model accuracy with the LSMSA method. In addition, the spherical approximation with the topographic corrections from the SRTM2gravity model provided better performance in regridding and densification of the Bouguer anomalies, and hence contributed to the accuracy improvement of the calculated geoid model. In conclusion, the geoid model solution obtained using the free air anomalies restored from 1'-resolution spherical complete Bouguer anomalies gave the most improved accuracy, with 8.6 cm standard deviation of geoid undulation differences at the GPS/leveling benchmarks. Regarding the validation statistics at the benchmarks, the densification of the gravity grids improved the geoid model accuracy by 25%. Employing the spherical Bouguer anomalies instead of the planar in the process improved the geoid model accuracies by 2%. The results of the validations carried out at the tide gauge (TG) stations supported and were consistent with the validation results obtained at the GPS/leveling points.

The study area and the terrestrial gravity data used are described in the section “Study Area and Data Used”. The preprocessing and preparation of the data sets for the computations of the 5' – and two 1'-resolution geoid models also are described in detail in the section “Study Area and Data Used”. Section “Geoid Modeling” briefly explains the formulation of the LSMSA technique. The details of the geoid modeling procedure and the validation results of the calculated geoid models at GPS/leveling and tide gauge stations as well as their area-based (grid-to-grid) comparison results also are provided in the section “Geoid Modeling”. The parameters adopted in modeling the gravimetric geoids and their effects on the accuracy of the models also are given and interpreted.

The paper concludes with a summary of the findings from the study in the section “Conclusion and Discussions”.

3.2 Study Area and the Used Data

3.2.1 Gravity data and preliminary preparation

The study area for the geoid modeling covers the entire country between the latitudes $36^{\circ} N - 42^{\circ} N$ and longitudes $26^{\circ} E - 45^{\circ} E$. The mean elevation in the study area is approximately 1200 m. The topography is rather moderate in the northwest parts of Turkey; however, it is, in general, is quite rugged and mountainous over the country. The elevations in the Eastern part of the country reach over 5000 m. Three sides of the country are surrounded by seas and through the coastlines, there are steep changes in the elevation between the land and sea, especially in the Mediterranean coasts in southern Turkey. The similar character of the topography causes steep changes of heights in the Black Sea region in the northeastern coast of Turkey where is one of the most problematic areas in Turkey by means of geoid modeling studies. As parallel with the topographical changes, the geoid is expected to have a higher frequency pattern in the eastern and southeastern parts of the country. The study area and the topography can be seen in Figure 3.1.

The terrestrial gravity data used in this study has been collected by the GDMRE of Turkey. The dataset originally refers to the Potsdam datum for gravity. It is available as a complete Bouguer anomaly in a gridded form with $5'$ ($\sim 9 \text{ km}$) spatial resolution (see Figure 3.2). In reduction of the gravity data by the GDMRE, the Bouguer plate was estimated with 2.67 g/cm^3 mass density of topography. The terrain correction was applied to the gravity data using Hammer chart up to J zone, which corresponds to 6.65 km radius (Hammer, 1939). Contrary to the assumption in Bouguer plate, the terrain correction was calculated assuming the mass density of topography is 2.40 g/cm^3 . The normal gravity values for the latitude correction were calculated using GRS67 reference ellipsoid parameters (Arslan, 2016).

In preparation of the gravity dataset to use in numerical tests, the gravity values were converted to International Gravity Standardization Net 1971 (IGSN71), which is the

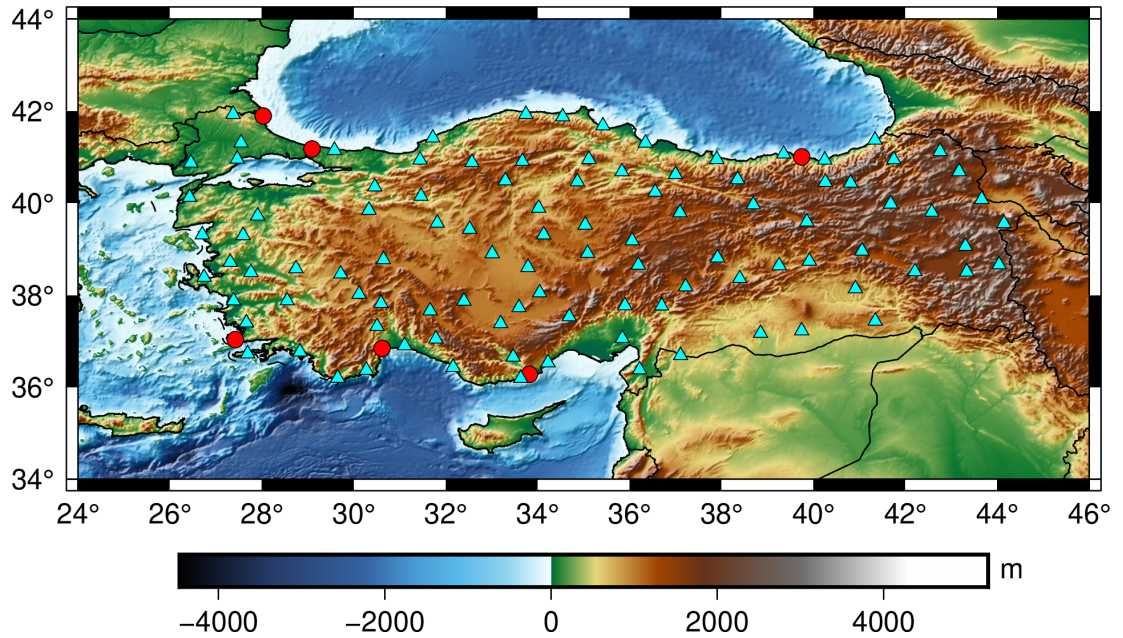


Figure 3.1 : Study area: distribution of GPS/leveling benchmarks (triangles) and tide gauge stations (circles) on the SRTM topography of Turkey. (Data from Jarvis et al., 2008).

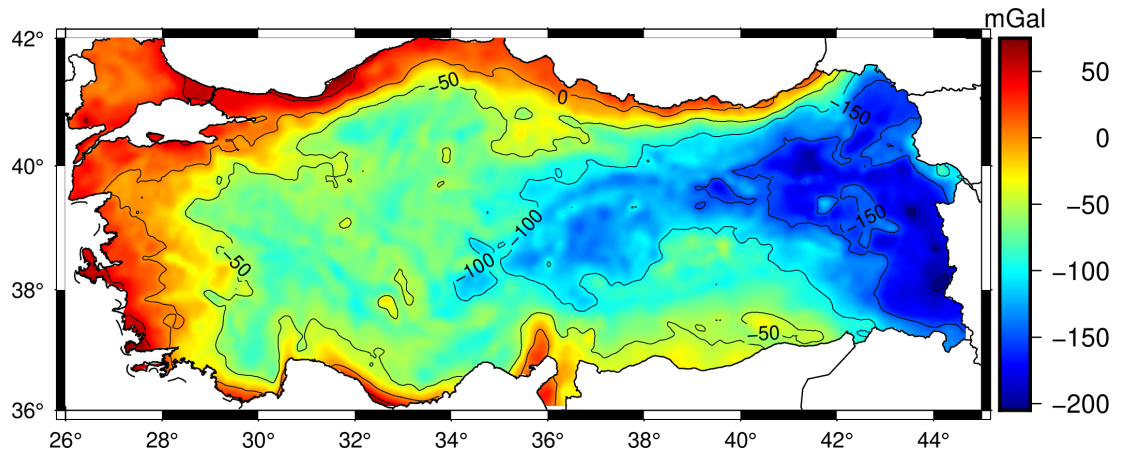


Figure 3.2 : Complete Bouguer anomalies in Turkey (original 5' resolution grid dataset shifted to IGSN71 gravity datum) (minimum = -205.07 mGal, maximum = 74.94 mGal, mean = -69.00 mGal, standard deviation = 55.45 mGal).

adopted gravity datum in Turkey, by subtracting 14 $mGal$ (Wppard, 1980). The normal gravity components (γ) of the given gravity anomalies that they have been calculated with respect to the GRS67 reference ellipsoid were converted to the GRS80 reference ellipsoid by restoring the differences between the normal gravity values of the two reference ellipsoids (GRS80 and GRS67), which were calculated using the given

equation and the physical constants in Featherstone and Dentith (1997) (ibid. p.1065, equation 5 and table 2, respectively).

In Figure 3.3, the data preparation and the geoid model computation procedures of numerical tests are shown step-by-step. In this flowchart, there are three different free-air gravity anomaly (denoted as Δg^{FA}) datasets, and corresponding three geoid models calculated using these datasets. In the preparation of the gravity anomalies, planar and spherical approximations are used to model the effect of topography. To be able to distinguish the datasets prepared using different approximations, the notations of the gravity anomalies have subscripts "P" and "S" for "planar" and "spherical" approximations, respectively. This notation was used in order to express the type of the Bouguer anomalies from which the free-air anomalies were calculated. In the figure, the validation steps of the calculated geoid models were defined as well.

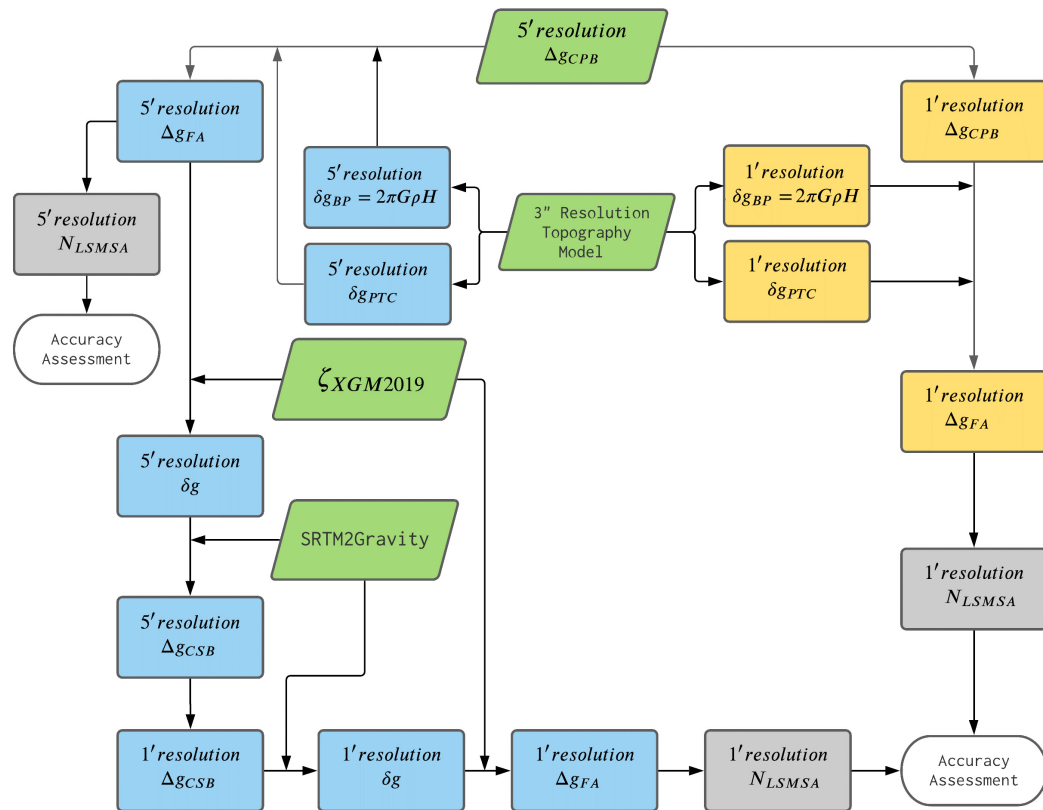


Figure 3.3 : Flowchart of the preparation of gravity anomaly datasets.

In the first section (see the upper-left corner of the flowchart) the complete Bouguer anomaly grid dataset (the original 5' resolution "complete planar-Bouguer anomalies";

Δg_{CPB} given by the map in Figure 3.2) was transformed into the free-air gravity anomalies via considering the Bouguer plate (δg_{BP}) and the terrain corrections (δg_{PTC} , which were calculated with the planar approximation, and using the parameters that have been previously used in their reduction process by GDMRE (6.65 km of the radius of computation, 2.67 g/cm^3 and 2.40 g/cm^3 of the constant mass density values for the computation of Bouguer plate and terrain corrections, respectively) according to Eq. 3.1.

$$\Delta g_{FA} = \Delta g_{CPB} + \delta g_{BP} - \delta g_{PTC} \quad (3.1)$$

In this equation, $\delta g_{BP} = 2\pi G\rho H_P$ is the gravitational attraction of the planar Bouguer plate of constant thickness H_P and constant mass density of topography ρ , and δg_{PTC} is the gravimetric terrain correction with planar approximation. The terrain correction values were calculated using $3''$ resolution SRTM v4.1 digital elevation model (Jarvis et al., 2008) according to Eq. 3.2 as given in Forsberg (1984).

$$\delta g_{PTC} = G \iint_{\sigma} \int_{H_P}^z \frac{\rho(x, y, z)(z - H_P)}{\ell^3 (x_p - x, y_p - y, z - H_p)} dz d\sigma \quad (3.2)$$

where $\rho(x, y, z)$ is the mass density of topography at the running point, ℓ is the distance calculated between the computation point P (x_P, y_P, H_P) and the running point that falls within the computation radius in the elevation model, H_P and z are the topographic heights at the computation point P and the running point, respectively, σ is the integration area. The distance kernel in Eq. 3.2 is given in Eq. 3.3 as,

$$\ell = \sqrt{(x_p - x)^2 + (y_p - y)^2 + (H_p - z)^2} \quad (3.3)$$

The terrain correction values were calculated using the "TC" module of the GRAVSOFT program package (Forsberg and Tscherning, 2008). The calculated terrain corrections (δg_{PTC}) for the country are shown in Figure 3.4. Since the effect of topography was handled in planar approximation for complete Bouguer anomaly in this step, the free-air anomaly in Eq. 3.1 includes the notation "P" for indicating the planar approximation. This $5'$ resolution free-air gravity anomaly was used in the computation of the $5'$ resolution geoid model (N_P^{5min}).

Thereafter, the $5'$ resolution Δg_{CPB} data were densified to the $1'$ resolution grid (upper-right corner of the flowchart in Figure 3.3) to have a denser complete Bouguer

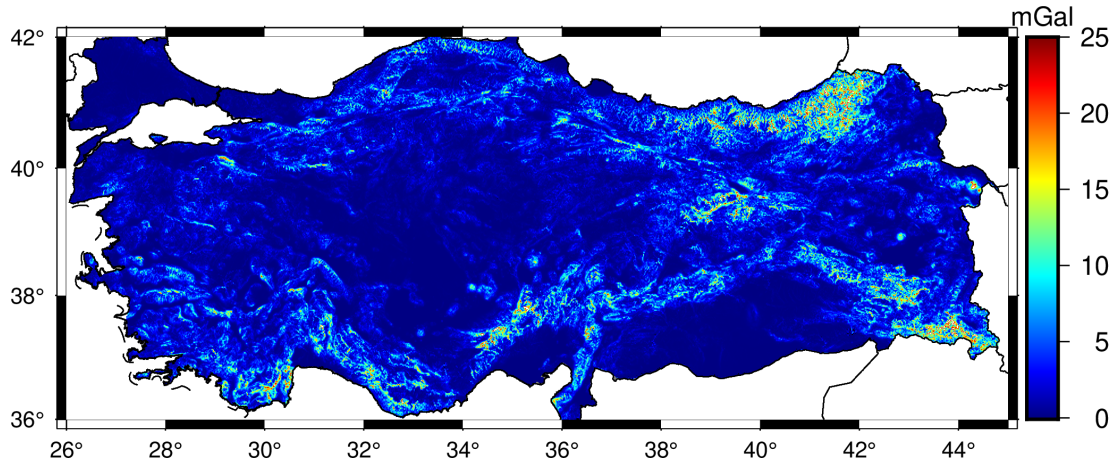


Figure 3.4 : Planar terrain corrections (δg_{PTC}) on gravity (unit: mGal) (minimum = 0.00 mGal, maximum = 168.82 mGal, mean = 2.34 mGal, standard deviation = 3.28 mGal).

anomaly grid with planar approximation. The densified Δg_{CPB} is transformed into $1'$ resolution free air gravity anomalies Δg_{FA} using $1'$ resolution planar Bouguer shell and terrain correction to calculate the $1'$ resolution geoid model (N_P^{1min}).

For the third dataset, the $5'$ resolution free air gravity anomalies were transformed to the $1'$ resolution Δg_{CSB} at first (see the lower-left corner of the flowchart) and then it densified to the $1'$ resolution Δg_{CPB} grids using SRTM2Grav. Thus, the second $1'$ resolution N_S^{1min} geoid model was calculated using the free air gravity anomalies derived from the $1'$ resolution Δg_{CPB} grids as it is shown at the lower-right corner of the schema. Contrary the planar Bouguer anomalies, the complete spherical Bouguer anomalies were converted from the gravity disturbances (δg) using full-scale gravity signal of the $3''$ resolution SRTM2gravity model ($\delta g_{SRTM2Gravity}$) (see Figure 3.5, for the complete spherical terrain corrections from the SRTM2gravity full signal model in Turkey) (Hirt et al., 2019). The full-scale gravity signal of the SRTM2gravity model represents the linear effect of the topography on gravity together with the gravity effect of all irregularities of the topography relative to the Bouguer shell (Hirt et al., 2019). Eq. 3.4 provides the relation between the gravity disturbance (δg) and the free air anomaly (Δg_S^{FA}) depending on the height anomaly (ζ), which has been obtained from a high-resolution global geopotential model.

$$\delta g - \Delta g_S^{FA} = \frac{2T}{R} \approx 0.3086\zeta \quad (3.4)$$

In this equation, T is the disturbing potential and R is the mean radius of spheroid. Using the gravity disturbances obtained from Eq. 3.4, the complete spherical Bouguer anomalies (Δg_{CSB}) were calculated using Eq. 3.5:

$$\Delta g_{CSB} = \delta g - \delta g_{SRTM2Gravity} \quad (3.5)$$

where, $\delta g_{SRTM2Gravity}$ is the complete spherical terrain correction from the SRTM2gravity model (see Figure 3.5).

Thus, 1' resolution gravity grids for both the planar and spherical Bouguer anomalies were generated via data interpolation using least squares collocation method with GEOGRID module of the GRAVSOFT Program Package (Forsberg and Tscherning, 2008). The densified 1' resolution Δg_{CPB} and Δg_{CSB} grid datasets were transformed to the Δg_P^{FA} and Δg_S^{FA} values, respectively, through the inverse use of the above given formulations for planar (Eqs. 3.1 and 3.2) and spherical (Eqs. 3.4, 3.5 and SRTM2gravity full signal model) approximations in order to use in geoid model calculations with LSMSA method.

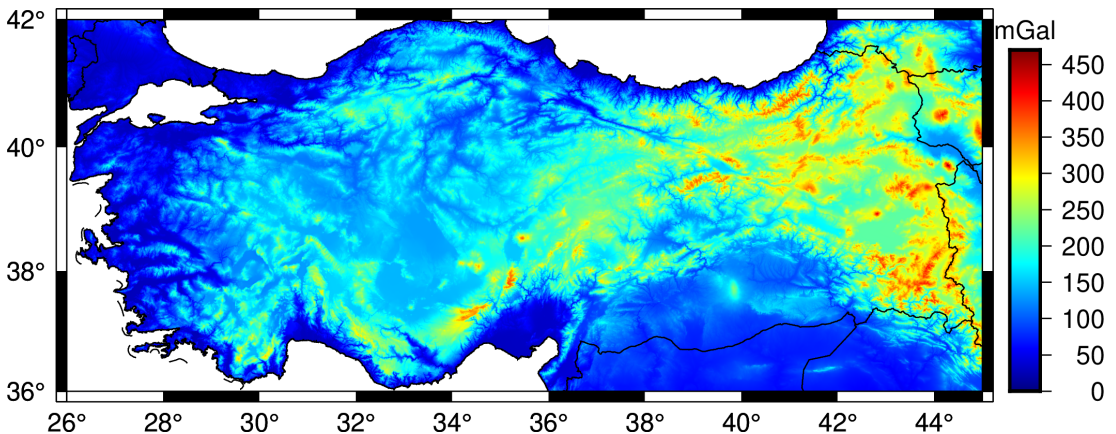


Figure 3.5 : SRTM2gravity full signal model ($\delta g_{SRTM2Gravity}$) (unit: mGal) (minimum = 17.65 mGal, maximum = 448.81 mGal, mean = 155.76 mGal, standard deviation = 72.60 mGal) (Data from Hirt et al., 2019).

The study area for the geoid modelling is the same area covered by the original gravity dataset, as well (as shown in the Fig. 3.2). However, in geoid model computations, to avoid the edge effects at the borders of the study area, we extended the region covered by the original dataset with the gravity anomalies computed from

a high-resolution global geopotential model, which is the eXperimental Gravity field Model (XGM2019e) (Zingerle et al., 2020).

The XGM2019e is a combined global geopotential model whose satellite data is from GOCO06s satellite-only model and terrestrial data is from 15' resolution grid provided by NGS (Zingerle et al., 2020). The gravity anomalies outside the borders of Turkey and the water bodies were filled with the gravity anomalies computed from the XGM2019e model up to 2190 degree/order of expansion; (see Barthelmes, 2009, p.23, Eq. 126) presented the calculation formula of the gravity anomaly using a spherical harmonic expansion model. In addition, the height anomalies (ζ) in Eq. 3.4 to convert the gravity disturbances into free air gravity anomalies in the land part were also calculated from XGM2019e model up to 2190 d/o with zero-degree term included with respect to the GRS80 ellipsoid. The spherical harmonic expansion equation for calculating the height anomaly is given by Barthelmes (2009) (ibid. p.22, Eq. 118). Tide-free system was adopted in all computations and no spectral or spatial smoothing was applied to the derived quantities.

The XGM2019e derived gravity anomalies for the extended land area, which includes gravity signal up to 10 km resolution, were spectrally enhanced using Residual Terrain Model (RTM) values obtained from the residual gravity product of the SRTM2gravity project (Hirt et al., 2019). This enhancement increased the spectral resolution of the gravity anomalies calculated from the model outside of the boundaries up to 90 m. The residual gravity signal (RTM) from SRTM2gravity model for the study area can be seen in Figure 3.6.

Figure 3.7a and Figure 3.7a show the 1' resolution surface gravity anomaly datasets, which were obtained from the planar and spherical Bouguer anomalies, respectively, and used in gravimetric geoid modeling. Table 3.1 lists the statistics for the grid-nodes inside of the country borders where the mean values and the standard deviations of the two datasets slightly vary. The difference map of two 1' resolution free air anomaly grids shows a high correlation with the topography (see Figure 3.7c). These differences are mainly due to the approximations adopted in the planar and spherical approaches in computation.

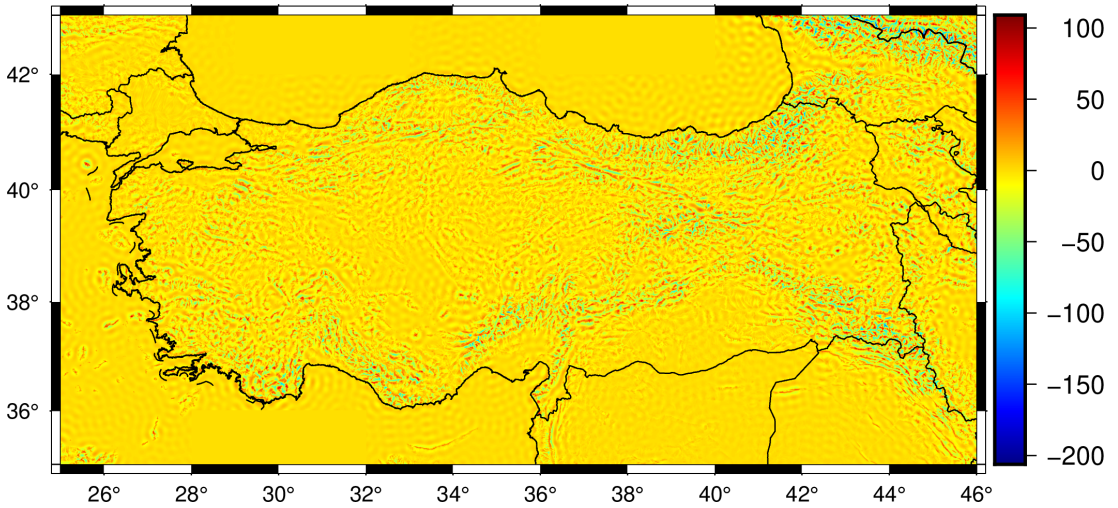


Figure 3.6 : Residual gravity signal from SRTM2gravity model (unit: mGal) (minimum = -206.190 mGal, maximum = 109.010 mGal, mean = -1.847 mGal, standard deviation = 14.675 mGal). (Data from Hirt et al., 2019).

Table 3.1 : Statistics of gravity anomaly datasets (only Turkey land area) [unit: mGal].

Data	Min	Max	Mean	Standard deviation
$\Delta g_P^{FA,5 \text{ min}}$	-79.25	295.63	57.42	43.55
$\Delta g_P^{FA,1 \text{ min}}$	-88.06	344.23	56.58	43.55
$\Delta g_S^{FA,1 \text{ min}}$	-84.99	299.89	56.56	42.96
$\Delta g_P^{FA,1 \text{ min}} - \Delta g_S^{FA,1 \text{ min}}$	-50.73	49.17	0.03	3.02

3.2.2 Validation datasets

The two datasets were employed for the validation of the calculated geoid models in the study. The first one includes homogeneously distributed 100 GPS/leveling benchmarks that belong to the Turkish National Fundamental GPS Network (TUTGA) (see Figure 3.1). The 3D coordinates of these stations are in the International Terrestrial Reference Frame (ITRF96) datum at epoch 2005.0. The orthometric heights of the benchmarks are referenced to the Turkey National Vertical Control Network (TNVCN-TUDKA) datum defined at the Antalya tide-gauge station on the Mediterranean coast of Turkey (Ayhan et al., 2002) and the estimated accuracy of the GPS/leveling data at these benchmarks is $\sim 1 - 3 \text{ cm}$. The orthometric heights of the benchmarks rise from the sea level up to ~ 2000 meters and almost 20% of these points are at the low altitudes between 2 m and 100 m. The dataset was used in this study to

assess the performance of the geoid models in terms of the statistics of the ΔN geoid height differences at the benchmarks ($\Delta N = N_{(GravimetricGeoid)} - N_{(GPS/levelling)}$).

The second validation dataset includes 6 tide-gauge (TG) stations around the coastlines of Turkey (see Figure 3.1), which are part of the Turkish National Sea Level Monitoring Network (TNSLM) (Simav et al., 2011; TUDES, 2021). The location information of the tide gauge stations used in this study for validation of the calculated geoid models at the coastline is given in Table 3.2.

Table 3.2 : Turkish National Sea Level Monitoring Network tide gauge stations.

Station name	Latitude (N)	Longitude (E)	Coastline
Antalya	36°50'09.6"	30°36'46.8"	Mediterranean (south)
Bodrum	37°01'44.4"	27°25'12.0"	Aegean Sea (west)
İğneada	41°53'24.0"	28°01'33.6"	Black Sea (northwest)
İstanbul	41°10'26.4"	29°05'16.8"	Marmara Sea (northwest)
Taşucu	36°16'30.0"	33°49'08.4"	Mediterranean (south)
Trabzon	41°00'03.6"	39°44'42.0"	Black Sea (northeast)

Source: Data from TUDES (2021).

The mean sea level (MSL) at these stations was calculated based on the 15 minutes' interval of the instantaneous sea level measurements. The high frequency instantaneous sea level measurements were down-sampled first to the hourly arithmetic mean values. Then the hourly time series were down-sampled to the daily time series using a low-pass filter, and eventually, the series were down-sampled to the monthly arithmetic mean values. Using least squares spectral analysis, harmonic analysis was applied to find the unknowns in the time series in Eq. 3.6.

$$M(t) = M(t_0) + v(t - t_0) + \left[\sum_{k=1}^2 A_k \cos(\omega_k(t - t_0) - \varphi_k) \right] + \varepsilon(t) \quad (3.6)$$

In this equation, $M(t)$ represents the monthly sea level time series, $M(t_0)$ is the mean sea level (MSL) at epoch t_0 , v is the linear trend of the time series which represents the rate of sea level change with respect to the epoch t_0 . The last term on the right-hand side of the equation represents the annual ($k = 1$) and semi-annual ($k = 2$) signals where A_k is the amplitude, ω_k is the angular frequency and φ is the phase of the annual and semi-annual signals of the time series. The term $\varepsilon(t)$ is the remaining un-modeled components of the time series. Similar to the used GPS/leveling benchmarks in the first

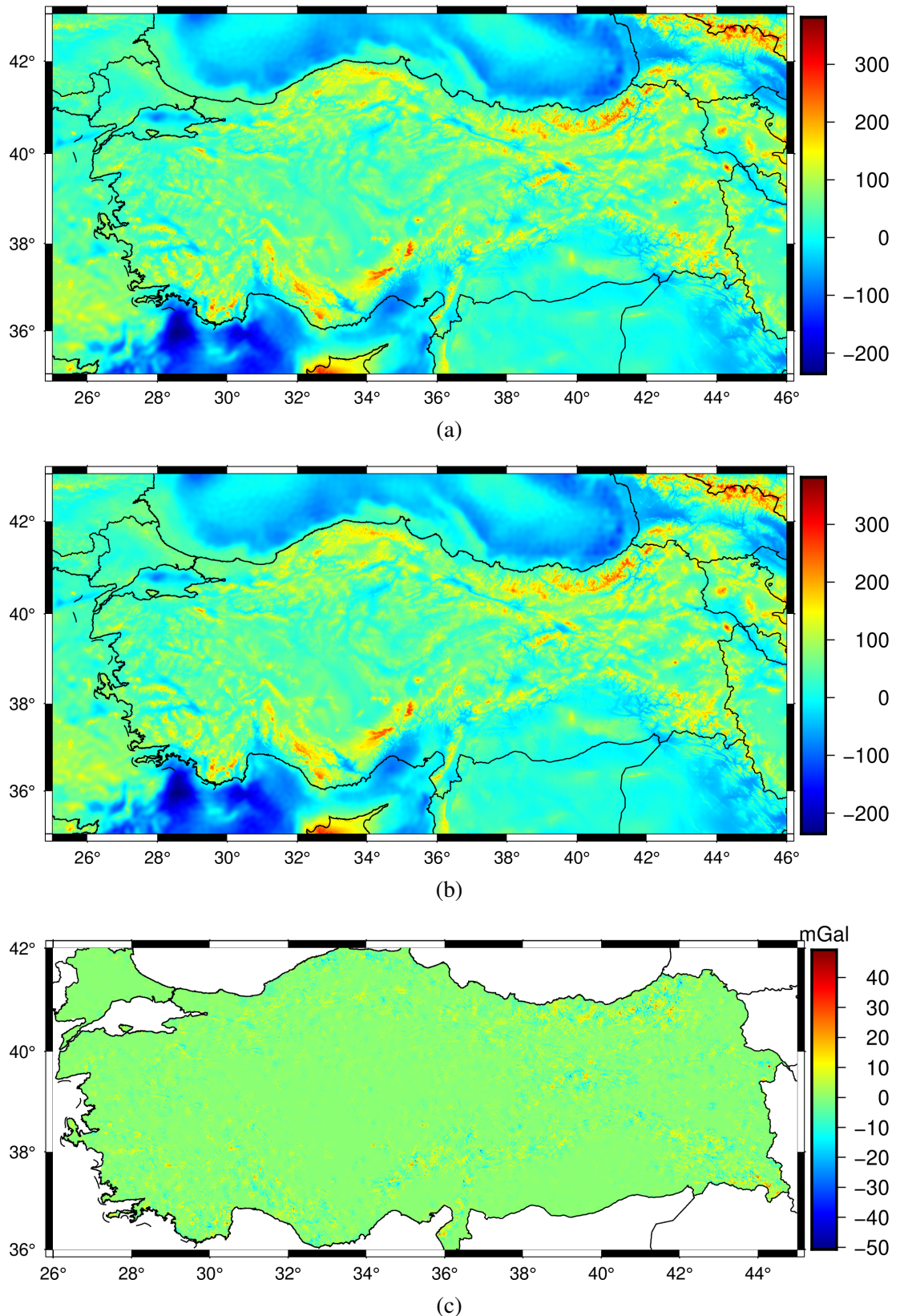


Figure 3.7 : Free-air gravity anomalies using: (a) the planar approximation $\Delta g_P^{(FA,1min)}$, (b) the spherical approximation $\Delta g_S^{(FA,1min)}$, (c) The difference map of gravity anomalies ($\Delta g_P^{(FA,1min)} - \Delta g_S^{(FA,1min)}$).

part of the validations, the calculated mean sea levels also refer to the TUDKA national vertical datum (NVD). The estimated accuracy of the mean sea levels calculated as a result of the spectral time series analysis is $\sim 1 - 2 \text{ cm}$.

For validations of the calculated geoid models at the tide gauge (TG) stations, the geoid undulation at tide gauge stations ($N_{TG}^{(MSS/MSL)}$), obtained by using the altimetry derived mean sea surface (MSS) values close to the coast (altimeter point (A) in Figure 3.8) and the mean sea level values at the tide gauge stations which are referenced to the national vertical datum (NVD - TUDKA), were compared with the geoid undulation at tide gauge stations (N_{TG}^{GG}) derived from the calculated gravimetric geoid models. The formulation of the validations carried out at the tide-gauge stations is given in Eq. 3.7 and the schema which explains this formulation is shown in Figure Figure 3.8.

$$\Delta N = N_{TG}^{GG} - N_{TG}^{MSS/MSL} = N_{TG}^{GG} - (MSS_A^{DTU} - MSL_{TG}^{NVD} + \delta N) \quad (3.7)$$

where the MSS_A^{DTU} is the mean sea surface interpolated for the altimetry point (A) close to the tide gauge station, MSL_{TG}^{NVD} is the mean sea level at the tide gauge station calculated from the spectral analysis of sea level time series (see $M(t_0)$ in Eq. 3.6), and δN is the datum shift between the gravimetric geoid and the national vertical datum at GPS/leveling benchmark (denoted as R in Figure 3.8) of tide gauge stations with an accuracy of $\sim 1 - 3 \text{ cm}$. The MSS values in this study were calculated from the global DTU13MSS model whose accuracy is approximated as $\sim 5 \text{ cm}$ near coastlines in Turkey (Andersen et al., 2016). Considering the law of error propagation, the accuracy of the validation data ($N_{TG}^{MSS/MSL}$) is estimated as $\sim 6 \text{ cm}$.

3.3 Geoid Modelling

3.3.1 Least squares modification of Stokes integral with additive corrections (LSMSA) method

Stokes integral requires gravity data all over the Earth to calculate the geoid height at a particular point. However, in practice, this is not possible due to the limited number of observations and data restrictions. This limits the integration area to a smaller region, which results in a truncation error in the computation. Stokes kernel

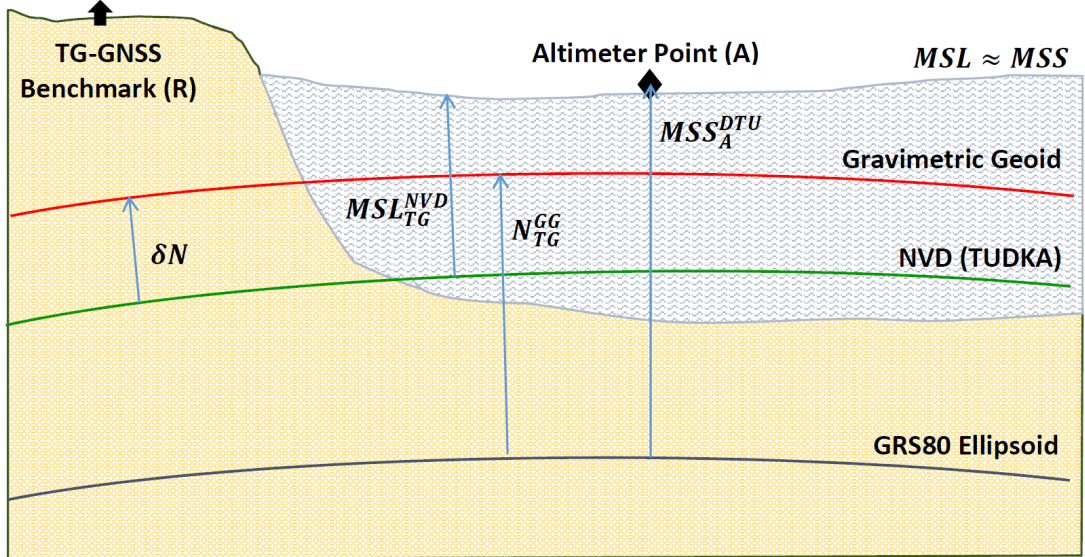


Figure 3.8 : Validation of geoid models at tide gauge stations.

needs to be modified to overcome this problem. There are many methods proposed in the geodetic literature to modify the Stokes kernel, either deterministic or stochastic (Featherstone et al., 1998; Meissl, 1971; Molodenskii et al., 1962; Sjöberg, 1980, 1981, 1984, 1991; Vaniček and Kleusberg, 1987; Vaniček and Sjöberg, 1991; Sjöberg, 2003b; Wong and Gore, 1969). In this paper, we use a geoid determination method, developed at the Royal Institute of Technology in Stockholm (KTH), which involves stochastic modification of Stokes integral that minimize the expected global mean square error by combining of global geopotential model and terrestrial gravity data in a least squares sense (Sjöberg, 2003c). In this technique, the Stokes' integral, truncated to a cap, is applied to the uncorrected surface gravity anomalies (Ågren et al., 2009).

In this method, the approximate geoid height \tilde{N} is composed of the near zone component calculated using gravity observations within the integration cap σ_0 , and the far zone component of the geoid signal calculated using the global geopotential model as follows:

$$\tilde{N} = \frac{R}{4\pi\gamma} \iint_{\sigma_0}^I S^L(\psi) \Delta g d\sigma + \frac{R}{2\gamma} \sum_{n=2}^M (s_n + Q_n^L) \Delta g_n^{GGM} \quad (3.8)$$

In this equation, σ_0 is the spherical cap, $S^L(\psi)$ is the modified Stokes' function of spherical distance ψ between the computation point and the integration points, Δg is the surface gravity anomalies, s_n are the modification parameters, Q_n^L are the truncation

coefficients, Δg_n^{GGM} are the Laplace harmonics of degree n calculated from the global geopotential model, M is the maximum expansion of the global geopotential model and L is the degree of the modification. The symbol s_n are calculated in a least squares sense so that the estimated global mean squares error of the modification would be minimized and the unbiased type of modification parameters are used (Ellmann, 2005a,b).

The modified Stokes' function is given as

$$S^L(\psi) = \sum_{n=2}^{\infty} \frac{2n+1}{n-1} P_n(\cos \psi) - \sum_{n=2}^L \frac{2n+1}{2} P_n(\cos \psi) \quad (3.9)$$

where the first term on the right-hand side of the equation is the closed form of the original Stokes function in spectral form and P_n are the un-normalized Legendre polynomials.

Laplace harmonics of gravity anomaly of degree n can be calculated as (Hofmann-Wellenhof and Moritz, 2006, Eq. 9-18),

$$\Delta g_n^{EGM} = \frac{GM}{a^2} \left(\frac{a}{r} \right)^{n+2} (n-1) \sum_{m=-n}^n C_{nm} Y_{nm} \quad (3.10)$$

where G is Newton's gravitational constant, M is the mass of the reference ellipsoid, a is the equatorial radius of the reference ellipsoid, r is the geocentric radius, C_{nm} are the fully normalized spherical harmonic coefficients from the global geopotential model and Y_{nm} are the fully normalized spherical harmonics (Hofmann-Wellenhof and Moritz, 2006).

The truncation coefficients in Eq. 5.8 are given as,

$$Q_n^L = Q_n - \sum_{k=2}^L \frac{2k+1}{2} s_k e_{nk} \quad (3.11)$$

where Q_n are the Molodensky truncation coefficients and e_{nk} are the Paul's coefficients by Paul (1973).

The estimated geoid model \hat{N} is computed by adding these so-called additive corrections to the approximate geoid height as:

$$\hat{N} = \tilde{N} + \delta N_{TOPO}^{COMB} + \delta N_{DWC}^{COMB} + \delta N_{ATM}^{COMB} + \delta N_{ELL}^{COMB} \quad (3.12)$$

where \tilde{N} is the approximate geoid heights, δN_{TOPO}^{COMB} is the combined topographic correction which involves both direct and indirect effects of the topographic masses (Kiahmehr, 2006), δN_{DWC}^{COMB} is the combined downward continuation correction which accounts for the analytical continuation of gravity anomalies from Earth's surface to the geoid (Sjöberg, 2003c), δN_{ATM}^{COMB} is the combined atmospheric correction which handles the atmospheric mass outside of the surface of the geoid (Kiahmehr, 2006), and δN_{ELL}^{COMB} is the combined ellipsoidal correction applied for the spherical approximation of geoid in the computation of Stokes integral (Sjöberg, 2004b).

3.3.2 Numerical test results

The geoid models were calculated with reference to the GRS80 ellipsoid. In gravimetrically determined geoid models, the zero-degree term represents the geoid height difference between the mean Earth ellipsoid of the global geopotential model and the reference ellipsoid. The zero-degree term geoid height (N_0) was calculated as (Sánchez and Sideris, 2017).

$$N_0 = \frac{(GM_{GGM} - GM_{GRS80})}{r_{P_0} \gamma_{Q_0}} - \frac{W_0 - U_0}{\gamma_{Q_0}} \quad (3.13)$$

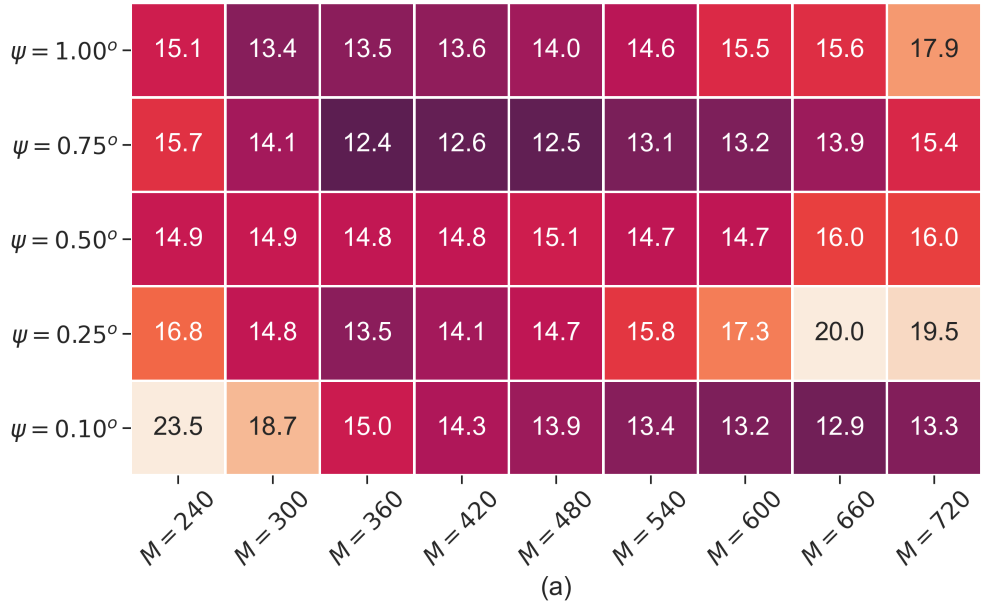
where GM_{GGM} and GM_{GRS80} are the product of gravitational constant (G) and mass of the Earth (M) for global geopotential model and GRS80 reference ellipsoid respectively, r_{P_0} is the geocentric radial distance, γ_{Q_0} is the normal gravity on the reference ellipsoid, W_0 is the conventional value of Earth's potential, and U_0 is the potential on the reference ellipsoid. The zero term (N_0) is computed as 0.936 m for this study. In order to find the optimum values of the modification parameters, we empirically determined the expansion degree of the geopotential model M and integration radius ψ . Since (Erol et al., 2020b) estimated the standard deviation of the dataset as 5 mGal, we constructed the error degree variance of the surface gravity anomalies using the band-limited white noise model where the standard deviation of the gravity anomalies was taken as 5 mGal. The long-wavelength components of the geoid models were computed using the XGM2019e model as it was used in the

pre-processing of the gravity dataset (see Sect. 3.2). The optimal expansion degree and integration radius were decided as a result of a trial and error based process. In the tests, the various values for the expansion degrees of the geopotential model M from 240 d/o to 720 d/o with 60 d/o increments were tested. Similarly, five different integration radii ($\psi = 0.1^\circ$, $\psi = 0.25^\circ$, $\psi = 0.5^\circ$, $\psi = 0.75^\circ$, and $\psi = 1.0^\circ$) were tested in geoid model solutions and trials for deciding the optimal parameters were repeated using each terrestrial gravity dataset in the numerical tests.

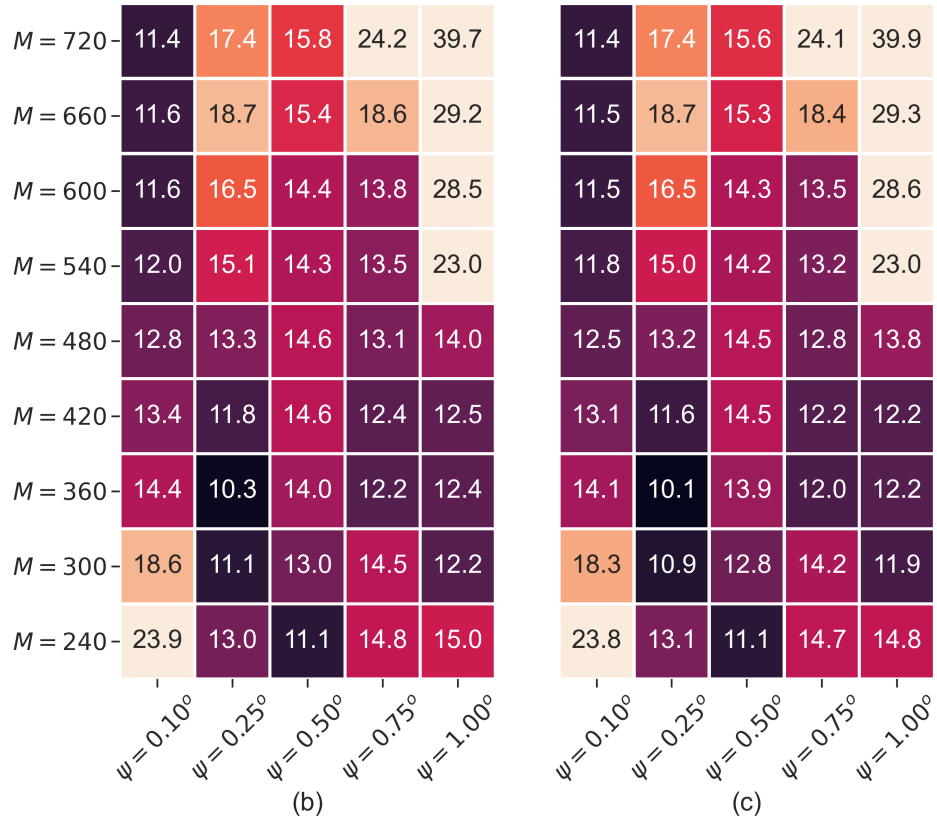
In the first part of the geoid modeling, $5'$ resolution free-air gravity anomalies computed from the complete planar Bouguer anomalies (the original dataset) were used. Figure 3.9a gives the statistics of the experiment results for determining the optimum modification parameters of the $5'$ resolution geoid model solutions. The best standard deviation (12.4 cm) was achieved for the 360 degree/order of the global model expansion degree (as well as the modification degree $L(M = L)$), and for the integration radius of $\psi = 0.75^\circ$. Nevertheless, the model fails to supersede the geoid model computed using XGM2019e global geopotential model.

In the second part of the geoid modeling, the $1'$ resolution free air gravity anomalies computed with densification of both the complete planar Bouguer anomalies and the complete spherical Bouguer anomalies were used. Figure 3.9b and Figure 3.9c show the geoid model accuracies due to the changing modification parameters for planar (Figure 3.9b) and spherical (Figure 3.9c) approximated datasets. The expansion degree of $M = 360$ and the integration radius $\psi = 0.25^\circ$ were found as the optimum parameters for both approaches. Accordingly, the best geoid model accuracies achieved with the $1'$ resolution free air gravity anomalies computed from the planar and spherical Bouguer anomalies are 10.3 cm and 10.1 cm , respectively. Both of the $1'$ resolution geoid solutions show better performance ($\sim 2\text{ cm}$) than XGM2019e model. The validation statistics of three geoid models that agree best with the GPS/leveling data were provided in Table 3.3.

The distribution of the residual geoid heights at the GPS/Leveling benchmarks for the $5'$ resolution geoid model, which will be called as $N_P^{5\text{ min}}$ in the rest of the article, is shown in Figure 3.10a. Similarly, Figure 3.10b and Figure 3.10c show



(a)



(b)

(c)

Figure 3.9 : Standard deviation of the residual geoid heights at GPS/Levelling stations for the varying computation (a) 5' resolution planar approximation (ΔN_P^5 min); (b) 1' resolution planar approximation parameters for: ($\Delta N_P^{1 \text{ min}}$); (c) the 1' resolution spherical approximation ($\Delta N_S^{1 \text{ min}}$) (units: cm).

Table 3.3 : The statistics of the residual geoid heights at GPS/leveling stations (cm).

Geoid	Min	Max	Mean	STD
$N_P^{5\text{min}}$	-25.8	41.0	8.3	12.4
$N_P^{1\text{min}}$	-23.8	30.3	1.2	10.3
$N_S^{1\text{min}}$	-23.9	29.4	1.1	10.1
N_{XGM2019e}	27.8	57.4	4.6	11.7

the distribution of the geoidal height differences of the $1'$ resolution geoid model solutions computed with the terrestrial gravity data prepared with planar (called as the $N_P^{1\text{min}}$ geoid model) and spherical (called as the $N_S^{1\text{min}}$ geoid model) approximations, respectively, from the GPS/leveling observations at the benchmarks. The graphics given in Figure 3.10d, Figure 3.10e, Figure 3.10f depict the distributions of the geoid height residuals with respect to the vertical locations of the GPS/leveling benchmarks in terms of their orthometric heights, for the $N_P^{5\text{min}}$, $N_P^{1\text{min}}$ and $N_S^{1\text{min}}$ geoid model solutions, respectively.

Considering the validation statistics at GPS/leveling benchmarks, the $1'$ resolution geoid models outperform the $5'$ resolution geoid model. When the graphics given in Figure 3.10, Figure 3.10e, Figure 3.10f are compared, the $1'$ resolution geoid models (both the $N_P^{1\text{min}}$ and $N_S^{1\text{min}}$ models) have better performance than the $N_P^{5\text{min}}$ model at the GPS/leveling stations at high altitudes (the benchmarks with topographical heights > 500 m). The GPS/leveling validations of the models showed that the $N_S^{1\text{min}}$ model provided slightly better performance compared to the $N_P^{1\text{min}}$ model. The accuracies of the $N_S^{1\text{min}}$ and the $N_P^{1\text{min}}$ models are 10.1 cm and 10.3 cm, respectively, and the difference between their accuracies is insignificant. Although the adopted gravity data reduction approximation (planar or spherical) for data gridding does not seem to make a significant effect on the geoid model accuracies, the contribution of the gravity grid densification to the geoid model accuracy improvement is considerable. It should also be noted that the validation data is insufficient to assess the effect of topographic reduction approaches on geoid modeling in terms of the benchmark topographic heights. Because it is natural that the topographic reduction effect on geoid models is most noticeable in high topographical regions. When the heights of the GPS/leveling points are considered, 35% of them are located below 500 meters,

and the rest of them reach up to 2000 meters. Thus, the effect of the adopted topographic reduction approach on the geoid model is clearly visible in area based (grid to grid) comparisons of the calculated 1' resolution geoid models, though this is barely recognized in the pointwise validation statistics. Using the gravity datasets densified from 5' to 1' resolutions revealed $\sim 17\%$ and 19% improvements in geoid model accuracy from 12.4 cm for the N_P^{5min} model to 10.3 cm for the N_P^{1min} model and 10.1 cm for the N_S^{1min} model, respectively.

In addition to the statistics given in Table 3.3, the geospatial distributions of the geoid height differences at the GPS/leveling benchmarks for each model solution in Figure 3.10a, Figure 3.10b, and Figure 3.10c are fairly helpful for an inspection of the geoid model performances in an absolute manner throughout the country.

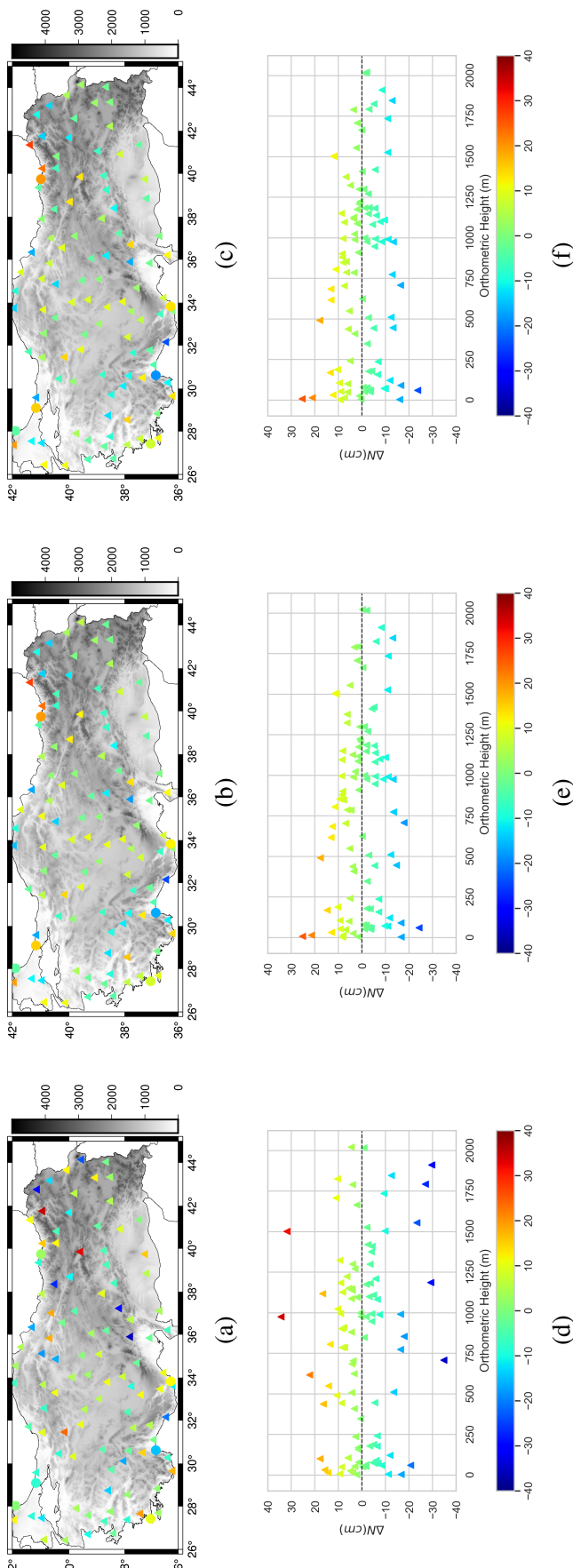


Figure 3.10 : The validation results at the GPS/levelling (triangles) and tide gauge (circles) stations (unit: cm): (a) distribution of the geoid height residuals at stations for the N_P^{5min} model; (b) distribution of the geoid height residuals at stations for the N_P^{1min} model; (c) distribution of the geoid height residuals at stations for the N_S^{1min} model; (d) correlations between the geoid height residuals and the heights of the GPS/levelling benchmarks for the N_P^{5min} model; (e) correlations between the geoid height residuals and the heights of the GPS/levelling benchmarks for the N_S^{5min} model; and (f) correlations between the geoid height residuals and the heights of the GPS/levelling benchmarks for the N_P^{1min} model.

However, to better interpret the obtained validation results, it is useful to have information about the distribution of all 100 GPS/leveling points according to the topographic heights. Accordingly, 15% of the benchmarks are located between 1500 m and 2000 m from the sea level. Between the 1000 m – 1500 m and 500 m – 1000 m, we have 24% and 26% of the benchmarks, respectively, and the 35% of these benchmarks are on topographical areas between the sea level and 500 m. In Figure 3.10d, Figure 3.10e, Figure 3.10f, the relations between the geoid height differences and the vertical position of the validation benchmarks are depicted. Considering the assessment of the 5' resolution N_P^{5min} model in Figure 3.10d, it is seen that there are geoid height differences over ± 20 cm at some of the benchmarks with an altitude higher than 500 m. On the other hand, when the 1' resolution N_P^{1min} and N_S^{1min} models in Figure 3.10e and Figure 3.10f are considered, at these benchmarks with altitudes higher than 500 m, the geoid height differences decrease whereas the discrepancies at the benchmarks along the coastline, specifically in the eastern Black Sea, are even bigger when compared with the 5' resolution N_P^{5min} model. This may indicate a possible degrading in the gravity anomalies along the coastlines while interpolating the grid values from 5 arc-minutes to 1 arc-minute resolution. The absence of marine gravity anomalies in the gridding procedure of original complete Bouguer anomalies in the first place, made by GDMRE, may affect the quality of gridding gravity anomalies along the coastal areas. Additionally, the errors that propagate by combining two datasets, terrestrial gravity data anomaly grid and gravity anomalies from the XGM2019e global gravity field model, may cause these large discrepancies in the GPS/leveling data set near the coastal areas. Considering that the XGM2019e model includes DTU13 gravity field data, we illustrated the interpolation error associated with the development of DTU13MSS model along the coastlines of Turkey in Figure 3.11. It is clear to see the errors located near Black Sea and Marmara Sea coastline are relatively bigger as the heights of the GPS/leveling points increase for the 1' resolution N_P^{1min} and N_S^{1min} models. Accordingly, the geoid height differences at the GPS/leveling benchmarks, which have topographic heights between 1000–2000 meters, remain $\sim \pm 10$ cm interval.

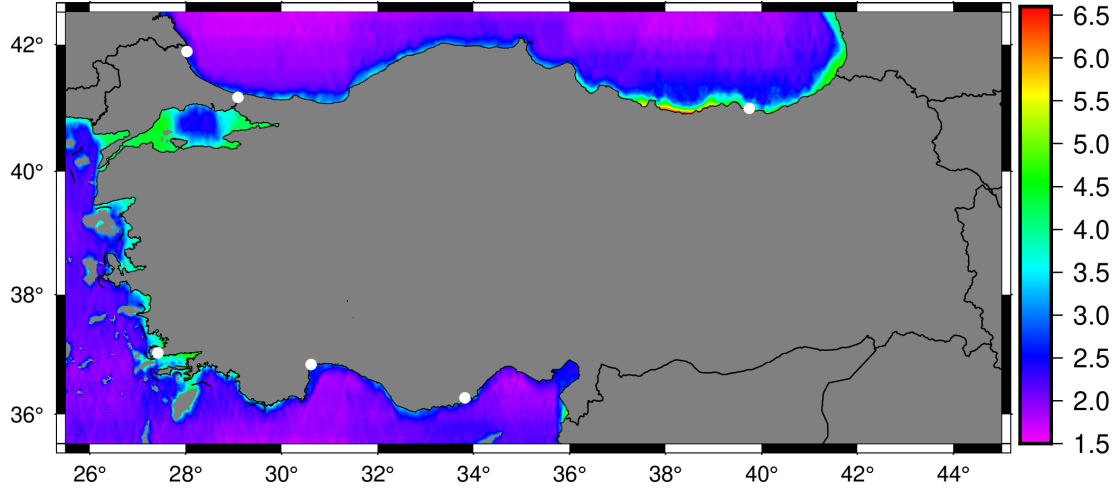


Figure 3.11 : The interpolation error associated with the DTU13MSS model along the coastlines of Turkey (unit: cm). The tide gauge stations are shown with white circles.

Because the GPS/leveling validation dataset does not include stations in the regions with an altitude higher than 2000 m, these validation results do not provide information regarding the absolute accuracies of the calculated models for the topographies higher than 2000 m. However, the area based (grid to grid) comparison of the geoid model solutions in equal resolutions (the N_S^{1min} and the N_P^{1min} models) provides an additional measure in terms of their relative performances throughout the country. Figure 3.12a shows the difference map between the two 1' resolution geoid model solutions (the N_S^{1min} and N_P^{1min} models). Similar to the free air anomaly difference map of the planar and spherical approaches given in Figure 3.7c, the surface pattern of the geoid heights difference map of two geoid model solutions in Figure 3.12a has a correlation with the topography. The graphic given in Figure 3.12b depicts the correlation of the discrepancies between the N_S^{1min} and N_P^{1min} models with the topographical heights. Considering these two figures, it is seen that the differences between the N_S^{1min} and N_P^{1min} models stay within ± 10 cm up to 1500 m, within ± 20 cm up to 3000 m. However, the differences sharply increase after 3000 m and reach up to ~ 60 cm in the regions with heights between 4000 m and 5000 m. Both models agree fairly well in lower elevations since Figure 3.7c and Figure 3.12a show no big differences. As it is seen in Figure 3.12b, the differences between the two solutions obtained by spherical and planar approaches are correlated with point heights. Thus, the effect of spherical and planar approaches on geoid model determination has been clarified. Considering

the elevation of GPS/leveling benchmarks, it is not possible to validate the performance of two models beyond 2000 meters. Contrary to the GPS/leveling validations, the area-based comparisons of the models make visible the differences between the two approaches.

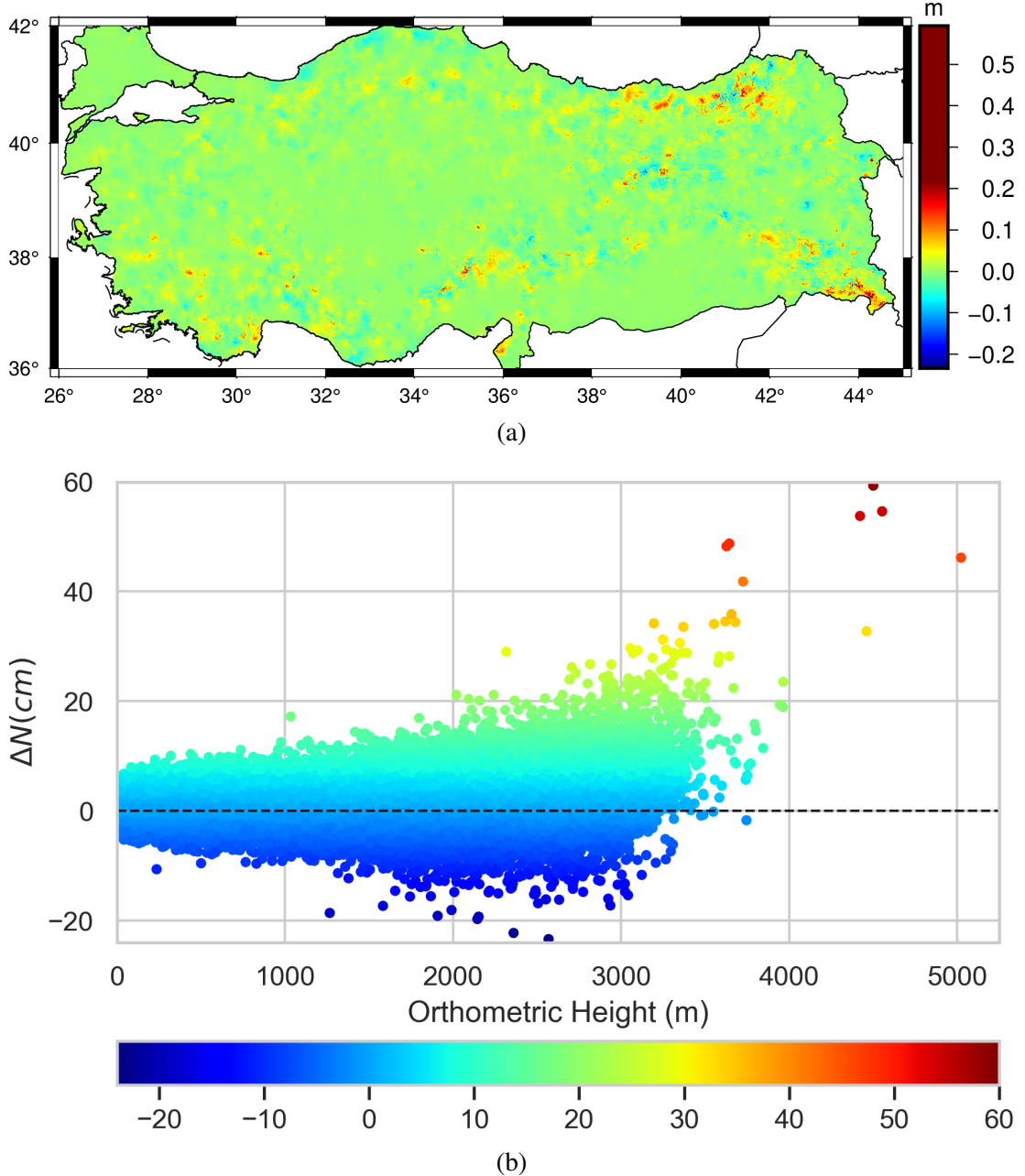


Figure 3.12 : (a) Differences between the two 1' resolution geoid models, $N_P^{1 \text{ min}} - N_S^{1 \text{ min}}$ (minimum = -0.234 m, maximum = 0.593 m, mean = 0.003 m, standard deviation = 0.018 m); and (b) distribution of these differences with respect to their orthometric heights (unit: centimeters).

In addition to the GPS/leveling benchmarks, the tide gauge stations also were used in the validations of the calculated geoid models following the described strategy in the section "Validation Data Sets". For this purpose, the observations of six tide-gauge stations (listed in Table 3.2 with their coordinates) located at the surrounding seas of Turkey were employed. The validations at the tide-gauge stations provided an additional check for the geoid model consistencies at the coastlines where the geoid models generally have reduced accuracies due to data gaps in sea-land transitions and sudden changes in topography. Since Turkey is surrounded by the seas on three sides, the coastal areas require special attention and to be concentrated in modeling Turkey geoid. Accordingly, in the validation results, the geoid height differences at the tide gauge stations were also provided in Figure 3.10(a-c) with the circle symbols colored according to the magnitude of geoid height differences. Also here, the list of the geoid height differences at the tide gauge stations for the calculated geoid model solutions and the XGM2019e model is given in Table 3.4. Considering the values given in the table, it can be said that the changes of the geoid height differences at the stations are reasonable, and there is no abrupt change in the values. The geoid models agreed reasonably at the tide gauge stations, and this result is supported by the validation results at the GPS/leveling stations along the coastline.

Table 3.4 : The validation results of the models at the tide gauge (TG) stations.

Station	Tide Gauge	Geoid Model Solutions			
		$N_P^{5\text{min}}$	$N_P^{1\text{ min}}$	$N_S^{1\text{min}}$	N_{XGM2019e}
Antalya	Mediterranean (south)	-16.3	-11.4	-13.3	-22.9
Bodrum	Aegean Sea (west)	6.1	4.4	3.9	9.6
İğneada	Black Sea (north-west)	-4.8	-8.2	-8.3	-8.0
Istanbul	Marmara Sea (north-west)	-17.3	2.9	2.7	-5.0
Tasucu	Mediterranean (south)	0.3	1.1	2.6	6.3
Trabzon	Black Sea (north-east)	12.3	27.8	28.1	21.9

A more detailed inspection of the ΔN values given in Table 3.4 showed that the geoid height differences at Antalya and Trabzon tide gauges exceed ± 10 cm for all geoid solutions. This result is primarily due to the rapid variations of the DTU13MSS model values from deep seas to shallow-water areas. Additionally, employing the values from different DTUMSS models revealed significant differences in the sea area close to the

Trabzon tide gauge station. Besides, the 1' resolution geoid models mostly provided consistent results at all stations. However, specifically at Trabzon tide gauge, the 1' resolution geoid models (the $N_S^{1\text{min}}$ and $N_P^{1\text{min}}$ models) provided worse performance than the 5' resolution geoid model (the $N_P^{5\text{ min}}$ model). This result is also consistent with the GPS/leveling validation results obtained at the benchmarks in the coastline area of the eastern Black Sea around the Trabzon tide gauge [Figure 3.10(a-c)]. In conclusion, the poorer performances of the 1' resolution models in comparison to the 5' resolution model in the region in issue can be attributed to the steep change of topography in the land to sea transition and relatively low accuracy of the gravity field data at sea. Because, whereas the 1' resolution high-frequency geoid models revealed the ascribed negativities in the geoid signal, the 5' resolution low-frequency model tolerated and did not reveal these effects in results caused by the topographic structure and measurement data around the Trabzon area. On the other hand, regarding the GPS/leveling validations, the systematic differences because of the datum shift between the geoid surface and the regional height reference surfaces in the validation statistics are unavoidable (Fotopoulos, 2013). In order to minimize these systematic effects in the validation results and to have comparable surfaces, the gravimetric geoid models are fitted to the GPS/leveling surface at the benchmarks and the validation statistics are once calculated after fitting with a mathematical surface equation. In this study, the systematic differences between the calculated geoid model surfaces and the local vertical datum (TUDKA) were modeled at the GPS/leveling benchmarks using a seven-parameter transformation equation (Fotopoulos, 2013, Table 11.3), and the accuracy of the calculated geoid models was also derived after fitting (see Table 3.5). Accordingly, in the test results, the 1' resolution $N_S^{1\text{min}}$ geoid model has shown the best performance. The accuracy of this model was calculated as 8.6 cm as a result of the validations at GPS/leveling benchmarks.

As a result of all the work, Figure 3.13f is the map of the $N_S^{1\text{min}}$ geoid model of Turkey without fitting, and its components calculated using the LSMSA algorithm are presented in Figs.13(a–e), and Table 3.6 gives the statistics of the calculated components and additive corrections of the $N_S^{1\text{min}}$ geoid model.

Table 3.5 : The statistics of the residual geoid heights at GPS/leveling stations after seven-parameter surface fitting (cm).

Geoid	Min	Max	Mean	STD
$N_P^{5\min}$	-34.5	34.3	0.0	11.5
$N_P^{1\min}$	-24.3	25.2	0.0	8.8
$N_S^{1\min}$	-23.8	25.3	0.0	8.6
$N_{XGM2019e}$	-21.9	36.1	0.0	10.0

Table 3.6 : The statistics of the $N_S^{1\min}$ geoid model components and additive corrections in LSMSA algorithm.

Component	Unit	Min	Max	Mean	STD
approximate geoid heights (\tilde{N})	m	10.511	41.780	31.236	6.445
combined topo. correction (δN_{TOPB}^{COM})	m	-2.721	0.000	-0.191	0.200
combined dwc. correction (δN_{FWMB}^{COM})	m	-1.817	2.950	0.032	0.088
comb. atmospheric corr. (δN_{ATM}^{COMB})	mm	-7.3	0.4	-1.7	1.0
comb. ellipsoidal corr. (δN_{ELI}^{COMB})	mm	-1.2	1.1	-0.3	0.2
final geoid model (\hat{N})	m	8.808	41.768	30.794	6.784

3.4 Conclusion and Discussions

In this study, we computed the gravimetric geoid models in Turkey with three different datasets using the least squares modification of Stokes integral (LSMSA) technique to understand the effect of grid densification on the geoid model accuracy and usability of the SRTM2gravity products in regional geoid modeling. In the first part of the study, using complete Bouguer anomalies, which were available in 5' resolution grid format, we modeled the free-air anomalies at the surface by restoring back the terrain corrections calculated following the planar approximation with the same parameters used to pre-generation of the Bouguer anomaly dataset. The geoid model computed with the original 5' resolution dataset has the accuracy of 11.5 cm as a result of validations at the 100 GPS/leveling benchmarks and 6 TG stations distributed as homogeneous as possible throughout Turkey. The second part of the study was carried out using densified gravity anomaly grids from the 5' to the 1' resolution with preserving or enhancing the spectral content of the gravity signal. As the success of this task depends highly on the forward modeling of the topographic masses,

the computation of gravimetric terrain correction played an important role in this experimentation. In this context, we used two terrain correction schemes: the planar and spherical approximations. Besides using classical formulas in generating the Bouguer anomalies according to the planar approximation for gravity grid densification purpose, we also used the terrain corrections from SRTM2gravity global model that is computed with the spherical approximation of Earth's topographic mass using 3'' SRTM topographic model.

Based on the findings of this study, we can conclude that the densification of the terrestrial gravity grids from the 5' (~ 9 km) to 1' (~ 2 km) resolution with restoring the high frequency content of the signal made a significant contribution to the geoid modeling accuracy. The geoid model computed with the 5' resolution free-air anomalies has 11.5 cm accuracy. This model failed to exceed the accuracy of the geoid model calculated from the XGM2019e global geopotential model using its maximum degree of expansion, which is found as 10 cm after the seven-parameter fitting. However, the geoid models calculated using densified 1' resolution gravity grids provided better accuracies. The 1' resolution geoid models (the N_S^{1min} and N_P^{1min} models) computed with the terrestrial gravity data, which were reduced and densified relying on the spherical and planar approximation schemes, respectively, provided almost similar accuracies. It should be noted that the residual geoid heights at the GPS/leveling benchmarks near coastal areas, especially for the Black Sea region, are relatively bigger for the 1' resolution geoid models. The same result is observed in the validation against the tide gauge stations. This problem may indicate a possible interpolation error in the original gridded complete Bouguer anomalies of land since there are no gravity measurements in the water bodies. The densification of the 5' gravity anomaly grid can magnify the effect of interpolation error in the original dataset. Another source of error in this problem is the inconsistency of sea and land gravity data obtained from different sources in different accuracies (the land-sea transition problem). The marine gravity anomalies are filled using the XGM2019e model which includes DTU13 global gravity field data. On the other hand, the validations at tide gauge stations include the use of DTU13 mean sea surface data. There is an apparent increase in the errors of DTU13 models along the coastlines with

maximum degrading near the Black Sea region. On the other hand, the densification of the gravity anomalies provided a better topographical signal in the mountainous parts which resulted in smaller residual geoid heights at GPS/leveling stations located in higher elevations. With 8.6 cm accuracy, the N_S^{1min} model provided the best performance. From this result, it is concluded that either spherical or planar approach can be used for obtaining the Bouguer anomalies to be used in the gravity data gridding, and the SRTM2gravity global model (full-signal product) performed very well in obtaining the Bouguer anomalies with the spherical approach. Thus, the computational burden and given efforts in obtaining the terrestrial corrections as with the classical formulas, in the calculation of the complete Bouguer anomalies from gravity observations is reduced. Although the usability of the SRTM2Gravity model has been clarified in the drawn conclusions of this study, further tests are required with better quality gravity datasets in order to see the potential contribution of this global product for determination higher (approximately $\sim 1 - 2 \text{ cm}$) accuracy geoid models.

Overall, a $\sim 25\%$ improvement in geoid model accuracy was obtained through using the densified version of the 5' resolution original gravity grid dataset. Although the accuracies of the N_S^{1min} and N_P^{1min} geoid models are similar as a result of GPS/leveling validations, area-based (grid to grid) comparison of two models showed significant differences at high mountains over 3000 m height. These differences could not be detected in validations because the control dataset does not include benchmarks at altitudes higher than 2000 m. Therefore, the adopted approximation in the computation of the Bouguer anomalies for gridding indirectly affects the geoid model accuracies at the places with rough topographical patterns. In order to criticize these discrepancies, we need a high accurate control data set at high altitudes.

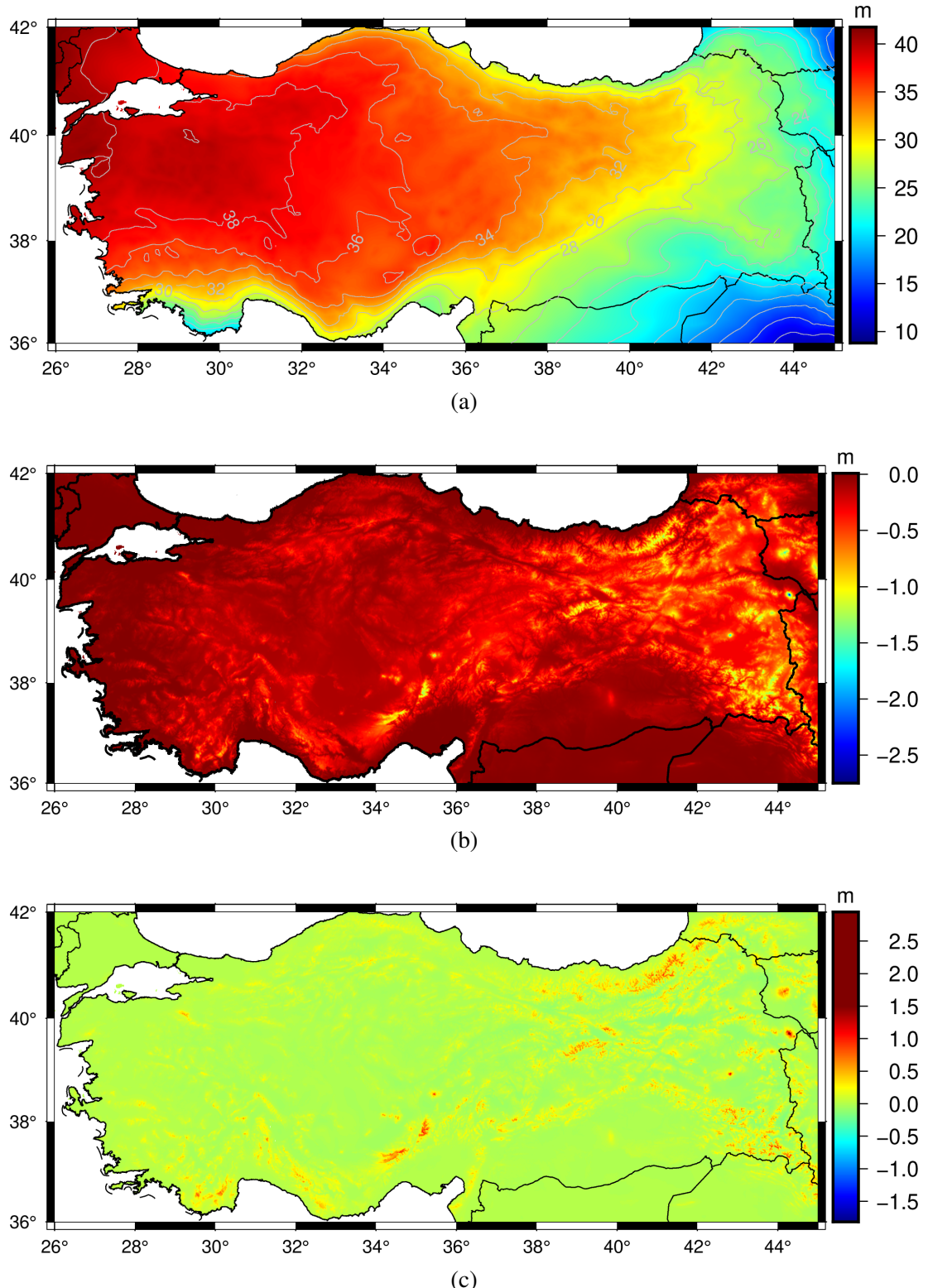


Figure 3.13 : $N_S^{1\min}$ geoid model: (a) approximate geoid heights (\tilde{N}); (b) combined topographic correction (δN_{TOMB}^{COM}); (c) combined downward continuation correction (δN_{DWC}^{COMB}); (d) combined atmospheric correction (δN_{ATM}^{COMB})); (e) combined ellipsoidal correction (δN_{ELL}^{COMB}); and (f) final geoid model (\hat{N}).

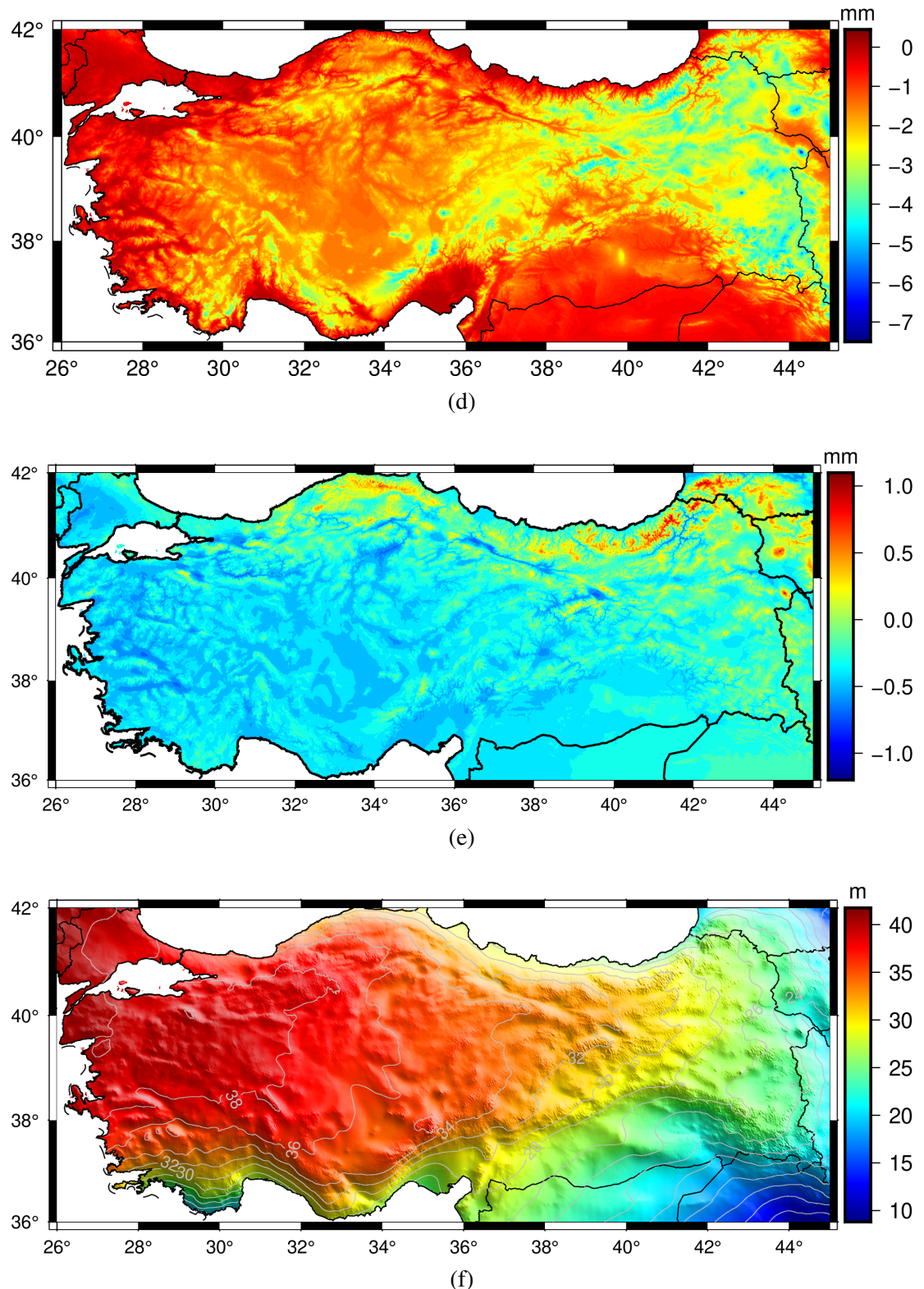


Figure 3.13 : Components of the $N_S^{1\min}$ geoid model: (a) approximate geoid heights (\tilde{N}); (b) combined topographic correction (δN_{TOMB}^{COMB}); (c) combined downward continuation correction (δN_{DWC}^{COMB}); (d) combined atmospheric (e) combined ellipsoidal correction (δN_{ELL}^{COMB}); (f) final geoid model (\hat{N}). correction (δN_{ATM}^{COMB})).
(cont.)

4. GEOID MODELING WITH LEAST SQUARES MODIFICATION OF HOTINE'S INTEGRAL USING GRAVITY DISTURBANCES IN TURKEY¹

4.1 Introduction

The geodetic boundary value problem solutions require gravity field observations, and the dominance in the utilization of Stokes's equation in gravimetric geoid modeling leads to the use of gravity anomalies. The fact that the height information of most of the archived gravity measurements comes from the traditional leveling techniques leads to the computation of gravity anomalies. In geoid modeling applications, the GNSS technique and the gravity measurements provide an opportunity to compute the gravity disturbances directly. Hotine's integral enables calculating the gravimetric geoid model using gravity disturbances instead of gravity anomalies (Hotine, 1969). Hotine's integral employs gravity disturbances calculated with the ellipsoidal height information of gravity measurement, which is much easier to acquire than the leveling based orthometric heights nowadays. However, Hotine's integral, as also in the case of Stokes's integral, needs to be modified to reduce the truncation error, which stems from the lack of gravity data in global coverage. The modification of Stokes's integral, first purposed by Molodenskii et al. (1962), has been studied in-depth in terms of both deterministic and stochastic approaches (Wong and Gore, 1969; Sjöberg, 1980, 1981, 1984, 1991, 2003b; Vaniček and Kleusberg, 1987; Vaniček and Sjöberg, 1991; Featherstone et al., 1998; Evans and Featherstone, 2000). However, compared with Stokes, the modification of Hotine's integral has been overshadowed in literature. Despite that it is more common to see the modification of Stokes's integral, there are several studies on the modification of Hotine's integral in the literature (Jekeli, 1979, 1980; Sjöberg, 1987; Zelin and Yecai, 1991; Sjöberg and Nord, 1992; Vanicek et al., 1992; Zhang, 1998; Novák and Heck, 2002; Novák et al., 2003; Sjöberg and

¹This chapter is based on : Isik, M. S., Erol, B., Çevikalp, M. R., & Erol, S. (2022). Geoid modeling with least squares modification of Hotine's integral using gravity disturbances in Turkey. Earth Science Informatics. <https://doi.org/10.1007/s12145-022-00843-2>

Eshagh, 2009; Featherstone, 2013). In these studies, besides explanations of the theoretical aspects regarding the modification and the use of Hotine's kernel, the satellite altimetry (at sea/ocean) and airborne gravimetry applications draw special attention since the computation of the gravity disturbances from these observations becomes more practical with the availability of the ellipsoidal height information from the GNSS technique (Zelin and Yecai, 1991; Zhang, 1998; Novák and Heck, 2002; Novák et al., 2003).

Märdla (2017) proposed a stochastic modification of Hotine's integral in the least squares sense to minimize the expected mean square error of the geoid/quasi-geoid estimator. The proposed modification is based on handling the absence of gravity measurements outside the geoid modeling area and considering the errors introduced by the gravity measurements and the global geopotential model, which is used as a reference for the long-wavelength gravity signal. This methodology was first implemented to Stokes's integral by Sjöberg (1981, 1984, 1991, 2003b) and has been successfully applied in areas with good quality dataset (Ågren et al., 2009; Yıldız et al., 2012; Sakil et al., 2021; Isik et al., 2021). The least squares modification of Stokes's formula with additive corrections (LSMSA), exploits the gravity anomaly calculated on the topography as an input for the modified Stokes's integral, without downward continuing it to the geoid surface, but rather correcting the so-called approximate geoid with the additive corrections for the assumptions in the integration. The Hotine counterpart so-called least squares modification of Hotine's integral with additive corrections (LSMHA), has been tested in the north of Sweeden by Märdla et al. (2018) and later in the Colorado region of the US, where high quality terrestrial and airborne gravity dataset is available, by Isik et al. (2021), and finally in Auvergne region of France using gridded and non-gridded gravity dataset by Sakil et al. (2021). A study conducted by Abbak et al. (2022) has recently demonstrated a case study using Auvergne dataset, together with providing software for the LSMHA method written in C programming language.

The accuracy of the gravimetric geoid models in Turkey has become more of an issue with the establishment of the Turkish National Fundamental GPS Network in 1999 (Ayhan et al., 2002). The increase in the use of GNSS technologies in

engineering projects has created the demand for an accurate geoid model that can be put into service to convert ellipsoidal height into orthometric height. However, the geoid models of Turkey released up to now are not accurate enough to replace the traditional geometric leveling (Ayhan, 1993; Kılıçoglu, 2002; Kılıçoglu et al., 2005; Yıldız et al., 2006; Yıldız, 2021; Kılıçoglu et al., 2011). Even though different geoid modeling methodologies were applied using more accurate global geopotential models, the accuracy of the models remained similar. The reason behind the unsuccess in increasing the accuracy of these models stems from the low quality of historical terrestrial gravity measurements. There are ongoing efforts to modernize the height system by renewing the current gravity measurement database. In this modernization effort, new terrestrial gravity measurements are being conducted in areas where the point density of gravity measurement is low. Furthermore, the General Directorate of Mapping is carrying out airborne gravity flight campaigns in lake regions of Turkey.

To investigate the advantage of kernel modification in the least squares sense, the performance of the LSMSA technique over the classical remove-compute-restore technique for the gravimetric geoid modeling in Turkey has been shown by Isik and Erol (2015, 2016) and Isik (2016), and the results demonstrated the superiority of the LSMSA technique. A similar study was conducted for a smaller area, Konya Closed Basin, located in central Turkey, by Abbak et al. (2012a), and it was stated that the LSMSA technique performed superior for the mountainous area with sparse gravity measurements. Aside from the many studies that showed the performance of the LSMSA technique, no study applied the LSMHA method in Turkey for modeling gravimetric geoid.

In this study, we investigated the performance of the LSMHA technique in Turkey as an alternative methodology to model the gravimetric geoid in a topographically challenging area where the quality of terrestrial gravity measurements is relatively low. Since the gravity anomaly dataset is already gridded and raw gravity measurements are not available for research purposes in Turkey, the gravity disturbance grid is computed from the gravity anomaly grid (1' spatial resolution) by using an existing geoid/quasi-geoid model. This conversion from gravity anomalies to gravity disturbances does not constitute a disadvantage in order to fulfill the purpose of this

study. The computed LSMHA geoid was tested at 100 GNSS/leveling benchmarks and compared with the geoid model computed using the LSMSA method. Additional 301 GNSS/leveling stations located in the Aegean region of Turkey were also included as a second validation dataset to analyze the geoid model's local behavior. The validations at the GNSS/leveling stations were presented in terms of both absolute and relative accuracies of the model. Though the Hotine's integral with the current archival gravity dataset provided performance similar to the commonly applied Stokes counterpart for geoid modeling in Turkey, the availability of ellipsoidal heights with the newly measured gravity data will bring the Hotine's integral method to the forefront in the future geoid modeling studies.

This section is followed by "Method and material" section, where the method and dataset used in this study are presented. "Method and material" section starts with a brief explanation of the formulation of the LSMHA technique and continues with the pre-processing and preparation of the gravity dataset for the gravimetric geoid modeling. "Gravimetric geoid modeling" section explains the details of the computation of the gravimetric geoid model and the validation results of the LSMHA geoid model at the GNSS/leveling benchmarks. The validation results are discussed in terms of the absolute and relative accuracy of the LSMHA geoid model and the accuracy assessment of the Stokes geoid model calculated using the same parameters. The paper is concluded with a summary of the findings from the study in "Conclusions" section.

4.2 Method and Material

4.2.1 Least squares modification of Hotine's integral with additive corrections method

Hotine's formula (Eq. 4.1) for the determination of geoid takes as input the gravity disturbance, which is accurately determined by the ellipsoidal heights (Hotine, 1969).

$$N = \frac{R}{4\pi\gamma} \iint_{\sigma} H(\psi) \delta g d\sigma \quad (4.1)$$

In this equation, R represents the mean radius of Earth, γ is the normal gravity on the reference ellipsoid, δg is the gravity disturbance, and $d\sigma$ is the surface element of the unit sphere.

Hotine's function $H(\psi)$ is given (Hotine 1969) as:

$$H(\psi) = \frac{1}{\sin(\frac{\psi}{2})} - \ln \left(1 + \frac{1}{\sin(\frac{\psi}{2})} \right) \quad (4.2)$$

Similar to Stokes's integral, applying the original Hotine's formula over the whole Earth is a necessity to determine the geoid height. In contrast, it is not possible to obtain gravity data on a global scale. A spherical distance ψ around the computation point should limit the integration area. Therefore, truncation error occurs at the borders of the computation area, as well as missing gravity signal at low degrees of harmonics which results in a far zone problem.

The least squares modification of Hotine's formula is based on the minimization of the expected global mean square error of the geoid estimator by spectrally weighting the gravity disturbances calculated from the gravity measurements and the global geopotential model based on their error estimates. Together with the additive corrections applied to the approximate geoid heights for the assumptions in the computation of Hotine's formula, the final equation that gives the combined geoid model can be written as

$$\bar{N} = \tilde{N} + \delta N_{\text{TOPO}} + \delta N_{\text{DWC}} + \delta N_{\text{ATM}} + \delta N_{\text{ELL}} \quad (4.3)$$

where \tilde{N} represents approximate geoid undulation, δN_{TOPO} is combined topographic effect, δN_{DWC} is downward continuation effect, δN_{ATM} is combined atmospheric correction, δN_{ELL} represents the combined ellipsoidal effect (Märdla, 2017).

Combining long-wavelength components from the global geopotential model (GGM) and terrestrial gravity data is used to reduce the truncation error, so Eq. 4.1 is rewritten as follows (Märdla, 2017):

$$\tilde{N} = \frac{R}{4\pi\gamma} \iint_{\sigma_0} H^L(\psi) \delta g d\sigma + \frac{R}{2\gamma} \sum_{n=0}^M (s_n + Q_n^L) \delta g_n \quad (4.4)$$

where $H^L(\psi)$ is the modified Hotine's function with L being an arbitrary upper limit for the expansion degree, s_n is the modification parameter. Q_n^L are the modified

truncation coefficients. δg_n is the Laplace harmonics of gravity disturbance, and its spherical harmonic representation is given in Heiskanen and Moritz (1967, Eq. 2–22) as

$$\delta g_n = \frac{GM}{a^2} \left(\frac{a}{r}\right)^{n+2} (n+1) \sum_{m=0}^n \{\bar{C}_{nm} \cos m\lambda + \bar{S}_{nm} \sin m\lambda\} \bar{P}_{nm}(\sin \phi) \quad (4.5)$$

where \bar{C}_{nm} and \bar{S}_{nm} are fully normalized spherical harmonic coefficients. \bar{P}_{nm} are fully normalized Legendre functions.

The modified Hotine's function $H^L(\psi)$ and the modified truncation coefficients Q_L^n are given as follows (Märdla, 2017)

$$H(\psi)^L = H(\psi) - \sum_{n=0}^L \frac{2n+1}{2} s_n P_n(\cos \psi) \quad (4.6)$$

and

$$Q_n^L(\psi_0) = Q_n(\psi_0) - \sum_{k=0}^L \frac{2k+1}{2} R_{nk} s_k \quad (4.7)$$

where $Q_n(\psi_0)$ are truncation coefficient calculated by the formula given by Jekeli (1979) and R_{nk} are Paul's coefficients (Paul, 1973).

Hotine's formula, as is the case for Stokes's formula, is based on the assumption that there are no topographic masses outside the geoid. The combined topographic effect is the sum of the direct and indirect topographical effects (Sjöberg, 2007) and can be calculated as:

$$\delta N_{\text{TOPO}} = N_{\text{dir}} + N_{\text{ind}} \approx -\frac{2\pi G\rho}{\gamma} \left(H_P^2 + \frac{2}{3} \frac{H_P^3}{r_P} \right) \quad (4.8)$$

where ρ represents the mean topographic mass density and is taken as 2.67 g/cm^3 . H is the orthometric height of the computation point.

The combined downward continuation effect (Märdla 2017) is given as:

$$\delta N_{\text{DWC}}(P) = \delta N_{\text{DWC}}^{(1)}(P) + \delta N_{\text{DWC}}^{L(1),\text{far}}(P) + \delta N_{\text{DWC}}^{L(2)}(P) \quad (4.9)$$

where

$$\delta N_{\text{DWC}}^{(1)}(P) = \frac{\delta g(P)}{\gamma} H_P + \frac{\zeta_P^0}{r_P} H_P - \frac{1}{2\gamma} \frac{\partial \delta g}{\partial r} \Big|_P H_P^2 \quad (4.10)$$

and

$$\delta N_{\text{DWC}}^{L(1),\text{far}}(P) = \frac{R}{2\gamma} \sum_{n=0}^M (s_n + Q_n^L) \left[\left(\frac{R}{r_P} \right)^{n+2} - 1 \right] \delta g_n^{\text{GGM}}(P) \quad (4.11)$$

and

$$\delta N_{\text{DWC}}^{L(2)}(P) = \frac{R}{4\pi\gamma} \iint_{\sigma_0} H^L(\psi) \left(\frac{\partial \delta g}{\partial r} \Big|_Q (H_P - H_Q) \right) d\sigma_Q \quad (4.12)$$

In these equations, $r_p = R + H_P$ and is the local radius at the computation point, σ_0 represents spherical cap with radius $\psi = \psi_0$ centered around P , and ζ_P^0 is the approximate height anomaly at P . Gravity gradient at the computation point is given in Heiskanen and Moritz (1967, Eq. 2–22)

$$\left(\frac{\partial \delta g}{\partial r} \Big| P \right) = \frac{R^2}{2\pi} \int_{\sigma_0} \frac{\delta g_Q - \delta g_P}{\ell_0^3} d\sigma_Q - \frac{2}{R} \delta g(P) \quad (4.13)$$

where ℓ_0 is the spatial distance between the computation point (P) and the running point (Q) $\ell_0 = 2R \sin \frac{\psi_{PQ}}{2}$.

The formulation of combined atmospheric correction (Ågren et al., 2009) is given as:

$$\begin{aligned} \delta N_{\text{ATM}}(P) &\approx \delta \zeta_{\text{ATM}}(P) \\ &= -\frac{2\pi RG\rho_A}{\gamma} \sum_{n=0}^M \left(\frac{2}{n+1} - s_n - Q_n^L \right) H_n(P) \\ &\quad - \frac{2\pi RG\rho_A}{\gamma} \sum_{n=M+1}^{\infty} \left(\frac{2}{n+1} - \frac{n+2}{2n+1} Q_n^L \right) H_n(P) \end{aligned} \quad (4.14)$$

where ρ_A represents the atmospheric density at sea level and H_n is Laplace harmonics of the topographic height.

The ellipsoidal correction is applied because of the spherical approximation of Stokes's/Hotine's integral. The combined ellipsoidal effect (Sjöberg, 2004a) is given as follows

$$\begin{aligned} \delta N_{\text{ELL}}(P) &\approx \delta \zeta_{\text{ELL}}(P) = \frac{R}{2\gamma} \sum_{n=0}^{\infty} \left(\frac{2}{n+1} - s_n^* - Q_n^L \right) \\ &\quad \times \left(\frac{a-R}{R} \delta g_n^{\text{GGM}}(P) + \frac{a}{R} (\delta g_e)_n \right) \end{aligned} \quad (4.15)$$

where

$$(\delta g_e)_n = \frac{e^2}{2a} \sum_{m=-n}^n \left\{ [3 - (n-3)F_{nm}] T_{nm} \right. \\ \left. - (n+2)G_{nm}T_{n-2,m} \right. \\ \left. - (n+5)E_{nm}T_{n+2,m} \right\} Y_{nm}(P) \quad (4.16)$$

In this equation, T_{nm} are the harmonic coefficients for disturbing potential. F_{nm} , G_{nm} and E_{nm} , are the ellipsoidal coefficients Sjöberg (2004b).

A flowchart, which shows the followed steps for gravimetric geoid modeling using the LSMHA method, is given in Figure 4.1. In the schema, the input data and parameters for calculating the approximate geoid undulation and the additive corrections are

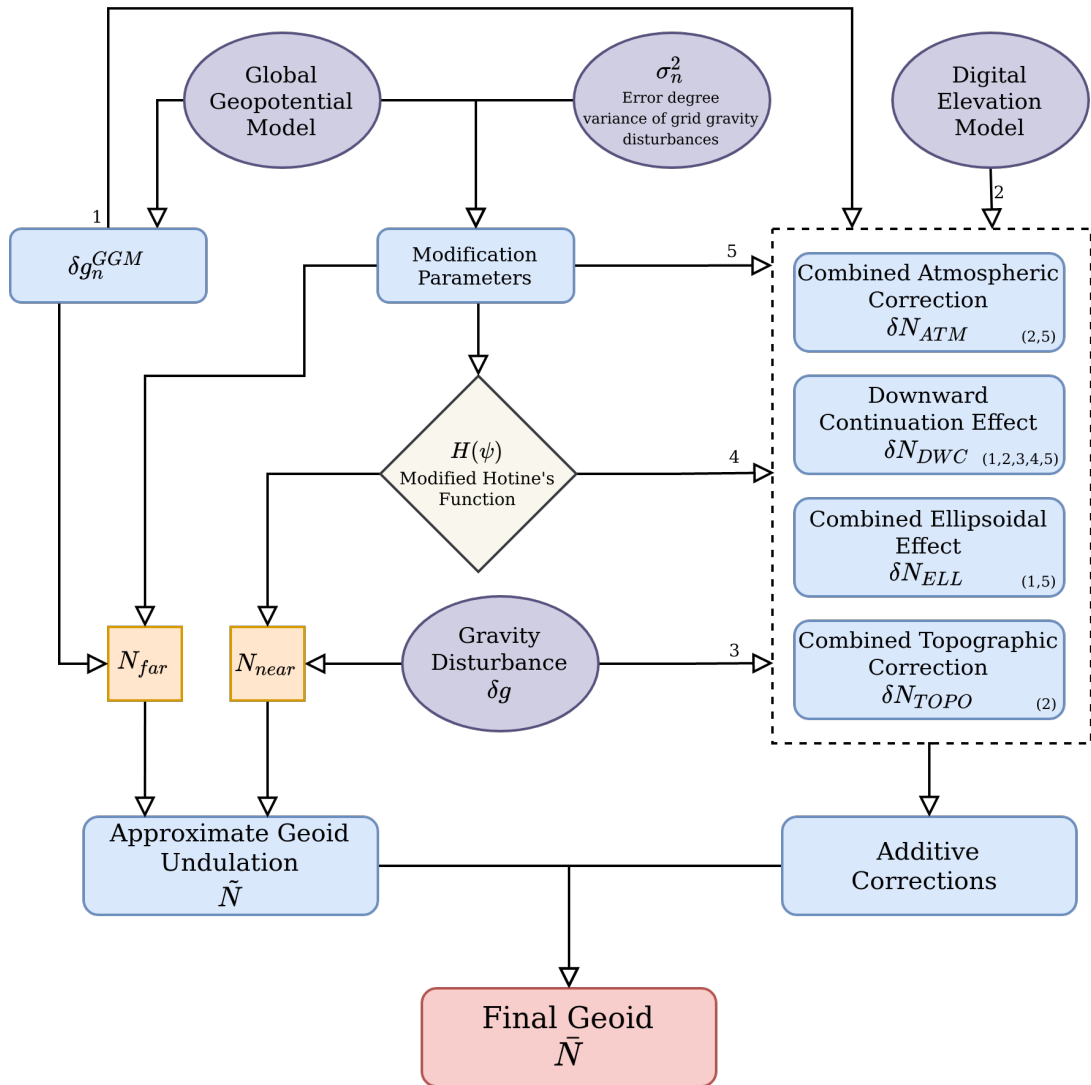


Figure 4.1 : The computation steps of the least squares modification of Hotine's integral with additive corrections (LSMHA) method.

shown in an individual section, and the input flow among the related computation steps is addressed with numbers.

4.2.2 Dataset and pre-processing

4.2.2.1 Terrestrial gravity data

The terrestrial gravity data collected by the General Directorate of Mineral Research and Exploration (GDMRE, or MTA as the original abbreviation) were used in this study. The dataset originally contains 64,469 gravity measurements collected for

mineral research and geophysical explorations throughout the country with $\sim 3.5 \text{ km}$ spacing between stations (see Figure 4.2a). All gravity measurements were conducted in the Potsdam gravity datum. The gravity data is distributed as a complete Bouguer anomaly grid, not as point-wise data. Thus, it contains preliminary assumptions for gravity reductions. The normal gravity values for the so-called latitude correction were calculated with reference to the Geodetic Reference System 1967 (GRS67). The Bouguer plate correction was applied using the density of the topographic masses equivalent to 2.67 g/cm^3 before the gridding process. The terrain correction was estimated up to Hammer zone J (6.5 km) (Hammer, 1939) with 2.40 g/cm^3 topographic density (Arslan, 2016).

The dataset contains a gridded complete Bouguer anomaly with 1-arcminute spatial resolution (see Figure 4.2b), and its accuracy is estimated about 5 mGal Erol et al. (see 2020b). The free-air gravity anomalies (Δg_P^{FA}) were calculated from the complete Bouguer anomalies (Δg^{BO}) by restoring the Bouguer plate (δg_{BP}) and removing the terrain corrections (δg_{TC}) as

$$\Delta g_P^{FA} = \Delta g^{BO} + \delta g_{BP} - \delta g_{TC} \quad (4.17)$$

In order to transform to International Gravity Standardization Net 1971 (IGSN 71) datum, 14 mGal were subtracted from the gravity values (Wppard, 1980). The normal gravity values based on the GRS67 ellipsoid were transformed to the GRS80 ellipsoid restoring the difference between the two ellipsoids using Somigliana's formula for the normal gravity (Eq. 4.18).

$$\gamma = \gamma_e \frac{1 + k \sin^2 \phi}{\sqrt{1 - e^2 \sin^2 \phi}} \quad (4.18)$$

where k is computed as,

$$k = \frac{b \gamma_p}{a \gamma_e} - 1 \quad (4.19)$$

In this equation, γ_e and γ_p are the normal gravity at the equator and the pole, respectively, ϕ is the geodetic latitude, and a and b are the semi-major and semi-minor axes of the reference ellipsoid, respectively.

As mentioned in "Least squares modification of Hotine's integral with additive corrections method" section, the gravity disturbances are the input values for Hotine's

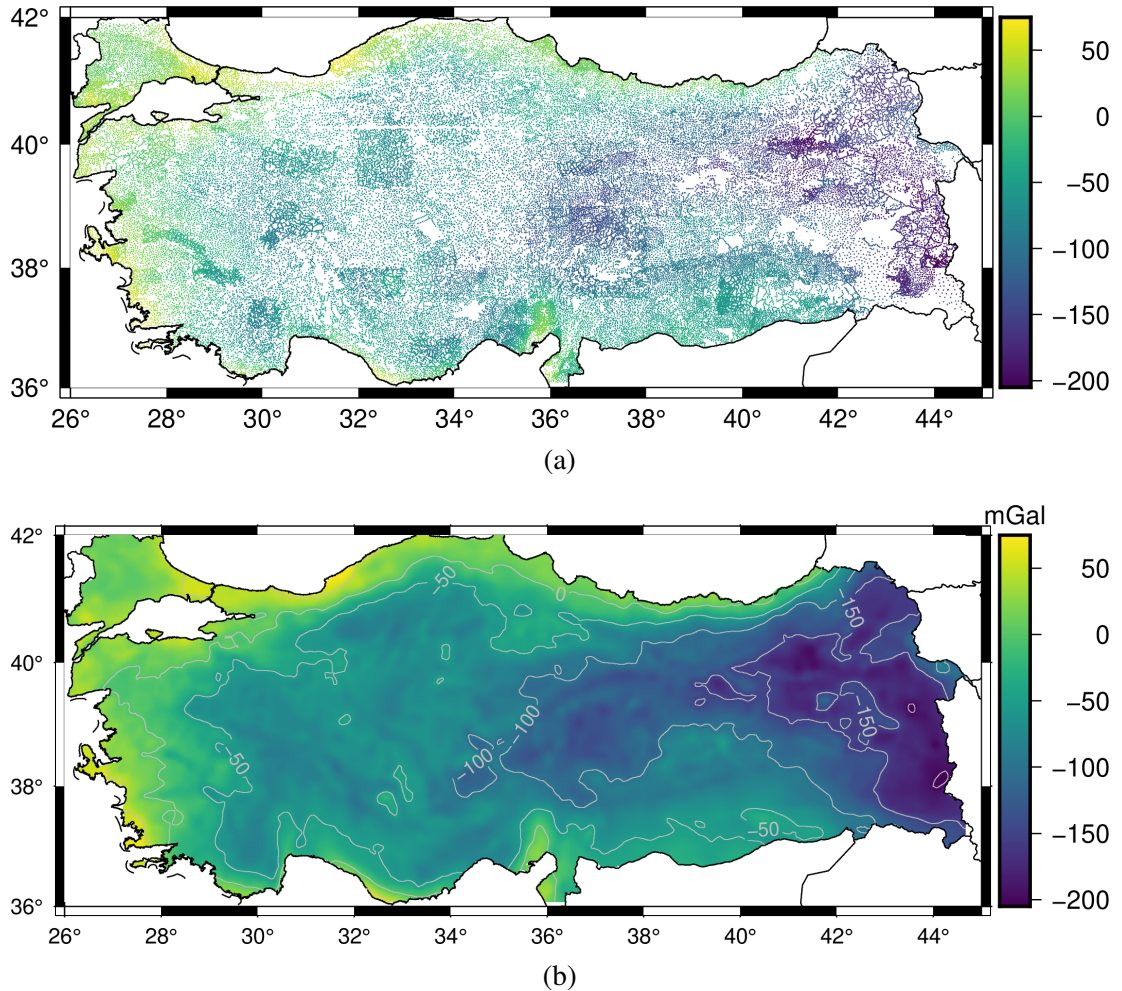


Figure 4.2 : (a) The location of the gravity observation points by the General Directorate of Mineral Research and Exploration with their complete Bouguer anomaly values [unit: mGal]. Please note that the complete Bouguer anomaly values at these locations were re-generated from the 1-arcminute grid given in (b) since the original point-wise gravity measurements are not available for this study.

integral. On the other hand, the free-air gravity anomalies, shown in Figure 4.3a, constitute an input for Stokesian geoid modeling approaches. Therefore, the free-air gravity anomalies were converted into gravity disturbances (see Figure 4.3b) using a simple relation that includes a geoid model (N) and the vertical gradient of normal gravity $\left(\frac{\partial\gamma}{\partial h}\right)$ via Eq. 4.20.

$$\delta g = \Delta g^{FA} - \frac{\partial\gamma}{\partial h}N \quad (4.20)$$

In the realization of this equation, the vertical gradient of normal gravity is approximated by -0.3086 mGal/m , and the geoid model is computed from a high

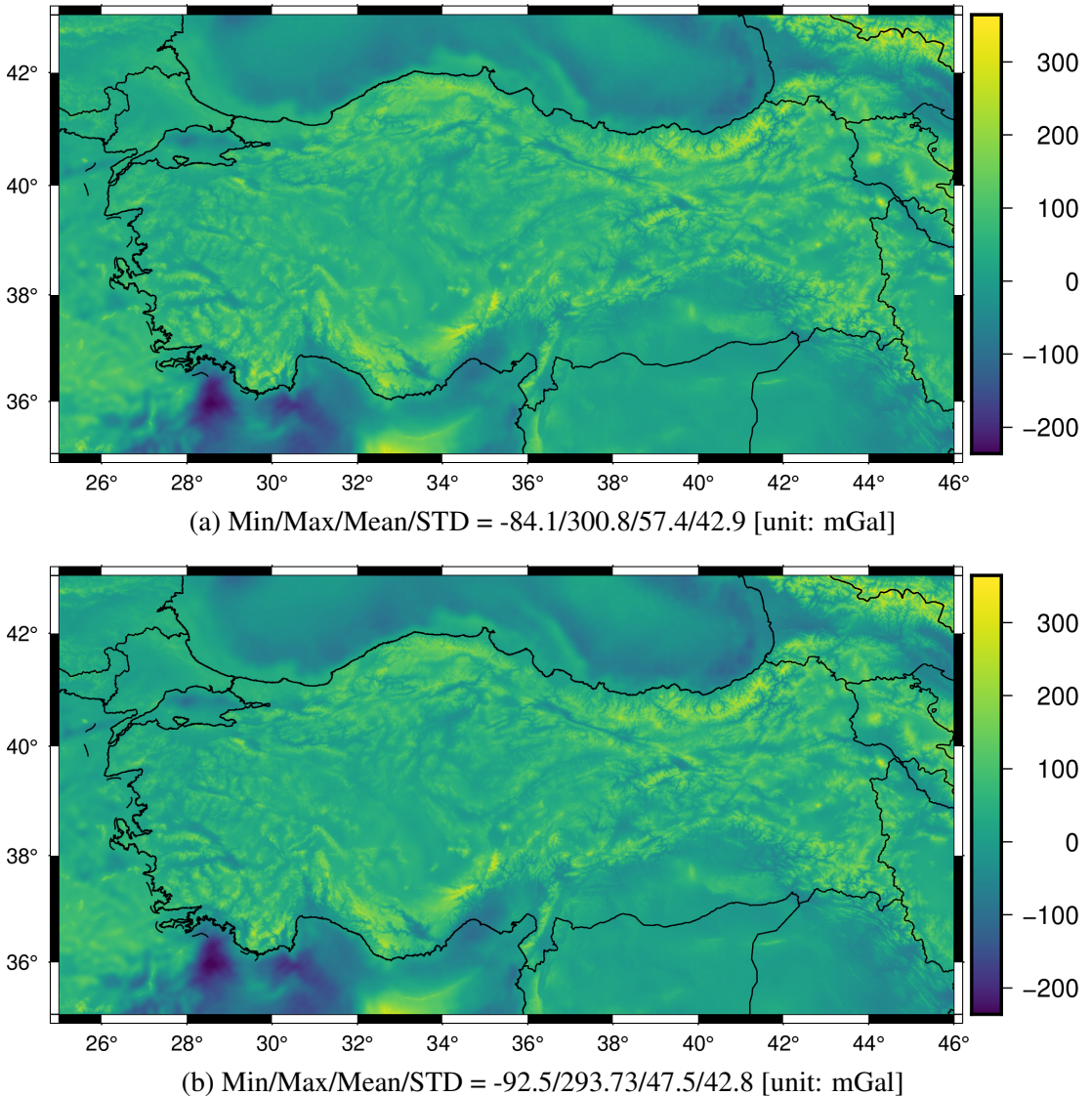


Figure 4.3 : (a) Gravity anomaly and, (b) gravity disturbance grids in Turkey.

degree global geopotential model XGM2019e up to 2190 degree/order (Zingerle et al., 2020). The success of this conversion from gravity anomalies to disturbances is not affected by the change in the geoid model since its magnitude is reduced by the multiplication of free-air correction (-0.3086 mGal/m), as long as the geoid model provides accuracy in decimeter level (Kirby, 2003). For the accuracy of the geoid model calculated using the XGM2019e geopotential model, please see Table 4.1 and Table 4.3 in Section 4.3: "Gravimetric Geoid Modeling". Furthermore, all of the studies that employed LSMHA methodology in the literature calculated the gravity disturbances from gravity anomalies using a geoid/quasi-geoid model since the

ellipsoidal height information is not available (Märdla et al., 2018; Sakil et al., 2021; Isik et al., 2021; Abbak et al., 2022). Additionally, the data gaps outside the borders of Turkey, as well as the water bodies inside, were filled with the XGM2019e model using the maximum degree of expansion. In these filled areas, the residual terrain effect on gravity is used from the SRTM2Gravity project (Hirt et al., 2019), a global model of gravimetric terrain corrections, to increase the spectral content of the gravity signal beyond 2190 degrees.

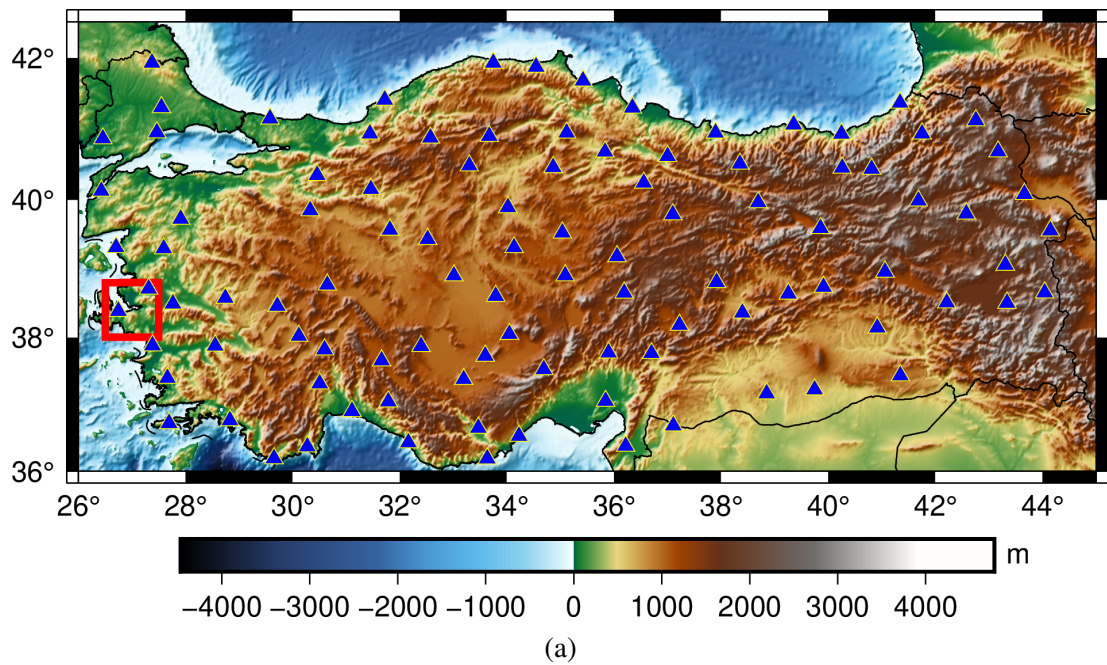
4.2.2.2 GNSS/leveling data

In this study, two GNSS/leveling dataset are available to validate the calculated geoid model. The first dataset consists of 100 GNSS/leveling benchmarks in the Turkish National Fundamental GPS Network (TUTGA) (see Figure 4.4a). The coordinates of the benchmarks are in the ITRF96 datum, and Helmert orthometric heights refer to the Turkish National Vertical Control Network 1999 (TUDKA99). The positional accuracy of GNSS/leveling points is reported as $\sim 1 - 3 \text{ cm}$ in horizontal and vertical components (Ayhan et al., 2002).

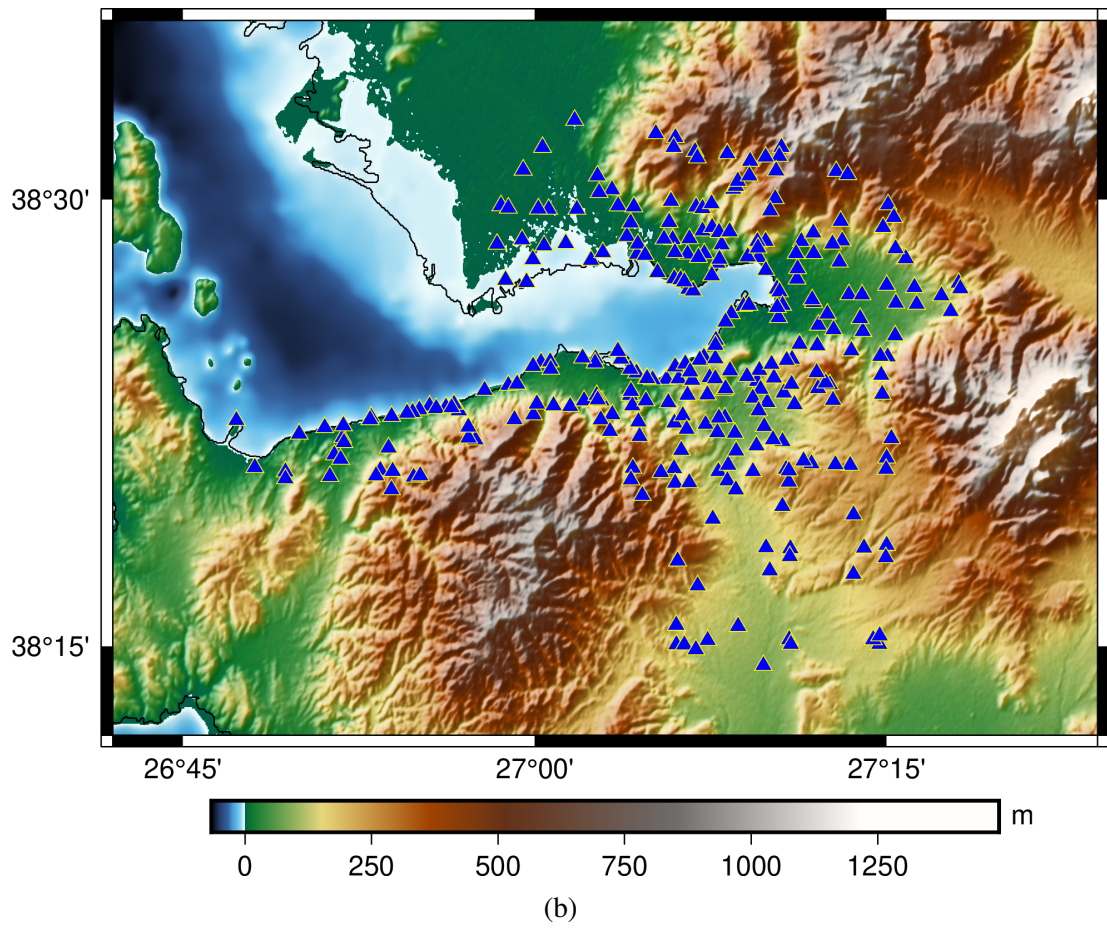
The second dataset consists of 301 GNSS/leveling benchmarks in Izmir province of Turkey (indicated by the rectangular frame in Figure 4.4a). Izmir is located between $38^{\circ}00' N \leq \phi \leq 38^{\circ}36' N$ latitudes and $26^{\circ}30' E \leq \lambda \leq 27^{\circ}30' E$ longitudes in the western part of Turkey near the Aegean Sea. The GNSS/leveling benchmarks were measured in the 'Izmir Geodetic Reference System (IzJRS-2001) project in 2001 (Ayan et al., 2001), and there is one benchmark per 8 km^2 area in the network (see Figure 4.4b). The positional accuracy of the GNSS/leveling points is reported as $\sim 1 - 2 \text{ cm}$ in horizontal and vertical components, respectively (Erol and Erol, 2021).

4.3 Gravimetric Geoid Modelling

The gravimetric geoid model covers an area between $36^{\circ} N \leq \phi \leq 42^{\circ} N$ latitudes and $26^{\circ} E \leq \lambda \leq 45^{\circ} E$ longitudes, and it has a grid spacing of 1-arcminute in both latitude and longitude. The geoid model computations are referenced to the GRS80 ellipsoid considering the zero-degree term in computations, and the tide-free system is adopted. XGM2019e is utilized as GGM for modeling the far zone contribution.



(a)



(b)

Figure 4.4 : The distribution of: (a) 100 TUTGA GNSS/leveling benchmarks in Turkey and, (b) 301 IzJRS GNSS/leveling benchmarks in Izmir province shown over the topography of Turkey.

As for the digital elevation model, 3'' resolution SRTM was selected to acquire the physical heights of the grid nodes (Jarvis et al., 2008). In order to be consistent with the gravity data grid, the SRTM was down-sampled to 1-arcminute resolution.

The selection of modification parameters is based on the experimentation of Stokes's integral counterpart of the methodology, where the maximum degree of expansion of the GGM is tested between 240 degree/order and 720 degree/order with a 60 degree/order increments while the integration radius is tested with varying degrees between $0.1^\circ - 1^\circ$. Based on the standard deviation of Stokes's solution of the gravimetric geoid model (Isik et al., 2022b), the optimum parameters are determined and adopted for the Hotine's solution. Accordingly, the integration radius (ψ_0) is taken as 0.25° . The maximum expansion degree/order of the model (M), as well as the maximum modification degree (L), is used as 360. The error degree variance of the gravity anomalies is constructed using a band-limited white noise model where the standard deviation of the gravity disturbance grid is taken as 5 mGal. For detailed information regarding the accuracy of the dataset, the readers are advised to see Erol et al. (2020b). The unbiased solution of modification parameters s_n are computed via Singular Value Decomposition (SVD).

The approximate geoid height and additive corrections are calculated using a Python programming language version of ITU-GRG software for the LSMHA solution (Sakil et al., 2021), originally written in MATLAB language. The components of the geoid model, as well as their combination, are presented in Figure 4.5.

In order to validate the calculated geoid model in absolute and relative manners, the two GNSS/leveling dataset mentioned above for the countrywide and local area were used. The differences between the geoid model and the local vertical datum were modeled by applying 1-parameter and 7-parameter (Eq. 4.21) Helmert similarity transformation to reduce the effect of random and systematic errors that may stem from datum inconsistency, vertical datum distortions, and measurement errors introduced by the GNSS/leveling dataset. 1-parameter model was used to remove the mean value between gravimetric geoid models (Stokes and Hotine) and the local vertical datum where the GNSS/leveling surface is referred to. 7-parameter model, on the other hand,

was opted for modeling datum shift parameters. Though, there are other techniques to fit the gravimetric geoid models to local vertical datum, such as 4-parameter, 5-parameter, and polynomial models, only these two parametric models (1-parameter and 7-parameter) were employed in this study, as they are commonly applied models for corrector surface fitting.

The residual geoid heights (ΔN) are fitted to a parametric model as,

$$\Delta N = N_{GNSS/leveling} - N_{\text{Model}} = \mathbf{a}_i^T \mathbf{x} + \varepsilon \quad (4.21)$$

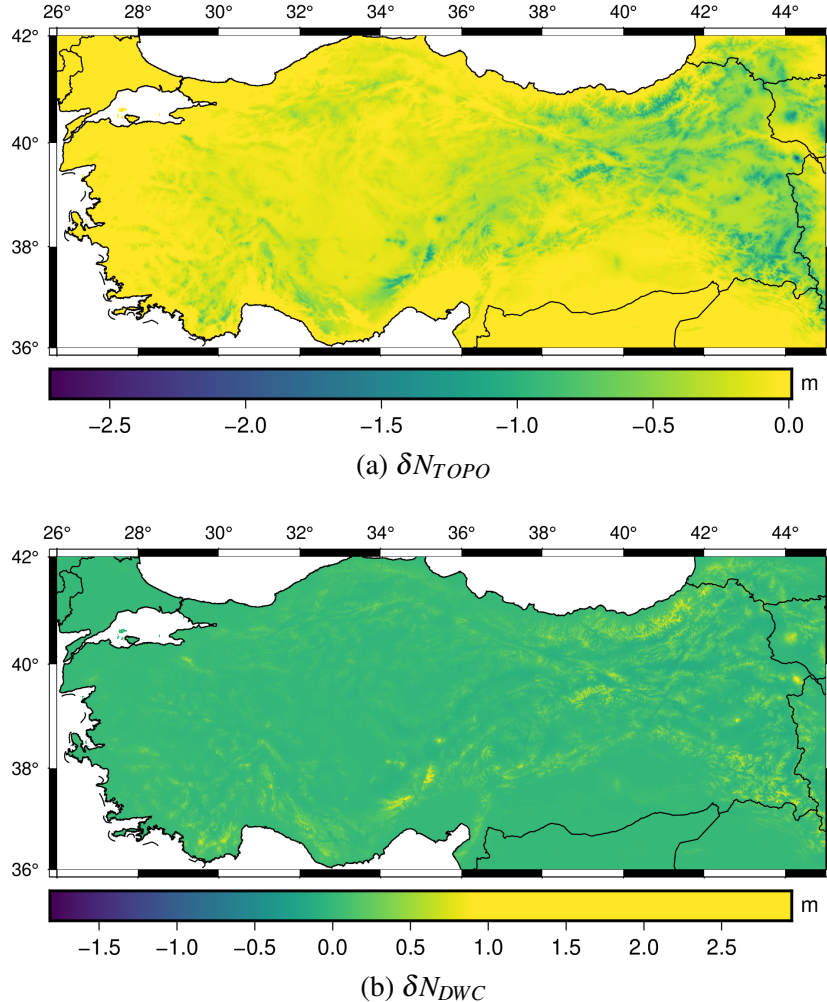


Figure 4.5 : N_S^{1min} geoid model: (a) approximate geoid heights ((\tilde{N})); (b) combined topographic correction (δN_{TOMB}^{COM}); (c) combined downward continuation correction (δN_{DWC}^{COMB}); (d) combined atmospheric correction (δN_{ATM}^{COMB})); (e) combined ellipsoidal correction (δN_{ELL}^{COMB}); and (f) final geoid model (\hat{N}).

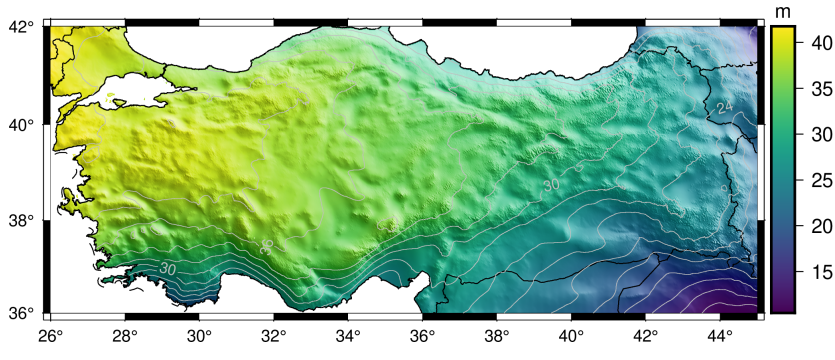
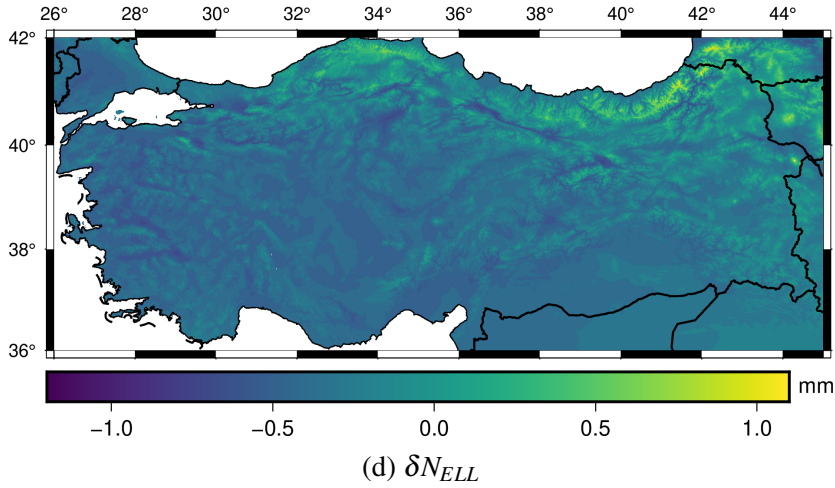
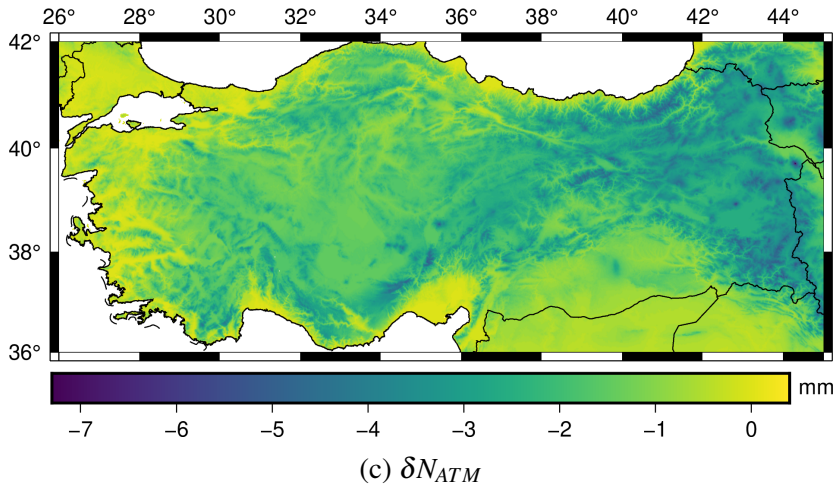


Figure 4.5 : The components of the LSMHA geoid model: (a) topographic correction (δN_{TOPO}), (b) downward continuation correction (δN_{DWC}), (c) atmospheric correction (δN_{ATM}), (d) ellipsoidal correction (δN_{ELL}), and (e) combined geoid model (\bar{N}).
(cont.)

where \mathbf{a} is the matrix of known coefficients, \mathbf{x} is the vector of unknowns of the parametric model, and ε is the random noise value. The vector of known coefficients

for the 1-parameter (mean removal) model is only $\mathbf{a}_i^T = [1]$ and the vector of unknowns $\mathbf{x} = [x_1]$ corresponds to the systematic shift between the local vertical datum and gravimetric geoid model. The formulation for the 7-parameter model is given as,

$$\begin{aligned}\mathbf{a}_i^T \mathbf{x} = & x_1 \cos \varphi_i \cos \lambda_i + x_2 \cos \varphi_i \sin \lambda_i + x_3 \sin \varphi_i + x_4 \left(\frac{\sin \varphi_i \cos \varphi_i \sin \lambda_i}{W} \right) + \\ & x_5 \left(\frac{\sin \varphi_i \cos \varphi_i \cos \lambda_i}{W} \right) + x_6 \left(\frac{1 - f^2 \sin^2 \varphi_i}{W} \right) + x_7 \left(\frac{\sin^2 \varphi_i}{W} \right)\end{aligned}\quad (4.22)$$

where $\mathbf{x} = [x_1 \dots x_7]$ is the vector of 7 unknown coefficients (hence the name 7-parameter model), φ_i and λ_i represent the geodetic latitude and longitude of GNSS/leveling station, W is formulated as $\sqrt{1 - e^2 \sin^2 \varphi_i}$, e is the first eccentricity, and f is the flattening of the reference ellipsoid (Fotopoulos, 2013).

Besides the absolute comparison of geoid models at GNSS/leveling benchmarks, the performance of models in a relative manner is assessed by calculating the residual geoid height differences at each baseline formed by the pairs of GNSS/leveling benchmarks (Eq. 4.23).

$$\delta \Delta N = \Delta N_{GNSS/leveling} - \Delta N_{Model} \quad (4.23)$$

In this equation, $\delta \Delta N$ is the misclosure value, $\Delta N_{GNSS/leveling}$ is the geoid height differences between two stations calculated from differences between ellipsoidal heights and orthometric heights of the stations ($\Delta N_{GNSS/leveling} = \Delta h_{GNSS} - \Delta h_{leveling}$), and ΔN_{Model} is the geoid height difference between the two stations interpolated from the geoid model. For detailed information on the absolute and relative comparison of the geoid models, please see Featherstone (2001).

For the countrywide assessment of the geoid models in an absolute manner, Table 4.1 shows detailed statistics of the residual geoid heights for the gravimetric geoid model and the model fitted to the local vertical datum at 100 TUTGA GNSS/leveling stations. Moreover, the statistics of the gravimetric geoid model calculated using the least squares modification of Stokes's integral in Turkey (Isik et al., 2022b) are included in this table to compare numerically with the gravimetric geoid model based on Hotine's formulation.

Based on the absolute comparison of geoid models against TUTGA stations, the two geoid model solutions reveal similar accuracy in terms of standard deviations (8.8 cm

Table 4.1 : The statistics of the geoid height differences at 100 TUTGA GNSS/leveling stations ($N_{(GNSS/Leveling)} - N_{Model}$) [unit: cm].

		Min	Max	Range	Mean	STD
Hotine	1-parameter	-28.6	21.3	49.9	0.0	10.4
	7-parameter	-27.3	20.2	47.5	0.0	8.8
Stokes	1-parameter	-25.0	28.3	53.3	0.0	10.1
	7-parameter	-23.8	25.3	49.1	0.0	8.6
XGM2019e	1-parameter	-32.4	52.8	85.2	0.0	11.7

for Hotine's solution and 8.6 cm for Stokes's solution). At the TUTGA GNSS/leveling benchmarks, the highest residual geoid heights in an absolute manner for both Hotine's solution and Stokes's solution are near the coastlines (see Figure 4.6a and Figure 4.6b). The problem near coastlines is not an unexpected behavior. The recent study by Yildiz (2021) shows similar discrepancies between Turkey Geoid 2020 (TG-20) and GNSS/leveling benchmarks near the coastal areas. Statistics given in Table 4.1 also show the validation results of the geoid model computed using the maximum expansion degree of the XGM2019e global geopotential model. According to the table, the XGM2019e geoid model has an accuracy of 10.0 cm. Thus, the Hotine and Stokes geoid models show an improvement of about 15% on XGM2019e.

Aside from the absolute comparison, the relative comparison results based on the geoid slopes calculated between each of the GNSS/leveling station pairs are presented. In both Stokes's and Hotine's solutions, the change in the standard deviation of the geoid models (mean removal and 7-parameter fitting) with respect to the change in the baseline increment is shown in Figure 4.7a. The standard deviations of the models after only 1-parameter fitting (removes only a shift) are between 8 cm – 10 cm through the baselines, which are quite close to their accuracy in absolute comparison. In the figure, the standard deviation of the models after 7-parameter fitting is better than 8 cm; evidently, the correlation between the relative accuracy of the models and the baseline length seems to be less significant as it is supposed to be. Figure 4.7b and Figure 4.7c indicate that 92% (for Stokes's solution) and 91% (for Hotine's solution) of the misclosure values after 1-parameter fitting fall within the error tolerance of the 3_{rd} order leveling network ($12mm\sqrt{S_{km}}$). This percentage rises to 94% for both

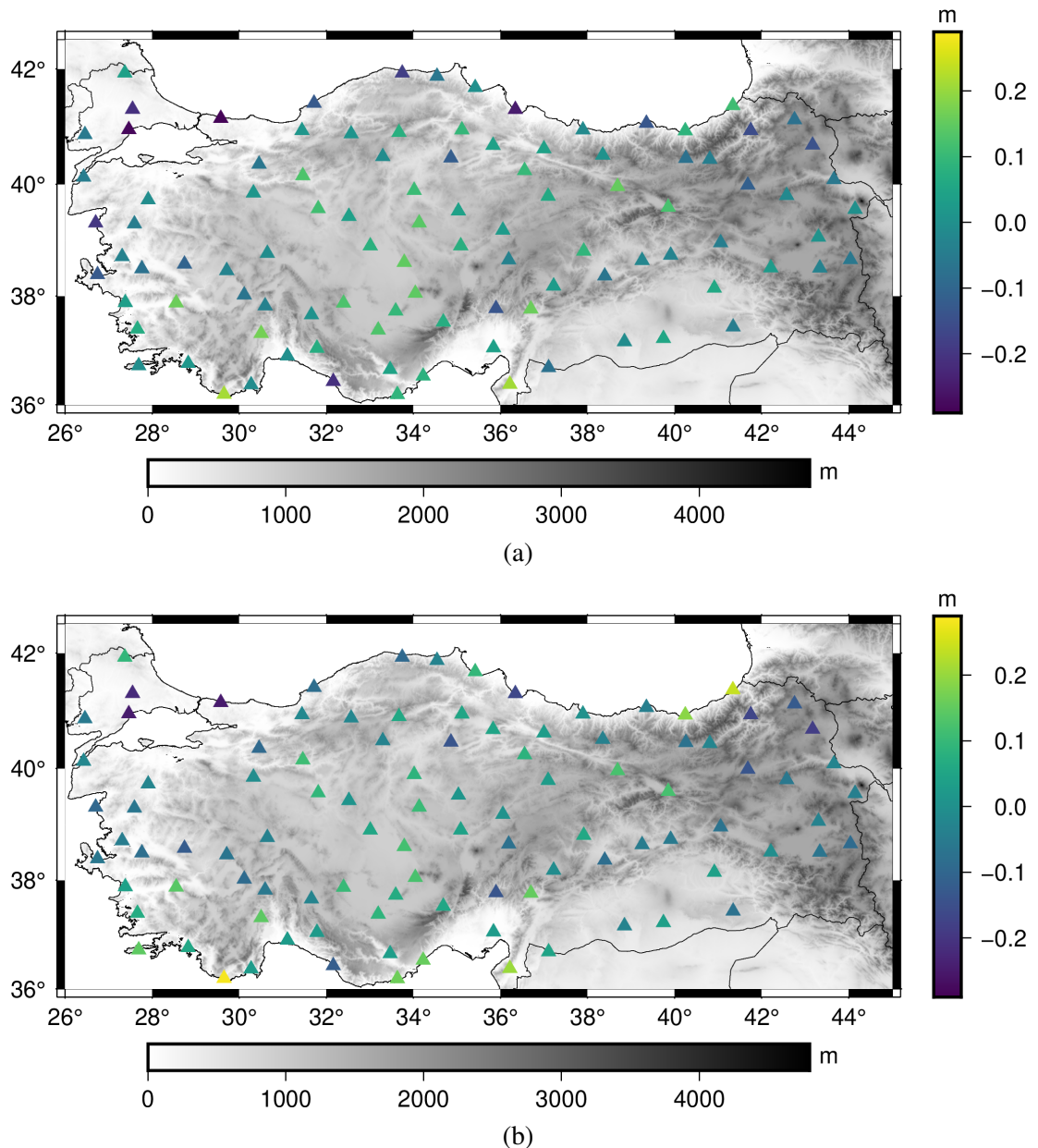


Figure 4.6 : Residual geoid heights (after 1-parameter fitting, which removes only a shift) at 100 TUTGA GNSS/leveling stations for Hotine (a) and Stokes (b) geoid solutions [unit: meters].

solutions after fitting the geoid models to the local vertical datum using 7-parameter transformation.

To evaluate if the misclosure values are dependent on height differences between the stations, the baselines that fall within the 500 m absolute height changes between 0 m - 2000 m are investigated separately, and the corresponding statistics are given in Table 4.2. The standard deviation of misclosure values that fall within the height

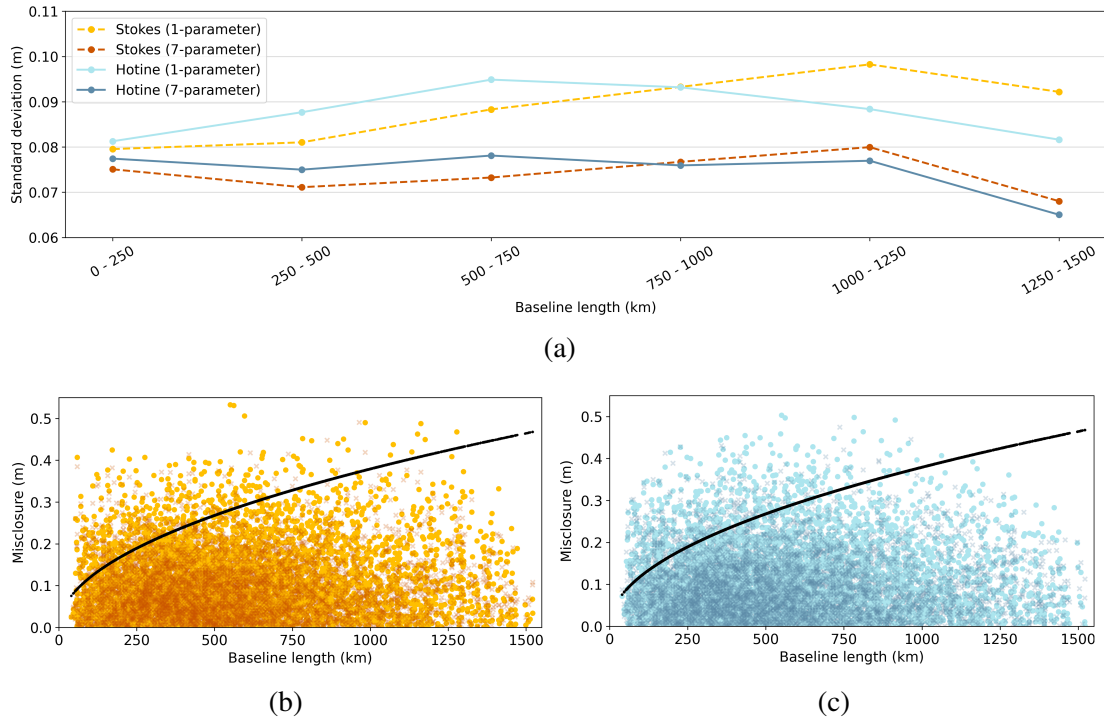


Figure 4.7 : Relative accuracies and misclosures for Stokes and Hotine geoid models according to 100 TUTGA GNSS/leveling benchmarks [unit: meters]: (a) the change in the relative accuracy of Stokes and Hotine geoid models with respect to increasing baseline length after 1-parameter and 7-parameter surface fitting; (b) and (c) the misclosure values for Stokes's and Hotine's solutions, respectively, along the baselines. The circular markers with the lighter tone of colors represent misclosures after 1-parameter fitting. The cross markers with the darker tone of colors represent misclosures after 7-parameter fitting. The black line represents the error tolerance limit of the 3_{rd} order leveling network for backward and forward leveling.

difference intervals shows the homogeneity of the accuracy of the gravimetric models, which is calculated as 7–8 cm for all intervals.

The accuracy assessment of the geoid models in the Aegean region of Turkey is carried out using 301 IzJRS GNSS/leveling benchmarks located in Izmir. The absolute comparison of geoid heights, given in Table 4.3, shows that the performance of Hotine and Stokes geoid models is higher in the western part of Turkey compared to the entire country.

This is expected since the topography of the western part is relatively moderate. While the orthometric height reaches above 5000 m in the eastern parts of the country, the maximum elevation observed near the IzJRS GNSS/leveling network is around

Table 4.2 : The statistics of the misclosure values for baselines of 100 TUTGA GNSS/leveling benchmarks, which are categorized based on the orthometric height difference for all baseline combinations [unit: cm].

Height Difference	No of Baselines	Solution	Min	Max	Mean	STD
0 – 500	2128	Hotine	0.0	47.5	10.1	7.7
		Stokes	0.0	49.1	9.7	7.4
500 – 1000	1586	Hotine	0.0	41.2	9.9	7.5
		Stokes	0.0	41.8	9.6	7.2
1000 – 1500	907	Hotine	0.0	40.2	10.2	7.5
		Stokes	0.0	35.6	10.1	7.4
1500 – 2000	329	Hotine	0.0	31.0	9.4	7.3
		Stokes	0.0	38.2	10.0	7.7

Table 4.3 : The statistics of the geoid height differences at 100 TUTGA GNSS/leveling stations ($N_{(GNSS/Leveling)} - N_{Model}$) [unit: cm].

			Min	Max	Range	Mean	STD
Hotine	1-parameter		-15.2	21.4	36.6	0.0	7.1
	7-parameter		-9.7	14.5	24.2	0.0	4.4
Stokes	1-parameter		-14.2	19.0	33.2	0.0	6.1
	7-parameter		-11.0	14.2	25.2	0.0	4.3
XGM2019e	1-parameter		-21.9	26.7	48.6	0.0	8.2
	7-parameter		-11.5	19.8	31.3	0.0	5.5

1300 m (see Figure 4.4 for a detailed view of the topography in the study area). Nevertheless, the residual geoid heights are larger in magnitude near the mountainous parts of the area (Figure 4.8a and Figure 4.8b), and a correlation between the increase in topographic heights of GNSS/leveling stations and the increase in the magnitude of residual geoid heights is apparent (Figure 4.8c and Figure 4.8d). The accuracy of Hotine’s and Stokes’s solutions after 7-parameter fitting are 4.4 and 4.3 cm, respectively. Both solutions perform approximately 22% better than the XGM2019e global geoid model, whose accuracy is found as 5.5 cm.

The relative accuracies of the models and the magnitude of the misclosures of the baselines for the IzJRS network are shown in Figure 4.9. The models’ relative accuracy after 7-parameter fitting is about 3.5 cm regardless of baseline length (Figure 4.9a). It was found that only 36% of the misclosure values satisfied the error tolerance of the 3rd order leveling network. After the 7-parameter fitting, only half of the misclosure values

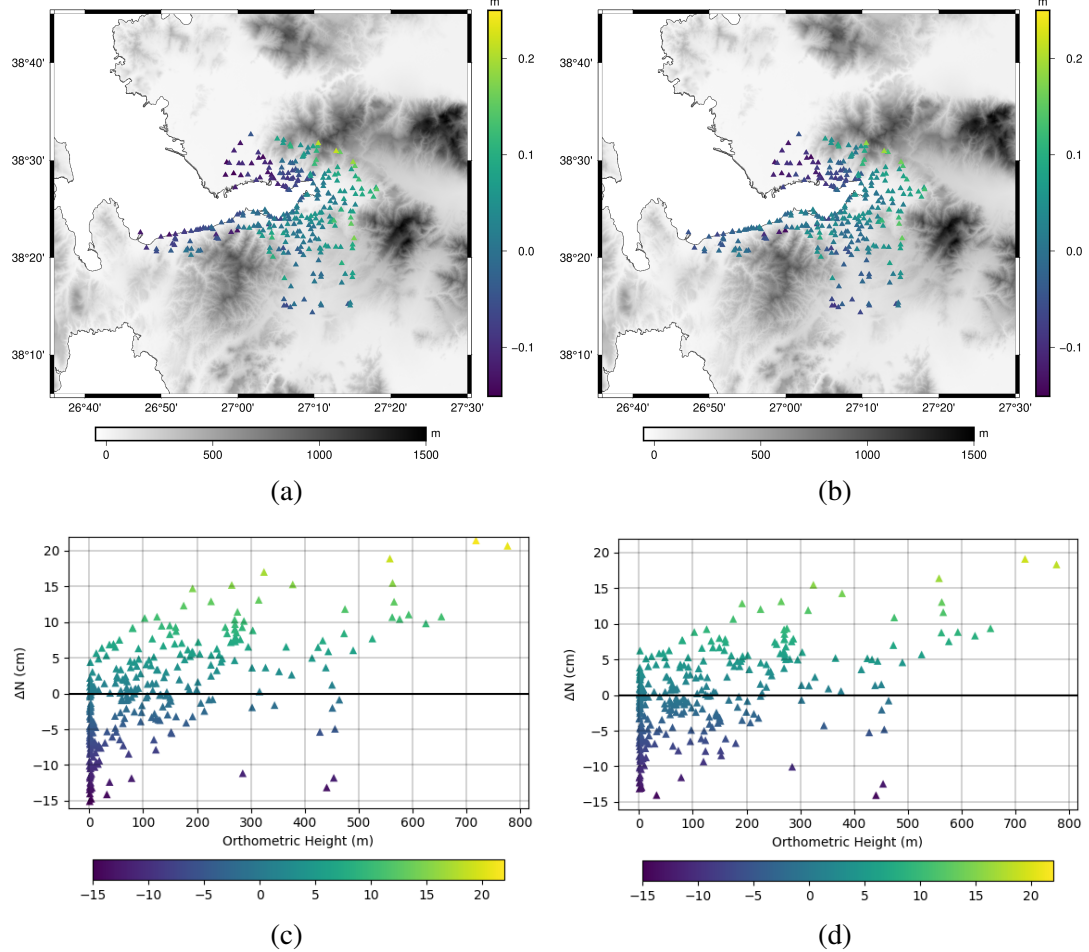


Figure 4.8 : Residual geoid heights (after 1-parameter fitting) at 301 IzJRS GNSS/leveling stations for Hotine (a) and Stokes (b) geoid solutions [unit: meters]. (c) and (d) show the distribution of the residual geoid heights w.r.t. the orthometric heights of the benchmarks.

fall within limits (Figure 4.9b and Figure 4.9c). The shortness of the baselines resulted in a strict error tolerance limit for the 3rd order leveling. Although, the absolute and relative accuracies of the geoid model computed with Hotine's integral, as well as Stokes counterpart, are enough to be used in practice to convert ellipsoidal height to orthometric height in the Izmir local area; when the minimum and maximum values of geoid height residuals in absolute validations and the misclosure values in relative validations are taken into account, it may be recommended to use precise leveling measurements to obtain orthometric heights rather than utilizing the geoid models in high precision engineering and surveying applications requiring sub-centimeter accuracy of heights.

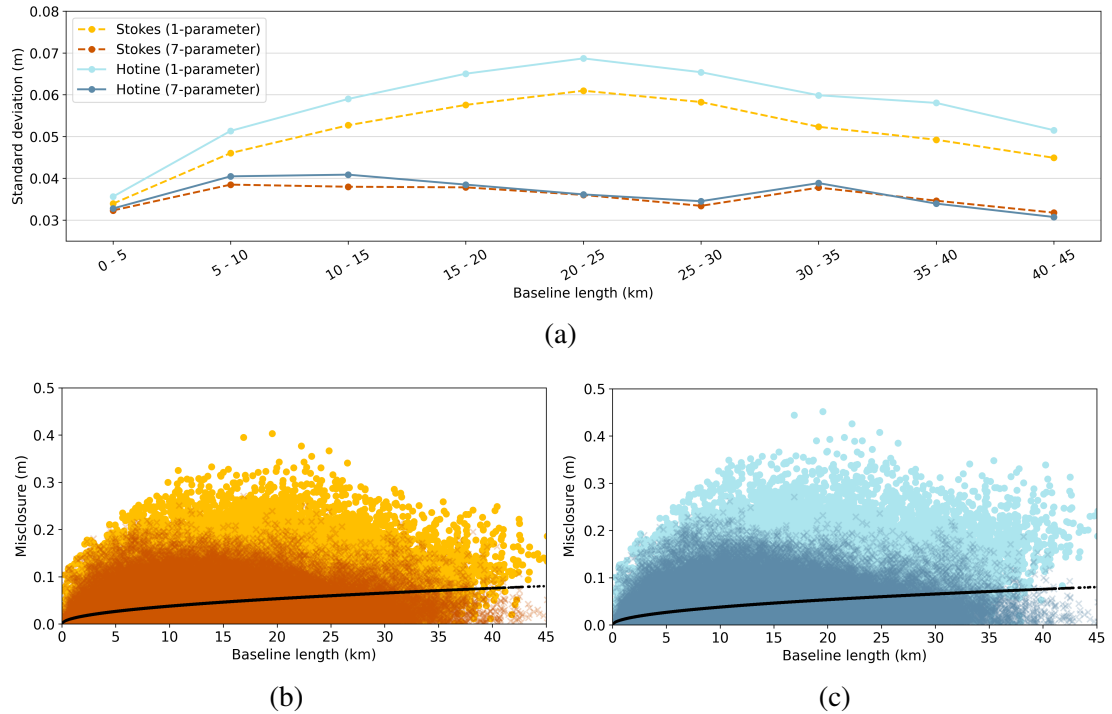


Figure 4.9 : Relative accuracies and misclosures for Stokes and Hotine geoid models according to 301 IZJRS GNSS/leveling benchmarks [unit: meters]: (a) the change in the relative accuracy of Stokes and Hotine geoid models with respect to increasing baseline length after 1-parameter and 7-parameter surface fitting; (b) and (c) the misclosure values for Stokes's and Hotine's solutions, respectively, along the baselines. The circular markers with the lighter tone of colors represent misclosures after 1-parameter fitting. The cross markers with the darker tone of colors represent misclosures after 7-parameter fitting. The black line represents the error tolerance limit of the 3_{rd} order leveling network for backward and forward leveling.

Considering the misclosure statistics and relative accuracies of the 7-parameter fitted geoid models with respect to the height difference between benchmarks given in Table 4.4, it is seen that the relative accuracy decreases as the height difference between the benchmarks increases.

4.4 Conclusions

In this study, a gravimetric geoid model for Turkey was computed using least squares modification of Hotine's integral with additive corrections method. The geoid model was evaluated in an absolute and relative manner at 100 GNSS/leveling benchmarks homogeneously scattered to the entire country. In the absolute comparison of the geoid height differences, the standard deviation of the geoid model was found

Table 4.4 : The statistics of the misclosure values for all baseline combinations of 301 IzJRS GNSS/leveling benchmarks categorized based on the orthometric height difference [unit: cm].

Height Difference	No of Baselines	Solution	Min	Max	Mean	STD
0 – 200	2128	Hotine	0.0	22.3	4.5	3.3
		Stokes	0.0	23.0	4.3	3.2
200 – 400	1586	Hotine	0.0	24.8	5.8	4.2
		Stokes	0.0	25.0	5.5	3.9
400 – 600	907	Hotine	0.0	26.2	7.4	4.7
		Stokes	0.0	25.1	7.2	4.4
600 – 800	329	Hotine	0.0	27.0	13.5	4.2
		Stokes	0.0	27.1	13.0	4.2

as 8.8 cm after the difference between the local vertical datum was minimized using 7-parameter surface fitting. The majority of the relative geoid differences between GNSS/leveling stations were found within the tolerance limit of the 3_{rd} order leveling network. However, the accuracy of the geoid model is not enough to transform ellipsoidal heights to orthometric heights yet in most engineering projects that require high-accuracy height information countrywide. The performance of the Hotine's solution is almost the same as the gravimetric geoid model computed using least squares modification of Stokes's integral with additive corrections. Additional validation in the western part of Turkey using 301 GNSS/leveling stations was performed in a local area. Based on the absolute comparison of geoid height differences, the accuracy of the geoid model using Hotine's approach was found as 4.4 cm. Stokes's approach had an almost equal performance with Hotine's method in the same area. The gravimetric geoid model solutions perform better in the western side of the country since the errors introduced by the roughness of the topography are less effective in the western part of Turkey.

The use of Hotine's integral has shown comparable accuracy with Stokes's integral for modeling the regional gravimetric geoid in Turkey. The availability of the ellipsoidal heights for the gravity measurements makes Hotine's solution more desirable since the gravity disturbance, which is the input for Hotine's integral, is calculated using only the ellipsoidal height of the station, as opposed to the gravity anomaly, which requires the physical height of the station. Traditionally the ellipsoidal heights are not available

for gravity measurements since most cases, they are historical datasets and acquired along with the leveling network measurements without GNSS observations. The recent efforts initiated by the General Directorate of Mapping (HGM) and Scientific and Technological Research Council of Turkey (TUBITAK) for the modernization of the height system in Turkey to re-define a geoid-based vertical datum included the collection of terrestrial gravity measurements throughout the entire country not only for the renewal of the existing gravity database but also for the verification of the quality of the historical data. Furthermore, physically challenging areas where the topography is not suitable for carrying out dense gravity measurements and the geoid modeling is potentially problematic, such as lakes, coastal zones, and rough mountains, were planned to be covered by airborne gravimetry campaigns. Hence, the renewed gravity database of Turkey will include the ellipsoidal height information of the gravity measurements, collected either on the topography or at flight height. The gravimetric geoid modeling based on Hotine's theory will be beneficial for achieving the desired accuracy (about 1-3 cm) of a geoid model that can be used for the transformation of GNSS-derived heights into physical heights for earth science engineering projects in practice. To this end, this study constitutes a base for future geoid modeling studies to be carried out with the new gravity measurements in Turkey.

5. IMPROVEMENT OF GOCE-BASED GLOBAL GEOPOTENTIAL MODELS FOR GRAVIMETRIC GEOID MODELING IN TURKEY¹

5.1 Introduction

The modeling of gravity field using satellites with low Earth orbit has opened a new era in the field of physical geodesy. From development of the first global gravity field models in the early 1960s to today's state-of-art global models that can represent the gravity field and its temporal change with unprecedented accuracy, geosciences benefit more and more from the information we can get about the Earth's gravity field and its interior mass significantly (Barthelmes, 2009). Earth's gravity field can be modeled with high accuracy using data from geodetic satellite missions that aims to contribute to gravity field studies, namely CHallenging Minisatellite Payload (CHAMP), Gravity Recovery and Climate Experiment (GRACE), and Gravity field and steady-state Ocean Circulation Explorer (GOCE).

The contribution of global geopotential models from state-of-art gravity field satellite missions and methodological improvements for gravimetric geoid modeling make the computation of a precise geoid model that can replace the existing vertical datum possible. Geoid based vertical datum facilitates obtaining orthometric heights from ellipsoidal heights precisely using Global Navigation Satellite System (GNSS) technologies, hence removing the need of a traditional geometric leveling to acquire physical heights. Height system based on the vertical control network and leveling measurements are gradually replaced with geoid based height systems in countries where a precise regional geoid model is available. In this context, acquiring the optimum data set for determination of precise geoid model is of great importance.

The performance of a global geopotential model over an area affects the quality of the gravity field modeling and its parameters. Gravimetric geoid modeling methodologies

¹This chapter is based on : Isik, M. S., Çevikalp, M. R., & Erol, B., Erol. S. (2022). Improvement of GOCE-based Global Geopotential Models for Gravimetric Geoid Modeling in Turkey. Submitted to Geosciences

exploit the global geopotential models in terms of modeling the long wavelength gravity signals to overcome the absence of these signals in the local gravity data sets. Thus, the increase in the quality of signal content of these models can contribute to accuracy of regional geoid models, as well. There are studies in the geodetic literature that showed the local enhancements of the GOCE mission to the regional gravity field modeling (Eshagh and Ebadi, 2013; Saari and Bilker-Koivula, 2018; Matsuo and Kuroishi, 2020; Borghi et al., 2020; Barzaghi et al., 2021). Moreover, this increase in the performance of global geopotential models contributed to the precise estimation of zero-level geopotential value of local vertical datums W_0^{LVD} within the efforts of height system unification studies (Gruber et al., 2012; Kotsakis et al., 2012; Vergos et al., 2018; Zhang et al., 2022).

The assessment of the GOCE based global geopotential models were conducted with both local and global data sets to report the progress made in the releases of GOCE models, and to clarify the achievement made by GOCE satellite mission (Gruber et al., 2011; Hirt et al., 2011; Pail et al., 2011; Rexer et al., 2014; Godah et al., 2018). These studies showed the contribution of GOCE satellite data to the medium wavelengths of gravity field in different regions. In Turkey, the performance of the third releases of direct (DIR) and time-wise (TIM) models, second releases of space-wise (SPW) and GOCO models, together with GRACE-only ITG2010S model, were presented in Ince et al. (2014). Later, Erol et al. (2020a) presented the assessment of all releases of DIR, TIM and SPW model series, GOCO05S and GOGRA04 models against the same GPS/leveling data set used in Ince et al. (2014), over the entire country. Erol et al. (2020a) expanded the validation with a closer look to the Marmara region (North-West of Turkey) with 81 GPS/leveling stations. All studies conducted in Turkey clearly showed the improvement in the medium wavelength components in the gravity field, specifically in the western parts of Turkey where there are precise local GPS/leveling networks. Nonetheless, the country-wide comparisons in these three studies failed to enunciate the contribution of GOCE considering the limited number of stations. Aside from the comparisons with GPS/leveling data, Simav and Yildiz (2019) presented the evaluation of the fifth releases of DIR, TIM, SPW and GOCO models against the densified network of relative gravity sites and 16 absolute gravity sites located in the

south-west part of Turkey, and showed the improvements in the gravity signals between 120 and 190 degrees.

This study presents the evaluation of GOCE based global geopotential models in Turkey using 100 GPS/leveling benchmarks distributed homogeneously throughout the entire country. All releases of satellite-only models that are developed based on DIR (R1 - R6), TIM (R1 - R6), SPW (R1 - R5), and GOCO (R1 - R6) model series were tested in the assessment. In this evaluation, global geopotential models, that represent only the part of the spectrum constrained by their maximum degree of expansion, were enhanced spectrally to match their signal content with the observation data which contains the full spectrum of the gravity signal. In this spectral enhancement method, the spectrum beyond the expansion degree of model was completed by an ultra-high resolution model EGM2008 (Pavlis et al., 2012) and residual terrain effect computed from ERTM2160 model (Hirt et al., 2014). The global geopotential model that showed the best agreement with the observation data has been used in the gravimetric geoid modeling based on the least squares modification of Stokes integral with additive corrections technique (LSMSA) (Sjöberg, 2003b). In geoid modeling, an additional reference geopotential model was created by mixing the best performing GOCE model and EGM2008. To ensure a smooth transition between the coefficients of two models, linear blending technique (Gilardoni et al., 2013) was applied to two coefficient sets near the optimum degree of the GOCE model. The contribution of the GOCE model to the accuracy of the gravimetric geoid model was clarified as a result of its comparison with the accuracy of gravimetric geoid model computed with EGM2008 model as the reference model.

This paper consists of five sections. This section introduces the background and objective of the study. Section 5.2 includes the theoretical background on the accuracy assessment procedure of global geopotential models, as well as the formulation for gravimetric geoid modeling. In Section 5.3, the tested global geopotential models are given together with the data used for the spectral enhancement method. The section follows with the explanation of the terrestrial gravity data and briefly describes the pre-processing of gravity anomaly grid for the gravimetric geoid modeling. The results and discussions on the GOCE based global geopotential model evaluations

and the contribution of mixed global geopotential model to the performance of the experimental gravimetric geoid models were presented in Section 5.4. The findings of this paper are summarized in Section 5.5.

5.2 Methodology

5.2.1 Spectral enhancement method

The quasi-geoid heights (ζ) can be calculated using coefficients of disturbing potential via spherical harmonic expansions as,

$$\zeta_{GGM} = \frac{GM}{r\gamma} \sum_{n=2}^{n_{max}} \left(\frac{a}{r}\right)^n \sum_{m=0}^n (\Delta\bar{C}_{nm} \cos m\lambda + \bar{S}_{nm} \sin m\lambda) \bar{P}_{nm}(\cos \theta) \quad (5.1)$$

where G is the gravitational constant, M is the mass of the Earth, a is the semi-major radius and γ is the normal gravity of the reference ellipsoid, $\Delta\bar{C}_{nm}$ and \bar{S}_{nm} are the spherical harmonic coefficients of disturbing potential at degree n and order m , \bar{P}_{nm} is the fully normalized Legendre functions, and finally θ , λ and r are the coordinates of the computation point which are co-latitude, longitude, and local radius, respectively. Since the coefficients of global geopotential model represent the gravity potential W , normal potential must be removed from the gravity potential to form disturbing potential T where $T = W - U$. This is handled as,

$$\Delta\bar{C}_{nm} = \bar{C}_{nm}^W - \bar{C}_{nm}^U \quad (5.2)$$

where \bar{C}_{nm}^W and \bar{C}_{nm}^U are the spherical harmonic coefficients of gravity potential W and normal potential U , respectively. Because of rotational and equatorial symmetry of normal potential, \bar{C}_{nm}^U contains only even zonal harmonics (Barthelmes, 2009).

In case the physical heights of the GPS/leveling stations are orthometric heights, as opposed to normal heights, the quasi-geoid heights, calculated from global geopotential model using Equation 5.1, must be converted to geoid heights using geoid-to-quasigeoid separation term. This term can be approximated using the simple Bouguer anomaly Δg_{BA} , the mean normal gravity $\bar{\gamma}$, and the orthometric height H at the computation point as (Hofmann-Wellenhof and Moritz, 2006, Eq. 8-113),

$$N - \zeta = \frac{\Delta g_{BA}}{\bar{\gamma}} H \quad (5.3)$$

While evaluating the performance of GGMs using GPS/leveling data in an absolute sense, the geoid heights from GGMs are compared with the geoid heights derived from the GPS/leveling observations. These observations, in nature, contain the full spectrum of the gravity signal, as opposed to the ones computed from global geopotential models. The geoid heights computed from the spherical harmonic expansions, as formulated in Equation 5.1, contain gravity signals up to a degree of expansion to which the global geopotential model is opened up. This shortage in the contained gravity signal is caused by the limitation of global geopotential model constrained by its maximum degree of expansion. The absence of gravity signals above the maximum degree in spherical harmonic expansion causes an error called *omission error* (Hirt et al., 2011).

In order to make the global geopotential model and observation data spectrally comparable and remove the effect of omission error as much as possible, the model can be enhanced by using another model with higher expansion degree (possibly an ultra-high resolution model) and residual terrain model to complete the short-scale gravity signals. The evaluation of geoid heights calculated from GGMs based on spectral enhancement method is as follow (Hirt et al., 2011),

$$N_{res} = N_{GPS/leveling} - \left(N_0 + N^{GOCE}|_2^n + N^{EGM2008}|_{n+1}^{2159} + N^{RTE}|_{2160}^{\infty} \right) \quad (5.4)$$

where N_{res} is the residual geoid heights, $N_{GPS/leveling}$ is the geoid heights derived from ellipsoidal height and orthometric heights at control station, N_0 is the zero-degree term geoid height, $N^{GOCE}|_2^n$ is the geoid height calculated from GOCE model in evaluation using harmonic degrees from 2 to n , $N^{EGM2008}|_{n+1}^{2159}$ is the geoid height calculated from a high resolution model such as EGM2008, and $N^{RTE}|_{2160}^{\infty}$ is the geoid height that represents the short wavelength signals beyond maximum degree of high resolution model $n_{max} = 2160$.

In Equation 5.4, the spherical harmonic expansion starts from degree 2, omitting the terms formed by zero-degree and first-degree. With the choice of coordinate system that coincides with the geo-center of the Earth, the first degree terms can be easily omitted. The zero-degree term is handled externally to account for different mass estimates of the global geopotential model that represents the gravity potential W and

the reference ellipsoid that represents the normal potential U in the computation of disturbing potential. The zero-degree term geoid height, given in Equation 5.4, is computed as follow (Sánchez and Sideris, 2017):

$$N_0 = \frac{(GM_{GGM} - GM_{ELL})}{r_{P_0}\gamma_{Q_0}} - \frac{W_0 - U_0}{\gamma_{Q_0}} \quad (5.5)$$

where r_{P_0} is the geocentric radial distance for the computation point, and γ_{Q_0} is the normal gravity on reference ellipsoid. The first term on the right-hand side of Equation 5.5 represents the component of zero-degree term caused by the mass difference δM between the global geopotential model and the reference ellipsoid ($\delta M = M_{GGM} - M_{ELL}$). The second term, on the other hand, is the result of the difference between the potential of the Earth W_0 , represented by the conventional value adopted by International Association of Geodesy (Sánchez et al., 2016), and the normal potential of the reference ellipsoid.

Residual Terrain Model (RTM) represents the forward modelling of gravity to achieve the short-scale gravity signals occurred by the existence of topographic masses. The residual terrain effect can be computed as,

$$N_{RTE} = 2\pi G\rho (H - H_{ref}) - c \quad (5.6)$$

where ρ is the mass density of Earth in land areas which can be approximated as 2.67 g/cm^3 , H is the orthometric height of the computation point, H_{ref} is mean reference surface from which the attraction is computed, and finally, c is the terrain correction term (Forsberg, 1984).

5.2.2 Gravimetric geoid modeling

The Stokes integral enables the computation of geoid using gravity observations, as the solution of geodetic boundary value problem. In this computation, there are certain assumptions and requirements to be able to model the geoid surface. One of which is the necessity of gravity data in the entire Earth since the integration is done globally for each computation point. This is not possible in practice for many reasons. The implementation of Stokes' integral in small region causes a truncation error. Furthermore, the absence of gravity observations outside the computation region,

and the limitations of the spatial resolution of the terrestrial gravity data set result in long-wavelength errors in the gravity field. These problems create the necessity to modify the Stokes' kernel. With the first study conducted by Molodenskii et al. (1962), and many more that attempt to modify the Stokes kernel in a deterministic or stochastic approach, the foundations of today's precise techniques of gravimetric geoid modeling is built. See Ellmann (2005a) for details of the prominent modification methods of Stokes integral with a case study for geoid modeling in Baltic countries. Sjöberg (2003b) proposes a new technique to determine gravimetric geoid by using spectrally modified Stokes kernel that deals with the truncation error, as well as the spectral weighting of satellite and terrestrial gravity data determined by their error information. In this method, the least squares modification of Stokes' formula is implemented to minimize the expected global mean square error by optimally combining global geopotential model and terrestrial gravity data. The main formula of this methodology is given as,

$$\hat{N} = \tilde{N} + \delta N_{COMB}^{TOPO} + \delta N_{COMB}^{DWC} + \delta N_{comb}^{ATM} + \delta N_{COMB}^{ELL} \quad (5.7)$$

where the first term on the right-hand side represents the approximate geoid heights, and the rest of the terms represent the so-called additive corrections to calculate the detailed geoid model.

The approximate geoid height \tilde{N} ,

$$\tilde{N} = \frac{R}{4\pi\gamma} \iint_{\sigma_0} S^L(\psi) \Delta g d\sigma + c \sum_{n=2}^M (s_n + Q_n^L) \Delta g_n^{GGM} \quad (5.8)$$

where the first term in the right-hand side of Equation 5.8 is the near-zone component calculated using the surface gravity anomalies Δg within the integration cap σ_0 via modified Stokes' kernel. The second term in this equation is the far-zone component of the geoid signal calculated from global geopotential model via Laplace harmonics of gravity anomalies Δg_n^{GGM} (Hofmann-Wellenhof and Moritz, 2006, Eq. 9-18).

Out of the corrections given in Equation 3.12, δN_{COMB}^{TOPO} is the combined topographic correction to deal with both direct and indirect topographic effects of the mass above the geoid surface (Sjöberg, 2007). δN_{COMB}^{DWC} is the combined downward continuation

correction to take into account the use of surface gravity anomalies in modified Stokes' integral, as opposed to gravity anomalies on geoid surface. This gives an advantage of not dealing with the downward continuation of gravity anomalies to the geoid surface, which is an ill-posed problem, but rather computing its effect directly on the geoid (Sjöberg, 2003c). δN_{comb}^{ATM} is the combined atmospheric correction for the atmospheric mass (Sjöberg and Nahavandchi, 2000), and finally, δN_{COMB}^{ELL} is the combined ellipsoidal correction for the spherical approximation of Stokes' integral in the computation of geoid (Sjöberg, 2004b).

5.3 Study Area and Data Set

The validation of global geopotential models and gravimetric geoid modeling were carried out in Turkey, between latitudes $36^{\circ} \leq \varphi \leq 42^{\circ}$ and longitudes $26^{\circ} \leq \lambda \leq 45^{\circ}$. In this section, we started by introducing GOCE-based global geopotential model that were used in the assessment, and continue with residual terrain model used to enhance these models spectrally. Following that, we presented the gravity data set used for the gravimetric geoid modeling and briefly explained its pre-processing steps. Finally, we described the GPS/leveling data set that was used to evaluate both global geopotential models and calculated experimental gravimetric geoid models in this study.

5.3.1 Global geopotential models

From March 17th, 2009 to November 11th, 2013, GOCE continued to revolve in its orbit with approximately 250 km altitude, providing an unprecedented detail of the stationary gravity field of Earth. The mission flew in its unusually low orbital height for four years, measuring the second derivative of the gravity potential using satellite gravity gradiometer (SGG) while being its orbit was tracked via high-to-low satellite to satellite tracking (hl-SST). The aim of the mission was to determine gravity anomalies with an accuracy of 1 *mGal* and the geoid with 1 – 2 *cm* at 100 *km* spatial resolution, corresponding to 200 degree/order harmonic expansion (Rummel, 2012).

So far, various gravity field solutions have been computed using GOCE satellite data. Specifically, the solutions of High-Level Processing Facility (HPF) of GOCE are of great importance for the processing GOCE data to produce gravity field solution using

three different approaches, namely direct, time-wise, and space-wise. The first releases of these model series include only 2 months of GOCE data. The second, third and the forth releases were computed using 8 months, 18 months, and 33 months of GOCE observations, respectively. The full mission data (48 months) is used for the fifth and sixth releases.

DIR approach is based on the computation of spherical harmonic coefficients using an iterative solution of SST and SGG normal equations together that are formed for each batches of 24 hours (daily) arcs. The normal equations of daily arcs are then stacked, and solved by using Cholesky decomposition. This approach requires a-priori weights from a reference gravity field model (Pail et al., 2011). In the first release of DIR models (DIR-R1), the a-priori gravity field information is taken from EIGEN5C model up to degree/order 360. In the second release (DIR-R2), the reference model is replaced by ITG-Grace2010s model up to 150 degree/order. The releases after DIR-R2 are used one release before as the a-priori model. In the TIM computation schema, SST and SGG data measured along the satellite orbit are treated as a time series. The gravity field models computed using TIM approach are pure GOCE solutions, containing no other measurements from CHAMP, GRACE or a-priori model. This is beneficial in terms of seeing how good of a solution can be achieved based on solely GOCE observation. SPW approach, on the other hand, is based on the solution of least squares collocation that uses spatial correlation of the gravity field with the distance to form a signal covariance. The method deals with the SST and SGG measurements in the spatial domain, as opposed to time/frequency domain, by gridding them via least squares collocation, as well. As a prior model, the first release (SPW-R1) uses EGM2008 in very low degrees and Quick-look gravity field model. From the second release (SPW-R2) to the last (SPW-R5), aside from the use of EIGEN model series for the signal covariance modeling and FES2004 tide model for ocean tide modeling, no a-priori model is used, which makes these releases GOCE-only solutions. For more details about the philosophy behind these methodologies and the computation schema of these approaches are well discussed in (Pail et al., 2011). To exploit GOCE satellite mission at best, the combination of the observations from other dedicated missions provides a better representation of long-wavelength signals. In this context,

the initiative called Gravity Observation Combination (GOCO) provides gravity field solutions for satellite-only models by combining the data from CHAMP, GRACE, GOCE and SLR (Pail et al., 2010b).

In this study, all releases of DIR (Bruinsma et al., 2010, 2013, 2014), TIM (Pail et al., 2010a, 2011; Brockmann et al., 2014, 2019), SPW (Migliaccio et al., 2010, 2011; Gatti et al., 2014, 2016) and GOCO (Pail et al., 2010b; Goiginger et al., 2011; Mayer-Gürr, 2012; Mayer-Gürr, 2015; Kvas et al., 2021) satellite-only models were included in determination of the most suitable GOCE-based global geopotential model for Turkey. The satellite data content and maximum degree of expansion of these models are given in Table 5.1.

Table 5.1 : Tested global geopotential models and their data content.

Model	Max degree	Data
DIR R1	240	GOCE(2m)
DIR R2	240	GOCE(8m)
DIR R3	240	GOCE(18m), GRACE(6.5y), SLR(6.5y)
DIR R4	260	GOCE(33m), GRACE(9y), SLR(>10y)
DIR R5	300	GOCE(48m), GRACE(>10y), SLR(>10y)
DIR R6	300	GOCE(48m), GRACE(>10y), SLR(>10y)
TIM R1	224	GOCE(2m)
TIM R2	250	GOCE(8m)
TIM R3	250	GOCE(18m)
TIM R4	250	GOCE(33m)
TIM R5	250	GOCE(48m)
TIM R6	300	GOCE(48m)
SPW R1	210	GOCE(2m)
SPW R2	240	GOCE(8m)
SPW R4	280	GOCE(33m)
SPW R5	330	GOCE(48m)
GOCO0S R1	224	GOCE(2m), GRACE(7.5y)
GOCO0S R2	250	GOCE(8m), GRACE(7.5y), SLR(5y)
GOCO0S R3	250	GOCE(18m), GRACE(7.5y), SLR(5y)
GOCO0S R5	280	GOCE(48m), GRACE(10.5y), CHAMP(6y), SLR(>10y)
GOCO0S R6	300	GOCE(48m), GRACE(15.5y), CHAMP(6y), SLR(>10y)

*m: month, y: year

5.3.2 Residual terrain model

Residual terrain models are used in many geodetic and geophysical applications that require the high frequency, accordingly short wavelength, gravity signal information. These models are mainly used in completion of gravity signals beyond the expansion degree of a global geopotential model to augment its spectral content. Another frequent use of RTM is seen in studies that deals with smoothing the gravity observations, either terrestrial or airborne, before interpolating them to create a gridded data (i.e remove-grid-restore), or to reduce the computational error of upward/downward continuation. Additionally, it is one of the main steps of well-known geoid modeling technique, remove-compute-restore.

In this study, our intent to use RTM is to enhance the global geopotential models spectrally beyond 2159 degree/order. We used ERTM2160 computed from 7.5" resolution SRTM topography that corresponds to the signal content between $\sim 10\ km$ to $\sim 250\ m$ (Hirt et al., 2014). The model includes the high frequency gravity signals for four gravity field parameters, namely quasigeoid/geoid, gravity disturbance, and North-South and East-West components of vertical deflection according to Helmert's definition. Since we are only interested to validate the global geopotential models against GPS/leveling data, we used only RTM effects on geoid. Figure 5.1 shows the magnitude of residual terrain effects from ERTM2160 model on geoid in Turkey, along with its statistics.

5.3.3 Gravity data

The gravity measurements, shown as blue scattered points in Figure 5.2, has been collected by the General Directorate of Mineral Research and Exploration (GDMRE) (Arslan, 2016). The data set originally contains 64,469 gravity measurements with 3.5 km spacing throughout the country. However, it must be noted that we only have the gridded version of the gravity data as a complete Bouguer anomaly. The scattered gravity data is not open for scientific use. This archival data set originally was tied to the Potsdam datum for the gravity. We added $-14\ mGal$ to the grid values to convert

it to International Gravity Standardization Net 1971 (IGSN71) datum. GDMRE processed the reduction the gravity data by taking the mass density of Bouguer plate as 2.67 g/cm^3 while assuming a mass density of topography as 2.40 g/cm^3 in the terrain correction. The effect of terrain on the gravity measurements was computed within 6.65 km radius for each gravity point, as the original data includes the terrain correction up to J-zone in Hammer chart (Hammer, 1939). To comply with these pre-processing parameters applied by GDMRE, we have employed the same parameters in the conversion of complete Bouguer anomalies to free-air anomalies. Finally, the normal gravity values that were originally calculated using GRS67 reference ellipsoid were converted to GRS80 ellipsoid. The complete (or refined) Bouguer anomalies were converted to free-air gravity anomalies to be used as an input for the gravimetric geoid modeling. Please refer to Isik et al. (2022b) for details of the processing of GDMRE complete Bouger anomaly grid for the computation of free-air anomalies shown in Figure 5.3.

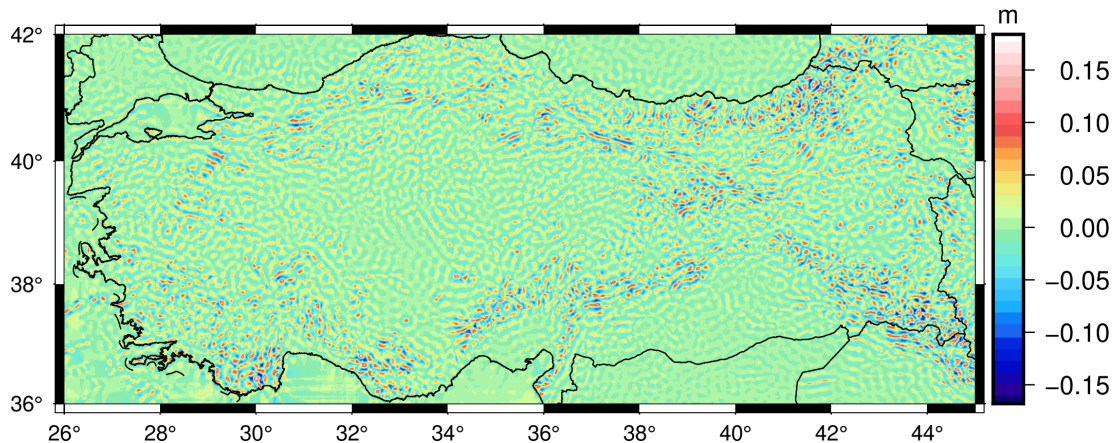


Figure 5.1 : Residual terrain effects on geoid from ERTM2160 model (*Minimum = -0.168 m , Maximum = 0.184 m , Mean = 0.000 m , SD = 0.025 m*).

5.3.4 Validation data set

In this study, we used 100 GPS/leveling stations that are part of common benchmarks of the Turkish National Fundamental GPS Network (TUTGA) and the Turkish National Vertical Control Network 1999 (TUDKA99). The GPS measurements in these benchmarks are at least 8 hours long, and the coordinates are in International Terrestrial Reference Frame 1996 (ITRF96) datum. The physical heights, on the other

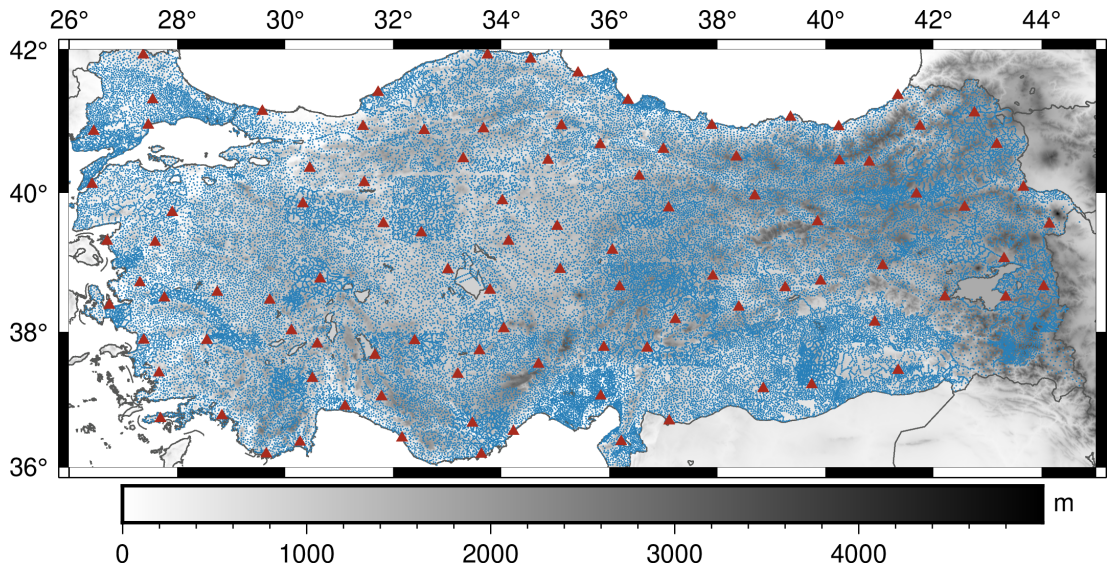


Figure 5.2 : Location of gravity measurements (blue points) and GPS/leveling benchmarks (red triangles) on topography of Turkey.

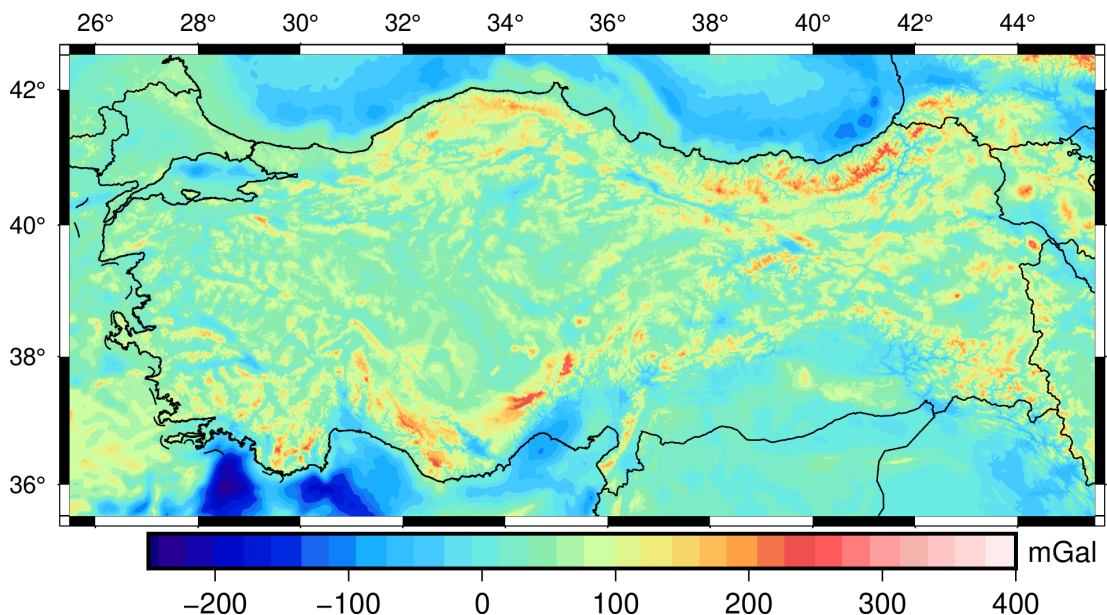


Figure 5.3 : Free-air anomaly grid used in this study ($\text{Min} = -236.2 \text{ mGal}$, $\text{Max} = 300.8 \text{ mGal}$, $\text{Mean} = 35.1 \text{ mGal}$, $\text{STD} = 55.6 \text{ mGal}$).

hand, are Helmert orthometric heights measured according to the regulation for the 1st order leveling network requirements with forward and backward leveling. The accuracy of these GPS/leveling data set is reported as $\sim 1 - 3 \text{ cm}$ (Ayhan et al., 2002). The distribution of the GPS/leveling stations above the topography of Turkey from SRTM 3" resolution digital elevation model (Jarvis et al., 2008) is given in Figure 5.2.

The geoid heights at GPS/leveling stations are computed as,

$$N_{GPS/leveling} = h - H \quad (5.9)$$

where h is the ellipsoidal height from GPS measurements and H is the Helmert orthometric height from geometric leveling. In the validation of geoid models, either gravimetric geoid or synthesized from global geopotential models, the geoid heights refer to tide-free permanent tide system. By convention, the ellipsoidal heights are computed in tide-free system. In order to make GPS/leveling derived geoid heights comparable with the others, the permanent tide system of Helmert orthometric heights at GPS/leveling stations were converted from mean-tide to tide-free system as,

$$H^{\text{tide free}} = H^{\text{mean tide}} - 0.68 (0.099 - 0.296 \sin^2 \varphi) \quad (5.10)$$

where $H^{\text{tide free}}$ and $H^{\text{mean tide}}$ are the tide-free (or non-tidal) mean-tide orthometric heights, and φ is the latitude of the GPS/leveling station (Ekman, 1989).

5.4 Results and Discussions

5.4.1 Evaluation of global geopotential models

We applied spectral enhancement to all global geopotential models given in Section 5.3.1 to calculate geoid heights for each degree of expansion from $n = 2$ to $n = n_{\max}$ with one degree/order increment. The zero-degree term geoid height N_0 was added to account for the systematic difference between the mean earth ellipsoid of global geopotential model and GRS80 ellipsoid on which we adopted to reference the computations. All computations of geoid heights were carried out in tide-free permanent tide system.

The standard deviations of residual geoid heights for each spectrally enhanced GOCE model are presented in Figure 5.4. The horizontal axis of the figures represents the degree to which the tested GOCE model is opened up. The rest of the gravity signals beyond this degree was filled from EGM2008 up to 2159 degree and residual terrain effect from 2159 to 90,000. The black dashed line represents the standard deviation achieved by expanding EGM2008 up to 2159 degree/order and enhancing with residual terrain effect, which corresponds to 14.1 cm accuracy.

In all four figures that represent performance of different model series, the contribution of GOCE mission between ~ 100 degree/order and ~ 250 degree/order is visible. The geoid heights from all releases of model series showed better agreement with the geoid heights at GPS/leveling benchmarks compared to EGM2008 model in these spectral bands. The results clearly show the improvement in the accuracy of models from first releases to the last for all model groups. The increase in the amount of GOCE satellite data led to a decrease in the standard deviations, as well as the spectral window of bands that showed improvement over EGM2008 is wider in the latest releases.

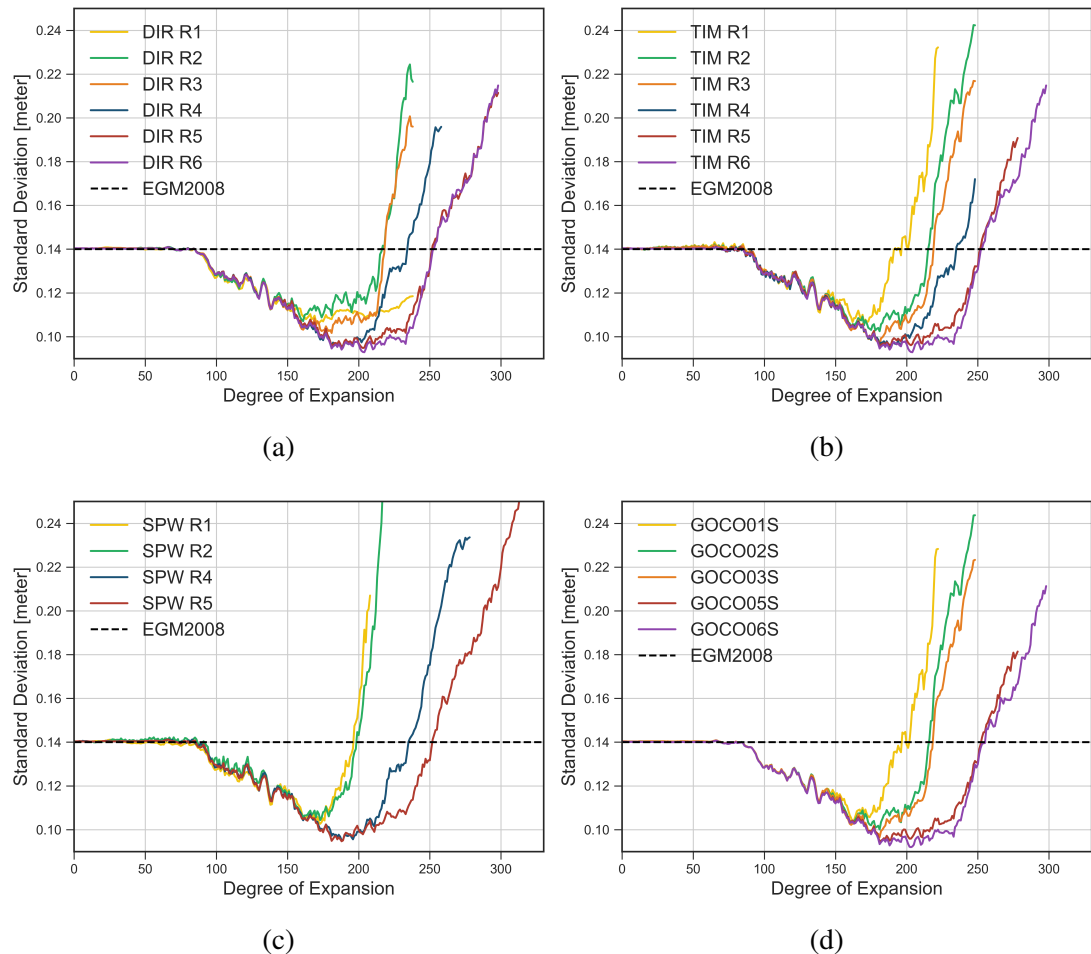


Figure 5.4 : Standard deviations of spectrally enhanced GOCE models at each expansion degree: (a) DIR models, (b) TIM models, (c) SPW models, and (d) GOCO models.

For DIR, TIM, and GOCO model series, the fifth and sixth releases showed similar improvements. Between ~ 200 and ~ 245 degree/order of the spectrum, the sixth releases of TIM and GOCO exceeded the performance of the fifth releases. Their

performances can be considered as equal outside of these spectral bands. For SPW model series, the fourth and the fifth releases gave almost the same result up to the degree/order ~ 210 . The fifth (and final) release became prominent after this degree, and SPW-R5 showed 5 cm better agreement at the maximum degree of SPW-R4 ($n_{max} = 280$).

From the first to the last releases, we see over 10% improvements in standard deviations of model series. With 9.3 cm accuracy around ~ 205 degree/order expansion, DIR-R6, TIM-R6, and GOCO06S models were found to be the best performing models in Turkey. The overall view of the best performing degree of GGMs are presented with their standard deviations and means in Figure 5.5.

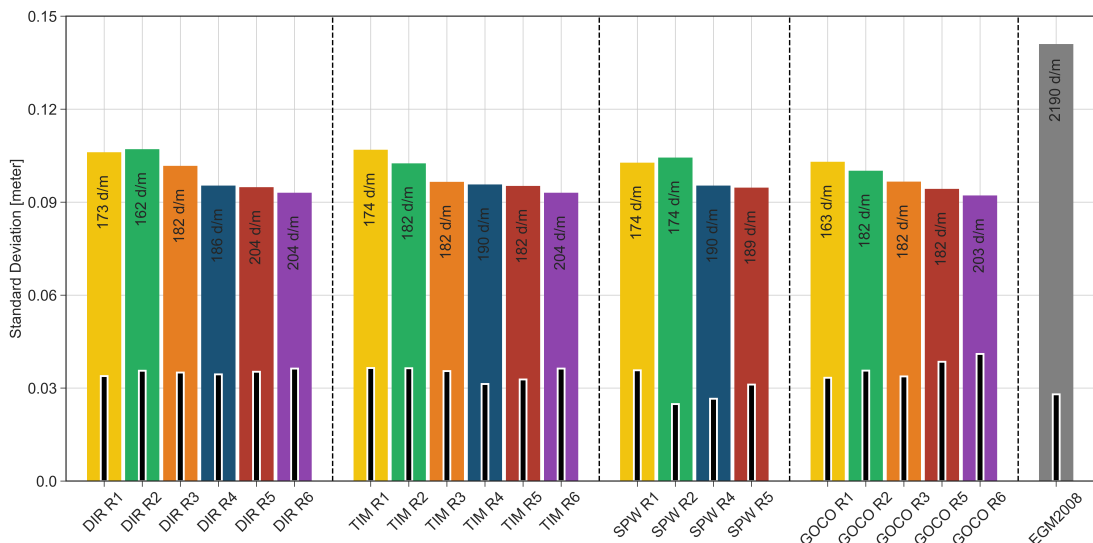


Figure 5.5 : The standard deviation (colored bars) of spectrally enhanced GOCE models at optimum expansion degree and their mean values (black bars).

5.4.2 Evaluation of gravimetric geoid models

We implemented the least squares modification of Stokes' integral approach to model the gravimetric geoid in Turkey based on EGM2008 and TIM-R6 global geopotential models. As a combined model with ultra-high resolution, EGM2008 was used in many regional geoid models, not only for former official Turkey Geoid models but also for other countries as well. Additionally, it was computed before GOCE era which makes this model valuable for showing the contribution of GOCE mission. As the best global geopotential model with smallest standard deviation against GPS/leveling

data set, TIM-R6 is the most suitable model to clearly show the improvements in the gravimetric geoid model, considering it is a pure GOCE model.

The experimental geoid models were computed in tide-free system and zero-degree term was calculated w.r.t. GRS80 reference ellipsoid. In the computation of the least squares modification parameters s_n and Q_n^L , the integration radius around the computation points was taken as $\psi_0 = 0.25^\circ$ in the Stokes' integral. The error degree variance of gravity anomalies were constructed using a band-limited white noise model where standard deviation is taken as $\sigma_{\Delta g} = 5 \text{ mGal}$. The values of modification parameters for the gravimetric geoid modeling were adopted from the experimentation conducted by Isik et al. (2022b) to empirically determine the optimum values of modification parameters ($\psi_0 = 0.25^\circ$, $M = 360$, and $\sigma_{\Delta g} = 5 \text{ mGal}$) for LSMSA technique in Turkey.

As an expansion (M) and modification degree (L) where $M = L$, we first implemented a modification degree $M = 205$ for gravimetric geoid models computed with EGM2008 (expGeoid-1) and TIM-R6 (expGeoid-2), since this expansion degree was found as the optimum degree for the last releases of GOCE models. Later, the global geopotential models were opened up to 360 degree to enhance the geoid accuracy. Though this degree can be implemented for EGM2008 model (expGeoid-3), it is not possible for TIM-R6 model because of its limited maximum degree ($n_{max}^{TIM-R6} = 300$). To improve the gravimetric modeling results, we combined the coefficients of EGM2008 with TIM-R6 model to make a mixed model up to 360 degree/order, as this degree was found as the optimum for regional geoid in Turkey (Isik et al., 2022b). The maximum combination degree of EGM2008 and GOCE model was determined based on the assessment results of TIM-R6 model using spectral enhancement method. The optimum combination degree was found to be 205 for GOCE model where the rest of the gravity spectrum was filled with EGM2008 and RTM. From degree $n = 2$ to $n = 205$, TIM-R6 model coefficients were used. The gravity spectrum between degree $215 - 360$ is filled with EGM2008 coefficients. The coefficients in spectral band between $205 - 215$, were determined by taking the mean of the coefficients of two models based on weights determined by their error information in order to blend the coefficients of two models linearly, as in the earlier studies that combined

EGM2008 with GOCE model to improve the long-wavelength signal (Gilardoni et al., 2013; Forsberg et al., 2014; Vu et al., 2019).

$$T_{mn} = \left[\frac{T_{mn}^{EGM2008}}{\left(\sigma_{T_{mn}}^2\right)^{EGM2008}} + \frac{T_{mn}^{TIM}}{\left(\sigma_{T_{mn}}^2\right)^{TIM}} \right] \left[\frac{1}{\left(\sigma_{T_{mn}}^2\right)^{EGM2008}} + \frac{1}{\left(\sigma_{T_{mn}}^2\right)^{TIM}} \right]^{-1} \quad (5.11)$$

where T_{mn} represents the new coefficients C_{mn} and S_{mn} of disturbing potential T , $T_{mn}^{EGM2008}$ and T_{mn}^{TIM} represent the corresponding coefficients of EGM2008 and TIM-R6 models, and $(\sigma_{T_{mn}}^2)^{EGM2008}$ and $(\sigma_{T_{mn}}^2)^{TIM}$ are the degree variances of $T_{mn}^{EGM2008}$ and T_{mn}^{TIM} , respectively. For more details about the methodology, please refer to Gilardoni et al. (2013).

The statistics of residual geoid heights computed from the gravimetric geoid models at GPS/leveling stations are given in Table 5.2, together with the statistics of the residual geoid heights after the geoid models were fitted to local vertical datum at GPS/leveling stations using seven parameter Helmert similarity transform (Fotopoulos, 2013). The experimental geoid models computed with EGM2008 and TIM-R6 models up to 205 degree/order expansion, namely expGeoid-1 and expGeoid-2, have shown 20 cm accuracy against GPS/leveling data set. Both models failed to supersede the performance of EGM2008 global geopotential model up to 2159 degree/order. The gravimetric geoid model computed with EGM2008 up to 360 degree/order (expGeoid-3) has the standard deviation of 11.5 cm (10.3 cm after-fit). The gravimetric geoid model computed with the mixed geopotential model (expGeoid-4) has shown 8.9 cm (7.7 cm after-fit). The results showed that the use of mixed geopotential model as a long-wavelength source has led to an improvement of $\sim 30\%$ in the accuracy of gravimetric geoid model.

The distribution of geoid height differences for the gravimetric geoid models computed using the EGM2008 (expGeoid-3) and the TIM-R6/EGM2008 mixed global geopotential model (expGeoid-4) at GPS/leveling benchmarks were plotted in Figure 5.6a and Figure 5.6b over topography of Turkey. The residual geoid heights for expGeoid-4 model are significantly smaller compared to expGeoid-3. The contribution of GOCE resulted in a decrease of 18.6 cm in the range of residual geoid heights, from 66.7 cm for expGeoid-3 to 48.1 cm for expGeoid-4. The varying behavior of these two

Table 5.2 : Statistics of gravimetric geoid model accuracy computed using TIM R6 and EGM2008 models. [unit: cm].

Geoid Model	Reference GGM		Min	Max	Mean	STD
expGeoid-1	EGM2008 ($M = 205$)	Before fit	-62.7	56.6	-1.2	20.5
		After fit	-50.5	59.7	0.0	19.3
expGeoid-2	TIM-R6 ($M = 205$)	Before fit	-58.5	53.2	-0.2	20.1
		After fit	-50.0	42.0	0.0	18.4
expGeoid-3	EGM2008 ($M = 360$)	Before fit	-37.0	29.7	-0.3	11.5
		After fit	-33.9	35.6	0.0	10.3
expGeoid-4	TIM-R6 + EGM2008 (mixed model - $M = 360$)	Before fit	-24.6	23.5	0.7	8.9
		After fit	-20.2	17.5	0.0	7.7

gravimetric geoid models, given as a difference grid in Figure 5.6c, can be attributed to the large amplitudes of long-wavelength geoid differences between EGM2008 and TIM-R6 model up to 205 degree/order expansion (Figure 5.6d). Since the expansion degree of both models in Figure 5.6d is the same, the geoid height differences are not affected by the omission errors of models. The large discrepancies between the residual geoid heights of expGeoid-3 and expGeoid-4 at GPS/leveling heights are visible in areas where the long-wavelength differences in Figure 5.6d are larger, specifically along the northern coastlines. A closer look to the north-east part of Turkey shows an abrupt change in the long-wavelength differences (from $\sim -70\text{ cm}$ to $\sim 50\text{ cm}$) between TIM-R6 and EGM2008 models.

The gravimetric geoid model, expGeoid-4, has shown the best performance compared to other three experimental geoid models against 100 GPS/leveling stations. Considering the accuracy of the geoid models reported by the previous studies that used the same terrestrial gravity data set, this model has the lowest standard deviation (Erol et al., 2020a). Most recently, the accuracy of the LSMSA geoid model computed using XGM2019e global geopotential model up to 360 degree/order was stated as 10.1 cm by Isik et al. (2022b), leading to $\sim 13.9\%$ better performance than expGeoid-3 and $\sim 13.5\%$ worse performance than expGeoid-4 at the same GPS/leveling benchmarks. Moreover, expGeoid-4 outperforms the geoid model presented by Isik et al. (2022b) in terms of the range of residual geoid heights by 5.2 cm . The models' performance

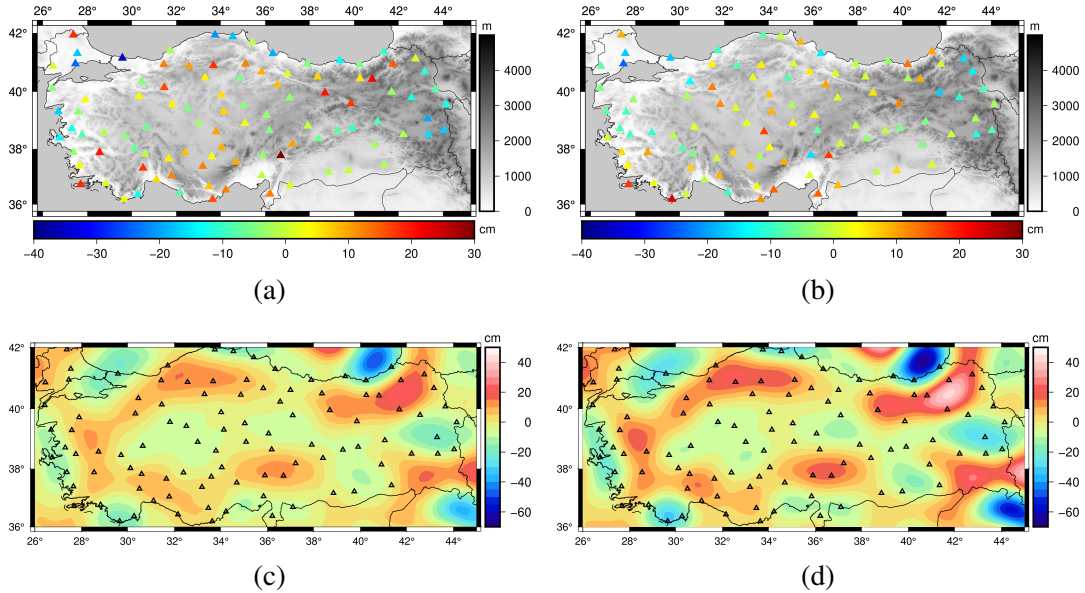


Figure 5.6 : Residual geoid heights of (a) gravimetric geoid model computed with EGM2008 (expGeoid-3) at GPS/leveling stations and (b) gravimetric geoid model computed with TIM-R6/EGM2008 mixed global geopotential model (expGeoid-4) at GPS/leveling stations. The long wavelength geoid height differences computed using TIM-R6 and EGM2008 GGMs at 205 degree/order are given in (c) where the statistics are: *Minimum = -49.8 cm, Maximum = 25.0 cm, Mean = -1.6 cm, SD = 9.3 cm.* Differences between expGeoid-3 and expGeoid-4 ($N_{\text{expGeoid-4}} - N_{\text{expGeoid-3}}$) are given in (d) where the statistics are: *Minimum = -67.0 cm, Maximum = 47.7 cm, Mean = -1.0 cm, SD = 13.9 cm.*

exceeds the accuracy of the gravimetric geoid model computed via least squares modification of Hotine's integral (LSMHA) method, which was reported as 10.4 cm by Isik et al. (2022a).

The expGeoid-4, as the gravimetric geoid model with the best standard deviation, is presented in Figure 5.7 together with its statistics. The accuracy of the geoid model after fitted to the local vertical datum at the GPS/leveling benchmarks is 7.7 cm.

5.5 Conclusions

In this study, the performances of DIR, TIM, SPW and GOCO satellite-only models were assessed based on their accuracy at 100 GPS/leveling benchmarks in Turkey. All releases of models, from release 1 to release 6, were included in the assessment. We applied the spectral enhancement method to the global geopotential models to complete the high-frequency part of their gravity spectrum using an ultra-high

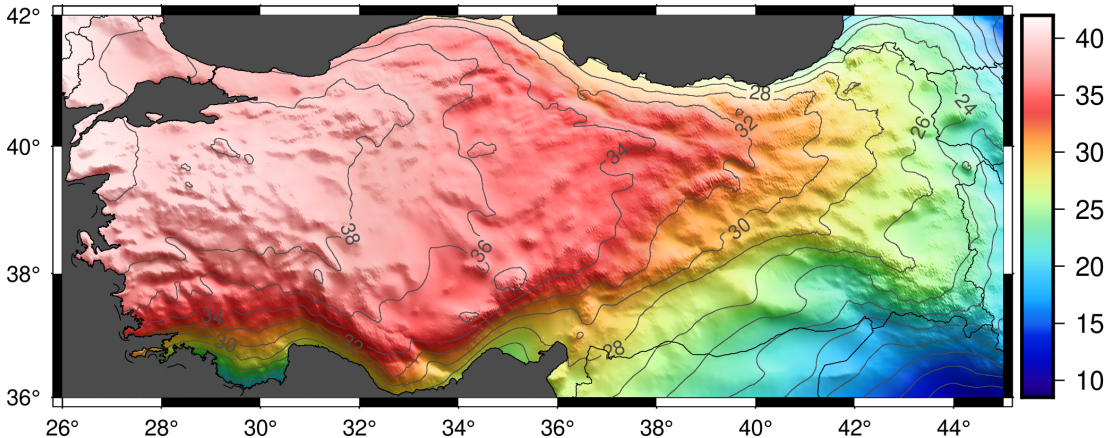


Figure 5.7 : Experimental gravimetric geoid model calculated with mixed global geopotential model as reference model (expGeoid-4; *Minimum* = 8.827 m, *Maximum* = 41.778 m, *Mean* = 30.793 m, *SD* = 6.781 m).

resolution geopotential model EGM2008 up to 2159 degree/order expansion and a residual terrain model to increase the coverage of the spectrum beyond 2160 degree/order up to $\sim 90,000$ degree/order. The results revealed the improvement from first release of model series to the last one, clearly. We observed a decrease in standard deviations of models as the amount of GOCE data increased. Since the time-span of the GOCE data is the same for the fifth and the sixth releases, we found the performance of these models quite close to each other in terms of optimum degree of expansions and their standard deviations, though there are spectral windows that the last releases of the model series showed superiority over the fifth, and by extension the earlier releases. Based on the statistical results, GOCE models showed up to 34% improvements in the standard deviation compared to the best accuracy achieved from EGM2008 model. DIR-R6, TIM-R6, and GOCO06S models have shown the best performance as 9.3 cm accuracy with their optimum expansion around 205 degree/order.

We produced a mixed global geopotential model by combining the coefficients of TIM-R6 GOCE model up to 205 degree and EGM2008 model from 215 to 360 degree. The coefficients in between were calculated by linear blending of two model's coefficients based on their error variances. This mixed model, along with the original version of TIM-R6 and EGM2008, were used in the computation of 1' resolution gravimetric geoid model via LSMSA technique. The mixed model has shown $\sim 23\%$ improvement over EGM2008 at the same expansion degree and

exceeded the best standard deviation achieved by expanding the EGM2008 model up to 2159 degree/order. It also takes the place of the gravimetric geoid models, reported in Isik et al. (2022a,b) recently, by showing approximately $\sim 12\% - 15\%$ better performance at the same GPS/leveling stations.

We conclusively showed the contribution of GOCE based global geopotential model to the gravimetric geoid modeling in Turkey. Currently, there are on-going initiatives to modernize the national vertical datum based on vertical control network, and replace it with a gravimetric geoid model with $1 - 3 \text{ cm}$ accuracy in Turkey. Accordingly, the terrestrial gravity database is being renewed and topographically challenging areas are being covered via airborne gravity campaigns. In this context, the findings of this study indicate a significant potential to increase the accuracy of regional geoid model and modernize the local vertical datum by replacing it with $1 - 3 \text{ cm}$ accuracy geoid model with the newly collected gravity data set. As the future work, GOCE-based models will be used as a base model for geoid modeling using the terrestrial and airborne gravity measurements in Turkey.

6. CONCLUSIONS

The Colorado geoid modeling studies for "the 1-cm geoid experiment", initiated under the IAG Joint Working Group 2.2.2, is of great importance to analyze the contribution of airborne gravity data geoid modeling in areas where gravity measurements are troublesome or geoid modeling is challenging. Colorado region is the 3rd stage of the geoid slope validation effort of NGS within the context of GRAV-D project (Smith, 2007). This study area has rough topography which makes the gravimetric geoid modelling challenging. The terrestrial gravity measurements have the shortage of spatial distribution in mountainous regions. Thus airborne gravity surveys provide quite essential information in these regions to be able to model highly accurate geoid.

In this first study, we presented our contributions to the "1 cm Colorado geoid experiment" initiated by IAG Joint Working Group 2.2.2 as Istanbul Technical University, Gravity Research Group (ITU-GRG). This paper presented the new geoid modeling solutions over Colorado using Stokes and Hotine Integrals, as well as the solution submitted to the Colorado experiment which is summarized in the paper, reported by Wang et al. (2021). In this study, we prepared three data set based on terrestrial-only, airborne-only and combined gravity data sets. Each data set was used to model the gravimetric geoid model of Colorado via least squares modification of Stokes integral (LSMSA) and Hotine integral (LSMHA) approaches. The performance of geoid models were tested at historical GPS/leveling data set and highly accurate GSVS17 benchmarks. As a result, we found that the combination of both terrestrial and airborne gravity data sets gave the best solutions for both methodologies. With 2.69 *cm* accuracy for LSMSA and 2.87 *cm* accuracy for LSMHA solutions, high resolution regional geoid model were successfully computed for Colorado experimentation. In conclusion, the contribution of airborne gravity data in topographically challenging region was shown.

Following the contribution brought by airborne gravimetry to the accuracy of gravimetric geoid of Colorado, we conducted series of studies that focused on the improvement of regional geoid model of Turkey by exploiting the latest GOCE-based global geopotential models and LSMSA and LSMHA which are proven to be successful approaches to compute high-resolution gravimetric geoid model.

In the second study, we investigated the effect of the densification of the complete Bouguer gravity anomaly grids obtained through planar and spherical approaches, respectively, on geoid modeling accuracy in Turkey. As the geoid model calculation method, the least squares modification of Stokes' integral with additive corrections method was used. We tested the calculated geoid models using homogeneously distributed GPS/leveling benchmarks as well as the tide-gauge stations along the surrounding coastlines. In conclusion, we obtained significant improvement in geoid model accuracy with using the densified gravity grid from the 5' to 1' resolution and restoring the attraction of the topographic masses through the appropriate schema. Densification of the Bouguer gravity anomaly grids with restored topographical effect has potential to improve geoid model accuracy using LSMSA method. Planar and spherical approximations in calculating complete Bouguer anomalies provide close results to each other.

In the third study, we investigated the use of gravity disturbances via Hotine's integral for gravimetric geoid modeling in Turkey. As the geoid model calculation method, we used the least squares modification of Hotine's integral with additive corrections (LSMHA), a promising new technique that gained importance with the availability of GNSS-derived heights for gravity measurements. We tested the calculated geoid models in terms of absolute and relative accuracy using two sets of GPS/leveling measurements. The first GPS/leveling dataset provides insight on the performance of the geoid model countrywide while the second dataset shows the local assessment results in the western part of Turkey where gravity measurements are of higher quality. In conclusion, we have shown that the use of Hotine's integral was shown promising results for modeling the regional gravimetric geoid in Turkey.

In the fourth study, we reported on the assessment of global geopotential models computed by ESA High Processing Facility, together with the Gravity Observation Combination (GOCO) model series over Turkey, and showed the contribution of GOCE-based models to the gravimetric geoid modeling. We believe the findings of this paper are significant for the re-definition of traditional vertical datums by introducing an accurate gravimetric geoid model, considering the enhancements in the long/medium wavelength signals of the gravity field achieved using GOCE observations. We evaluated the performance of GOCE based global geopotential models using Spectral Enhancement Method at GPS/leveling stations in Turkey to show the level of improvement brought by GOCE satellite mission data to the medium wavelength signals of Earth's gravity field. We reported that the latest releases of GOCE models exceed the performance of EGM2008 model by 34% around 205 degree of expansion. To show how it affects the gravimetric geoid modelling, we combined the sixth release of time-wise global geopotential model, which is a pure GOCE model, with EGM2008 ultra high-resolution model at the optimum degree using linear blending of two models' coefficients to form a mixed model up to 360 degree/order, and used it in the geoid modeling via least squares modification of Stokes' integral with additive corrections technique. We observed 23% improvement in the standard deviation compared to the gravimetric geoid model computed using EGM2008 as a reference model.

As a future work, it is aimed to combine the recently collected terrestrial gravity measurements and airborne gravity surveys conducted in Turkey. Though the spatial distribution of the new terrestrial gravity surveys is not high enough to model the geoid signals affected by the rough topography of Turkey, airborne gravity surveys are expected to close this gap. The new gravity database has the advantage of direct computation of gravity disturbances which promotes the use of Hotine integral in the gravimetric geoid modeling studies.

REFERENCES

- Abbak, R. A., Ellmann, A., and Ustun, A.** (2022). A practical software package for computing gravimetric geoid by the least squares modification of Hotine's formula. *Earth Science Informatics*, 15(1):713–724.
- Abbak, R. A., Erol, B., and Ustun, A.** (2012a). Comparison of the KTH and remove-compute-restore techniques to geoid modelling in a mountainous area. *Computers & Geosciences*, 48:31–40.
- Abbak, R. A., Sjöberg, L. E., Ellmann, A., and Ustun, A.** (2012b). A precise gravimetric geoid model in a mountainous area with scarce gravity data: a case study in central Turkey. *Studia Geophysica et Geodaetica*, 56(4):909–927.
- Ågren, J.** (2004). *Regional Geoid Determination Methods for the Era of Satellite Gravimetry Synthetic Earth Gravity Models*. PhD Thesis, KTH Royal Institute of Technology.
- Ågren, J. and Sjöberg, L. E.** (2014). Investigation of Gravity Data Requirements for a 5 mm-Quasigeoid Model over Sweden. In Marti, U., editor, *Gravity, geoid and height systems*, pages 143–150. Springer.
- Ågren, J., Sjöberg, L. E., and Kiamehr, R.** (2009). The new gravimetric quasigeoid model KTH08 over Sweden. *Journal of Applied Geodesy*, 3(3):143–153.
- Ahlgren, K., Wang, Y.-M., Li, X., and Youngman, M.** (2018). Towards a more consistent geoid model for north america. In *FIG Congress 2018 Proceedings*, Istanbul, Turkey.
- Alberts, B. and Klees, R.** (2004). A comparison of methods for the inversion of airborne gravity data. *Journal of Geodesy*, 78(1-2).
- Andersen, O., Knudsen, P., and Stenseng, L.** (2016). The DTU13 MSS (Mean Sea Surface) and MDT (Mean Dynamic Topography) from 20 Years of Satellite Altimetry. In Jin, S. and Barzaghi, R., editors, *IGFS 2014*, pages 111–121, Cham. Springer International Publishing.
- Arslan, S.** (2016). Geophysical regional gravity maps of Turkey and its general assessment. *Bulletin of the Mineral Research and Exploration*, 2016(153):203–222.
- Ayan, T.** (1976). *Astrogeodätische Geoidberechnung für das Gebiet der Türkei*. PhD Thesis, Geodätisches Institut, Universität Fridericiana Karlsruhe.

- Ayan, T.** (1978). Türkiye geoidi. *Harita Dergisi*, 85:5–17.
- Ayan, T., Deniz, R., Çelik, R. N., Denli, H. H., ÖzluDEMİR, M. T., Erol, S., Erol, B., Akyilmaz, O., and Güney, C.** (2001). *İzmir Geodetic Reference System-2001* (Technical Report 2000/2294). Istanbul: İstanbul Technical University.
- Ayhan, M. E.** (1993). Geoid determination in Turkey (TG-91). *Bulletin Géodésique*, 67(1):10–22.
- Ayhan, M. E., Demir, C., Lenk, O., Kılıçoglu, A., Aktuğ, B., Açıkgöz, M., Fırat, O., and ... Özerkan, A.** (2002). Türkiye Ulusal Temel GPS Ağı-1999 (TUTGA-99A). *Harita Dergisi*, 145:1–14.
- Barthelmes, F.** (2009). *Definition of functionals of the geopotential and their calculation from spherical harmonic models* (Technical Report STR09/02). Potsdam: Deutsches GeoForschungsZentrum GFZ.
- Barzaghi, R., Carrion, D., Kamguia, J., Kande, L., Yap, L., and Betti, B.** (2021). Estimating gravity field and quasi-geoid in cameroon (cgm20). *Journal of African Earth Sciences*, 184:104377.
- Borghi, A., Barzaghi, R., Al-Bayari, O., and Madani, S. A.** (2020). Centimeter precision geoid model for jeddah region (saudi arabia). *Remote Sensing*, 12:2066.
- Brockmann, J. M., Schubert, T., Mayer-Gürr, T., and Schuh, W.-D.** (2019). The Earth's gravity field as seen by the GOCE satellite - an improved sixth release derived with the time-wise approach (GO_CONS_GCF_2_TIM_R6). GFZ Data Services. DOI:10.5880/ICGEM.2019.003.
- Brockmann, J. M., Zehentner, N., Höck, E., Pail, R., Loth, I., Mayer-Gürr, T., and Schuh, W. D.** (2014). EGM-TIM-RL05: An independent geoid with centimeter accuracy purely based on the GOCE mission. *Geophysical Research Letters*, 41(22):8089–8099.
- Bruinsma, S. L., Förste, C., Abrikosov, O., Lemoine, J.-M., Marty, J.-C., Mulet, S., Rio, M.-H., and Bonvalot, S.** (2014). ESA's satellite-only gravity field model via the direct approach based on all GOCE data. *Geophysical Research Letters*, 41(21):7508–7514.
- Bruinsma, S. L., Förste, C., Abrikosov, O., Marty, J.-C., Rio, M.-H., Mulet, S., and Bonvalot, S.** (2013). The new ESA satellite-only gravity field model via the direct approach. *Geophysical Research Letters*, 40(14):3607–3612.
- Bruinsma, S. L., Marty, J.-C., Balmino, G., Biancale, R., Förste, C., Abrikosov, O., and Neumayer, K. H.** (2010). GOCE Gravity Field Recovery by Means of the Direct Numerical Method. In *The 2010 ESA Living Planet Symposium*.

- Ekman, M.** (1989). Impacts of geodynamic phenomena on systems for height and gravity. *Bulletin Géodésique*, 63(3):281–296.
- Ellmann, A.** (2005a). Computation of three stochastic modifications of Stokes's formula for regional geoid determination. *Computers & Geosciences*, 31(6):742–755.
- Ellmann, A.** (2005b). Two deterministic and three stochastic modifications of Stokes's formula: A case study for the Baltic countries. *Journal of Geodesy*, 79(1-3):11–23.
- Ellmann, A., Märdla, S., and Oja, T.** (2020). The 5 mm geoid model for Estonia computed by the least squares modified Stokes's formula. *Survey Review*, 52(373):352–372.
- Erol, B., Isik, M. S., and Erol, S.** (2020a). An Assessment of the GOCE High-Level Processing Facility (HPF) Released Global Geopotential Models with Regional Test Results in Turkey. *Remote Sensing*, 12(3):586.
- Erol, B., Isik, M. S., and Erol, S.** (2020b). Assessment of Gridded Gravity Anomalies for Precise Geoid Modeling in Turkey. *Journal of Surveying Engineering*, 146(3):05020005.
- Erol, S. and Erol, B.** (2021). A comparative assessment of different interpolation algorithms for prediction of GNSS/levelling geoid surface using scattered control data. *Measurement*, 173:108623.
- Eshagh, M. and Ebadi, S.** (2013). Geoid modelling based on EGM08 and recent Earth gravity models of GOCE. *Earth Science Informatics*, 6(3):113–125.
- Evans, J. D. and Featherstone, W. E.** (2000). Improved convergence rates for the truncation error in gravimetric geoid determination. *Journal of Geodesy*, 74(2):239–248.
- Featherstone, W. E.** (2001). Absolute and relative testing of gravimetric geoid models using Global Positioning System and orthometric height data. *Computers & Geosciences*, 27(7):807–814.
- Featherstone, W. E.** (2013). Deterministic, stochastic, hybrid and band-limited modifications of Hotine's integral. *Journal of Geodesy*, 87(5):487–500.
- Featherstone, W. E. and Dentith, M. C.** (1997). A Geodetic approach to gravity data reduction for geophysics. *Computers & Geosciences*, 23(10):1063–1070.
- Featherstone, W. E., Evans, J. D., and Olliver, J. G.** (1998). A Meissl-modified Vaniček and Kleusberg kernel to reduce the truncation error in gravimetric geoid computations. *Journal of Geodesy*, 72(3):154–160.
- Forsberg, R.** (1984). *A study of terrain reductions, density anomalies and geophysical inversion methods in gravity field modelling* (Technical Report 355).

- Forsberg, R.** (1987). A new covariance model for inertial gravimetry and gradiometry. *Journal of Geophysical Research*, 92(B2):1305.
- Forsberg, R., Olesen, A. V., Einarsson, I., Manandhar, N., and Shreshta, K.** (2014). Geoid of Nepal from Airborne Gravity Survey. In Rizos, C. and Willis, P., editors, *Earth on the Edge: Science for a Sustainable Planet. International Association of Geodesy Symposia*, pages 521–527. Springer, Berlin, Heidelberg, Berlin, Heidelberg.
- Forsberg, R. and Tscherning, C.** (2008). Gravsoft. geodetic gravity field modelling programs (overview manual).
- Forsberg, R. and Tscherning, C. C.** (1981). The use of height data in gravity field approximation by collocation. *Journal of Geophysical Research: Solid Earth*, 86(B9):7843–7854.
- Fotopoulos, G.** (2013). Combination of Heights. In Sansò, F. and Sideris, M. G., editors, *Geoid Determination: Theory and Methods*, pages 517–544. Springer Berlin Heidelberg, Berlin, Heidelberg.
- Gatti, A., Reguzzoni, M., Migliaccio, F., and Sansò, F.** (2014). Space-wise grids of gravity gradients from GOCE data at nominal satellite altitude. In *5th international GOCE user workshop*, pages 25–28. UNESCO, Paris, France.
- Gatti, A., Reguzzoni, M., Migliaccio, F., and Sansò, F.** (2016). Computation and assessment of the fifth release of the goce-only space-wise solution. In *The 1st joint commission 2 and IGFS meeting, 19-23 September 2016, Thessaloníki, Greece*, pages 19–23.
- Gilardoni, M., Reguzzoni, M., Sampietro, D., and Sansò, F.** (2013). Combining EGM2008 with GOCE gravity models. *Bollettino di geofisica teorica ed applicata*, 54(4).
- Godah, W., Krynski, J., and Szelachowska, M.** (2018). The use of absolute gravity data for the validation of Global Geopotential Models and for improving quasigeoid heights determined from satellite-only Global Geopotential Models. *Journal of Applied Geophysics*, 152:38–47.
- Goiginger, H., Rieser, D., Mayer-guerr, T., Pail, R., and Schuh, W.-d.** (2011). The combined satellite-only global gravity field model GOCO02S. In *Geophysical Research Abstracts*, volume 13, pages 10571–10571.
- Gruber, T., Gerlach, C., and Haagmans, R.** (2012). Intercontinental height datum connection with GOCE and GPS-levelling data. *Journal of Geodetic Science*, 2(4):270–280.
- Gruber, T., Visser, P. N. A. M., Ackermann, C., and Hosse, M.** (2011). Validation of GOCE gravity field models by means of orbit residuals and geoid comparisons. *Journal of Geodesy*, 85(11):845–860.

- Gürkan, O.** (1978). Astrojeodezik ağların deformasyonu ve Türkiye I. Derece triyangülasyon ağı. Scientific Technical Rep. 10. Trabzon, Türkiye: Karadeniz Teknik Üniversitesi.
- Hammer, S.** (1939). Terrain Corrections for Gravimeter Stations. *Geophysics*, 4(3):184–194.
- Heiskanen, W. and Moritz, H.** (1967). *Physical Geodesy*. Freeman, San Francisco.
- Hirt, C., Gruber, T., and Featherstone, W. E.** (2011). Evaluation of the first GOCE static gravity field models using terrestrial gravity, vertical deflections and EGM2008 quasigeoid heights. *Journal of Geodesy*, 85(10):723–740.
- Hirt, C., Kuhn, M., Claessens, S., Pail, R., Seitz, K., and Gruber, T.** (2014). Study of the Earth's short-scale gravity field using the ERTM2160 gravity model. *Computers & Geosciences*, 73:71–80.
- Hirt, C., Yang, M., Kuhn, M., Bucha, B., Kurzmann, A., and Pail, R.** (2019). SRTM2gravity: An Ultrahigh Resolution Global Model of Gravimetric Terrain Corrections. *Geophysical Research Letters*, 46(9):4618–4627.
- Hofmann-Wellenhof, B. and Moritz, H.** (2006). *Physical Geodesy*. Springer Vienna.
- Hotine, M.** (1969). *Mathematical geodesy*, volume 2. US Government Printing Office.
- Huang, J., Sideris, M. G., Vaníček, P., and Tziavos, I. N.** (2003). Numerical investigation of downward continuation techniques for gravity anomalies. *Bollettino di geodesia e scienze affini*, 62(1):33–48.
- Hwang, C., Hsiao, Y.-S., and Shih, H.-C.** (2006). Data reduction in scalar airborne gravimetry: Theory, software and case study in Taiwan. *Computers & Geosciences*, 32(10):1573–1584.
- Hwang, C., Hsiao, Y.-S., Shih, H.-C., Yang, M., Chen, K.-H., Forsberg, R., and Olesen, A. V.** (2007). Geodetic and geophysical results from a Taiwan airborne gravity survey: Data reduction and accuracy assessment. *Journal of Geophysical Research: Solid Earth*, 112(B4).
- Ince, E. S., Erol, B., and Sideris, M. G.** (2014). Evaluation of the GOCE-Based Gravity Field Models in Turkey. In Marti, U., editor, *Gravity, Geoid and Height Systems*, pages 93–99, Cham. Springer International Publishing.
- Isik, M. S.** (2016). An investigation on the contribution of GOCE satellite mission to regional geoid modelling in Turkey. M.Sc. Thesis, Graduate School of Science, Engineering and Technology, Istanbul Technical University.
- Isik, M. S. and Erol, B.** (2015). Geoid Modelling in Turkey Using Remove-Compute-Restore and Least Squares Modification of Stokes' Integral Methods. IUGG General Assembly 18, June 22 - July 02, Prague, Czech Republic.

- Isik, M. S. and Erol, B.** (2016). Geoid Determination Using GOCE-Based Models in Turkey. EGU Gen. Assem. 2016, Vol. 18, EGU2016–883, April 17–22, Vienna, Austria.
- Isik, M. S., Erol, B., Erol, S., and Sakil, F. F.** (2021). High-resolution geoid modeling using least squares modification of Stokes and Hotine formulas in Colorado. *Journal of Geodesy*, 95(5):49.
- Isik, M. S., Erol, B., Çevikalp, M. R., and Erol, S.** (2022a). Geoid modeling with least squares modification of hotine's integral using gravity disturbances in turkey. *Earth Science Informatics*, 15:1889–1904.
- Isik, M. S., Erol, S., and Erol, B.** (2022b). Investigation of the Geoid Model Accuracy Improvement in Turkey. *Journal of Surveying Engineering*, 148(3):1–14.
- Isik, M. S., Çevikalp, M. R., and Erol, B.** (Under Review, 2022c). Improvement of GOCE-based Global Geopotential Models for Gravimetric Geoid Modeling in Turkey. *submitted to Earth Science Informatics*, 1.
- Jarvis, A., Reuter, H. I., Nelson, A., Guevara, E., and others** (2008). Hole-filled SRTM for the globe Version 4. Available from the CGIAR-CSI SRTM 90m Database: <http://srtm.csi.cgiar.org>, Accessed on 15 Aug 2022.
- Jekeli, C.** (1979). *Global accuracy estimates of point and mean undulation differences obtained from gravity disturbances, gravity anomalies and potential coefficients* (Technical Report 288). Ohio: The Ohio State University.
- Jekeli, C.** (1980). Comparison of undulation difference accuracies using gravity anomalies and gravity disturbances. *Bulletin Géodésique*, 54(2):137–147.
- Kiahmehr, R.** (2006). *A hybrid precise gravimetric geoid model for Iran based on recent GRACE and SRTM data and the least squares modification of Stokes's formula*. PhD Thesis, KTH Royal Institute of Technology.
- Kirby, J. F.** (2003). On the combination of gravity anomalies and gravity disturbances for geoid determination in Western Australia. *Journal of Geodesy*, 77(7-8):433–439.
- Kotsakis, C., Katsambalos, K., and Ampatzidis, D.** (2012). Estimation of the zero-height geopotential level W_0^{LVD} in a local vertical datum from inversion of co-located gps, leveling and geoid heights: a case study in the hellenic islands. *Journal of Geodesy*, 86(6):423–439.
- Kvas, A., Brockmann, J. M., Krauss, S., Schubert, T., Gruber, T., Meyer, U., Mayer-Gürr, T., Schuh, W.-D., Jäggi, A., and Pail, R.** (2021). GOCO06s – a satellite-only global gravity field model. *Earth System Science Data*, 13(1):99–118.

- Kılıçoğlu, A.** (2002). Updated Turkish Geoid TG99A (in Turkish). Güncelleştirilmiş Türkiye Jeoidi 1999 (TG99A). In *Proceedings of the Tectonics and Geodetic Networks Workshop, Scientific Meeting of TNGC, TUJK*, pages 153–166, Boğaziçi Univ., Istanbul, Turkey.
- Kılıçoğlu, A., Direnç, A., Yıldız, H., Bölme, M., Aktuğ, B., Simav, M., and Lenk, O.** (2011). Regional gravimetric quasi-geoid model and transformation surface to national height system for Turkey (THG-09). *Studia Geophysica et Geodaetica*, 55(4):557–578.
- Kılıçoğlu, A., Firat, O., and Demir, C.** (2005). Observations and methods used in the computation of new Turkish geoid (TG-03). In *Proceedings of the Geoid and Vertical Datum Workshop, Scientific Meeting of TNGC*, Ankara, Turkey: General Directorate of Mapping.
- LAPACK-Linear Algebra Package** (2000). Version 3.0. web site: <http://www.netlib.org/lapack>, accessed 15 aug 2022.
- Li, X., Ahlgren, K., Hardy, R., Krcmaric, J., and Wang, Y.** (2019). The development and evaluation of the experimental gravimetric geoid model 2019, https://beta.ngs.noaa.gov/GEOID/xGEOID19/xGeoid19_tech_details.v10.pdf. Technical report.
- Märdla, S.** (2017). *Regional geoid modelling by the least squares modified Hotine formula using gridded gravity disturbances*. PhD Thesis, Tallinn University of Technology, Tallinn.
- Märdla, S., Ellmann, A., Ågren, J., and Sjöberg, L. E.** (2018). Regional geoid computation by least squares modified Hotine's formula with additive corrections. *Journal of Geodesy*, 92(3):253–270.
- Matsuo, K. and Kuroishi, Y.** (2020). Refinement of a gravimetric geoid model for Japan using GOCE and an updated regional gravity field model. *Earth, Planets and Space*, 72(1):33.
- Mayer-Gürr, T.** (2015). The combined satellite gravity field model GOCO05s. In *EGU General Assembly Conference Abstracts Vol 17*, volume 18, pages EGU2016–7696.
- Mayer-Gürr, T.** (2012). The new combined satellite only model GOCO03s. *presented at International Symposium on Gravity, Geoid and Height Systems 2012 Venice, Italy*.
- Meissl, P.** (1971). *Preparation for the numerical evaluation of second order Molodenskii type formulas*. Technical report, Department of Geodetic Science, The Ohio State University, Columbus.
- Migliaccio, F., Reguzzoni, M., Gatti, A., Sansò, F., and Herceg, M.** (2011). A GOCE-only global gravity field model by the space-wise approach. In *Proceedings of the 4th international GOCE user workshop*, volume 31.

- Migliaccio, F., Reguzzoni, M., Sanso, F., Tscherning, C. C., Veicherts, M., and Others** (2010). *GOCE data analysis: the space-wise approach and the first space-wise gravity field model*. In Proceedings of the ESA living planet symposium, volume 28. Citeseer.
- Molodenskii, M. S., Eremeev, V. F., and Yurkina, M. I.** (1962). *translated from Russian*. Methods for Study of the External Gravitational Field and Figure of the Earth, .
- Molodensky, M., Eremeev, V., and Yurkina, M.** (1962). *Methods for study of the external gravity field and figure of the Earth. Translations from Russian*. Israel Program for Scientific Translations, 248.
- Moritz, H.** (1980). Advanced Physical Geodesy. *Herbert Wichmann, Karlsruhe, Germany*.
- Moritz, H.** (2000). *Geodetic Reference System 1980*. Journal of Geodesy, 74(1):128–133.
- Novák, P. and Heck, B.** (2002). *Downward continuation and geoid determination based on band-limited airborne gravity data*. Journal of Geodesy, 76(5):269–278.
- Novák, P., Kern, M., Schwarz, K.-P., Sideris, M. G., Heck, B., Ferguson, S., Hammada, Y., and Wei, M.** (2003). *On geoid determination from airborne gravity*. Journal of Geodesy, 76(9-10):510–522.
- Olesen, A. V.** (2003). Improved airborne scalar gravimetry for regional gravity field mapping and geoid determination. *PhD Thesis, University of Copenhagen*.
- Pail, R., Bruinsma, S. L., Migliaccio, F., Förste, C., Goiginger, H., Schuh, W. D., and ...Tscherning, C. C.** (2011). *First GOCE gravity field models derived by three different approaches*. Journal of Geodesy, 85(11):819–843.
- Pail, R., Fecher, T., Barnes, D., Factor, J., Holmes, S., Gruber, T., and Zingerle, P.** (2016). *The experimental gravity field model xgm2016*. In International Symposium on Gravity, Geoid and Height System 2016-1st Joint Commission 2 and IGFS Meeting, Thessaloniki, Greece.
- Pail, R., Fecher, T., Barnes, D., Factor, J. F., Holmes, S. A., Gruber, T., and Zingerle, P.** (2018). *Short note: the experimental geopotential model XGM2016*. Journal of Geodesy, 92(4):443–451.
- Pail, R., Goiginger, H., Mayrhofer, R., Schuh, W.-D., Brockmann, J. M., Krasbutter, I., Höck, E., and Fecher, T.** (2010a). *GOCE gravity field model derived from orbit and gradiometry data applying the time-wise method*. In Proceedings of the ESA living planet symposium, volume 28, page 8. European Space Agency Bergen, Norway.

- Pail, R., Goiginger, H., Schuh, W. D., Heck, E., Brockmann, J. M., Fecher, T., Güruber, T., Mayer-Gürr, T., Kusche, J., Jäggi, A., and Rieser, D.** (2010b). *Combined satellite gravity field model GOCE01S derived from GOCE and GRACE*. Geophysical Research Letters, 37(20).
- Paul, M. K.** (1973). *A method of evaluating the truncation error coefficients for geoidal height*. Bulletin géodésique, 110(1):413–425.
- Pavlis, N. K., Holmes, S. A., Kenyon, S. C., and Factor, J. K.** (2012). *The development and evaluation of the Earth Gravitational Model 2008 (EGM2008)*. Journal of Geophysical Research: Solid Earth, 117(B4).
- Rapp, R. H., Nerem, R. S., Shum, C., Klosko, S. M., and Williamson, R. G.** (1991). *Consideration of permanent tidal deformation in the orbit determination and data analysis for the topex/poseidon mission. Technical report*.
- Rexer, M., Hirt, C., Pail, R., and Claessens, S.** (2014). *Evaluation of the third- and fourth-generation GOCE Earth gravity field models with Australian terrestrial gravity data in spherical harmonics*. Journal of Geodesy, 88(4):319–333.
- Rummel, R.** (2012). *Height unification using GOCE*. Journal of Geodetic Science, 2(4):355–362.
- Saari, T. and Bilker-Koivula, M.** (2018). *Applying the GOCE-based GGMs for the quasi-geoid modelling of Finland*. Journal of Applied Geodesy, 12(1):15–27.
- Sakil, F. F.** (2018). *Geoid Modeling by the Least Squares Modified Hotine Formula Using Voronoi Cell Structures*. Master's thesis, Istanbul Technical University, Istanbul.
- Sakil, F. F., Erol, S., Ellmann, A., and Erol, B.** (2021). *Geoid modeling by the least squares modification of Hotine's and Stokes' formulae using non-gridded gravity data*. Computers & Geosciences, 156:104909.
- Sánchez, L., Čunderlík, R., Dayoub, N., Mikula, K., Minarechová, Z., Šíma, Z., Vatrt, V., and Vojtíšková, M.** (2016). *A conventional value for the geoid reference potential W_0* . Journal of Geodesy, 90(9):815–835.
- Sánchez, L. and Sideris, M. G.** (2017). *Vertical datum unification for the International Height Reference System (IHRS)*. Geophysical Journal International, 209(2):570–586.
- Simav, M.** (2020). *Results from the first strapdown airborne gravimetry campaign over the Lake District of Turkey*. Survey Review, :1–7.
- Simav, M., Becker, D., Yıldız, H., and Hoss, M.** (2020). *Impact of temperature stabilization on the strapdown airborne gravimetry: a case study in Central Turkey*. Journal of geodesy, 94(4):1–11.

- Simav, M., Türkezer, A., Sezen, E., Akyol, S., İnam, M., Cingöz, A., Lenk, O., and Kılıçoğlu, A.** (2011). *Data Quality Control and Management System of Turkish Sea Level Monitoring Network (In Turkish)*. Harita Dergisi, (145).
- Simav, M. and Yıldız, H.** (2019). *Evaluation of EGM2008 and latest GOCE-based satellite only global gravity field models using densified gravity network: a case study in south-western Turkey*. Bollettino di Geofisica Teorica ed Applicata, 60(1).
- Simav, M., Yıldız, H., Direnç, A., and Türkezer, A.** (2013). *Terrestrial Gravity Measurements towards Turkish Height System Modernization*. EGU General Assembly 2013, 15(iii):12260.
- Sjöberg, L. E.** (1980). *Least squares combination of satellite harmonics and integral formulas in physical geodesy*. Gerlands Beiträge zur Geophysik, 89:371–377.
- Sjöberg, L. E.** (1981). *Least squares combination of satellite and terrestrial data in physical geodesy*. In *Annales de Geophysique*, volume 37, pages 25–30.
- Sjöberg, L. E.** (1984). *Least-Squares modification of Stokes' and Vening-Meinez' formula by accounting for truncation and potential coefficients errors*. Manusc. Geod., 9:209–229.
- Sjöberg, L. E.** (1987). *The Modification of Stokes' and Hotine's Formulas: A Comparison*. In *Figure and Dynamics of the Earth, Moon and Planets*, page 323.
- Sjöberg, L. E.** (1991). *Refined least squares modification of Stokes' formula*. Manuscripta geodaetica, 16(6):367–375.
- Sjöberg, L. E.** (2003a). *A computational scheme to model the geoid by the modified Stokes formula without gravity reductions*. Journal of Geodesy, 77(7-8):423–432.
- Sjöberg, L. E.** (2003b). *A general model for modifying Stokes' formula and its least-squares solution*. Journal of Geodesy, 77(7-8):459–464.
- Sjöberg, L. E.** (2003c). *A solution to the downward continuation effect on the geoid determined by Stokes' formula*. Journal of Geodesy, 77(1-2):94–100.
- Sjöberg, L. E.** (2004a). *A spherical harmonic representation of the ellipsoidal correction to the modified Stokes formula*. Journal of Geodesy, 78(3):180–186.
- Sjöberg, L. E.** (2004b). *The ellipsoidal corrections to the topographic geoid effects*. Journal of Geodesy, 77(12):804–808.
- Sjöberg, L. E.** (2007). *The topographic bias by analytical continuation in physical geodesy*. Journal of Geodesy, 81(5):345–350.

- Sjöberg, L. E. and Eshagh, M.** (2009). *A geoid solution for airborne gravity data*. Studia Geophysica et Geodaetica, 53(3):359–374.
- Sjöberg, L. E. and Nahavandchi, H.** (2000). *The atmospheric geoid effects in Stokes' formula*. Geophysical Journal International, 140(1):95–100.
- Sjöberg, L. E. and Nord, T.** (1992). *Geoidal undulation computation by modifying Stokes's kernel versus Hotine's kernel from gravity anomalies*. Manuscr Geod, 17:135–140.
- Smith, D.** (2007). *The grav-d project: gravity for the redefinition of the american vertical datum*. NOAA website: http://www.ngs.noaa.gov/GRAV-D/pubs/GRAV-D_v2007_12_19.pdf.
- Sneeuw, N.** (1994). *Global spherical harmonic analysis by least-squares and numerical quadrature methods in historical perspective*. Geophysical Journal International, 118(3):707–716.
- Stokes, G. G.** (1849). *On the variation of gravity on the surface of the earth*. Trans. Camb. Phil. Soc., 8:672–695.
- The GRAV-D Team** (2018). *Gravity for the redefinition of the american vertical datum (grav-d) project, airborne gravity data - block ms05*. https://www.ngs.noaa.gov/GRAV-D/data_products.shtml. accessed 21 sept 2020.
- Tscherning, C. C., Rubek, F., and Forsberg, R.** (1998). *Combining Airborne and Ground Gravity Using Collocation*. In Forsberg, R., Feissel, M., and Dietrich, R., editors, *Geodesy on the move*. International Association of Geodesy Symposia, vol 119, pages 18–23. Springer, Berlin.
- TUDES** (2021). *Turkish national sea level monitoring system - türkiye ulusal deniz seviyesi İzleme ağı*. "accessed november 23, 2021. <https://tudes.harita.gov.tr/?lang=us>.
- van Westrum, D., Ahlgren, K., Hirt, C., and Guillaume, S.** (2021). *A Geoid Slope Validation Survey (2017) in the rugged terrain of Colorado, USA*. Journal of Geodesy, 95(1):9.
- Vaniček, P. and Kleusberg, A.** (1987). *The Canadian geoid-stokesian approach*. Manuscr. Geodaet., 12:86–98.
- Vaniček, P. and Sjöberg, L. E.** (1991). *Reformulation of Stokes's theory for higher than second-degree reference field and modification of integration kernels*. Journal of Geophysical Research: Solid Earth, 96(B4):6529–6539.
- Vaniček, P., Sun, W., Ong, P., Martinec, Z., Najafi, M., Vajda, P., and ter Horst, B.** (1996). *Downward continuation of Helmert's gravity*. Journal of Geodesy, 71(1):21–34.

- Vanicek, P., Zhang, C., and Sjöberg, L. E.** (1992). *A comparison of Stokes's and Hotine's approaches to geoid computation.* Manuscr Geod, 17(1):29–35.
- Vergos, G. S., Erol, B., Natsiopoulos, D. A., Grigoriadis, V. N., Isik, M. S., and Tziavos, I. N.** (2018). *Preliminary results of GOCE-based height system unification between Greece and Turkey over marine and land areas.* Acta Geodaetica et Geophysica, 53(1):61–79.
- Vu, D. T., Bruinsma, S., and Bonvalot, S.** (2019). *A high-resolution gravimetric quasigeoid model for Vietnam.* Earth, Planets and Space, 71(1):65.
- Wang, Y. M.** (1988). *Downward continuation of the free-air gravity anomalies to the ellipsoid using the gradient solution, poisson's integral and terrain correction-numerical comparison and computations.* Technical report, Ohio State Univ Columbus Dept of Geodetic Science and Surveying.
- Wang, Y. M., Sánchez, L., Ågren, J., Huang, J., Forsberg, R., Abd-Elmotaal, H., and ... Zingerle, P.** (2021). *Colorado geoid computation experiment: overview and summary.* Journal of Geodesy, 95(12):127.
- Wenzel, H.-G.** (1982). *Geoid computation by least squares spectral combination using integral kernels.* Proceedings of the General Meeting of the IAG, :438–453.
- Wenzel, H.-G.** (1985). *Hochauflösende kugelfunktionsmodelle für das gravitationspotential der erde.* Wissenschaftliche Arbeiten der Fachrichtung Vermessungswesen der Universität Hannover, (137):1–154.
- Wppard, G. P.** (1980). *New Gravity System - Changes in International Gravity Base Values and Anomaly Values.* Geophysics, 44(8):1352–1366.
- Wong, L. and Gore, R.** (1969). *Accuracy of Geoid Heights from Modified Stokes Kernels.* Geophysical Journal International, 18(1):81–91.
- Wu, Y., Abulaitijiang, A., Featherstone, W. E., McCubbine, J. C., and Andersen, O. B.** (2019). *Coastal gravity field refinement by combining airborne and ground-based data.* Journal of Geodesy, 93(12):2569–2584.
- Yıldız, H.** (2021). *Quantifying the individual contributions of GOCE gradients for regional quasi-geoid modeling in a relatively rough topography.* Journal of Applied Geophysics, 187:104289.
- Yıldız, H., Firat, O., Simav, M., and Ünver, Y.** (2006). *The high resolution geoid model for Turkey, TG-07.* In 1 st International Symposium of the International Gravity Field Service (IGFS), Gravity Field of the Earth, Program & Abstract Book, Sayfa, volume 18, page 28.
- Yıldız, H., Forsberg, R., Ågren, J., Tscherning, C. C., and Sjöberg, L. E.** (2012). *Comparison of remove-compute-restore and least squares modification of Stokes' formula techniques to quasi-geoid determination over the Auvergne test area.* Journal of Geodetic Science, 2(1):53–64.

- Yıldız, H., Simav, M., Sezen, E., Akpinar, , Akdoğan, Y. A., Cingöz, A., and Akabali, O. A.** (2021). *Determination and validation of the Turkish Geoid-2020 (TG-20)*. *Bollettino di Geofisica Teorica ed Applicata*, 62(3):495–512.
- Zelin, G. and Yecai, L.** (1991). *The determination of oceanic geoid using modified hotine integral*. In Rapp, R. H. and Sansò, F., editors, *Determination of the Geoid*, pages 86–94. Springer New York, New York, NY.
- Zhang, C.** (1998). *Estimation of dynamic ocean topography in the Gulf Stream area using the Hotine formula and altimetry data*. *Journal of Geodesy*, 72(9):499–510.
- Zhang, P., Bao, L., Guo, D., and Li, Q.** (2022). *Estimation of the height datum geopotential value of Hong Kong using the combined Global Geopotential Models and GNSS/levelling data*. *Survey Review*, 54(383):106–116.
- Zhao, Q., Xu, X., Forsberg, R., and Strykowski, G.** (2018). *Improvement of downward continuation values of airborne gravity data in Taiwan*. *Remote Sensing*, 10(12):1951.
- Zingerle, P., Pail, R., Gruber, T., and Oikonomidou, X.** (2020). *The combined global gravity field model XGM2019e*. *Journal of Geodesy*, 94(7):1–12.

CURRICULUM VITAE

Name Surname: Mustafa Serkan IŞIK

EDUCATION :

- **B.Sc.** : 2014, Istanbul Technical University, Faculty of Civil Engineering, Department of Geomatics Engineering
- **M.Sc.** : 2016, Istanbul Technical University, Institute of Science, Engineering, and Technology, Department of Geomatics Engineering

PUBLICATIONS AND PRESENTATIONS ON THE THESIS:

- **Işık, M. S., Çevikalp, M. R., Erol, B., Erol, S.** (Under Review). *Improvement of GOCE-based Global Geopotential Models for Gravimetric Geoid Modeling in Turkey*, Submitted to Geosciences.
- **Işık, M. S., Erol, B., Çevikalp, M. R., Erol, S.** (2022). *Geoid Modeling with Least Squares Modification of Hotine's Integral using Gravity Disturbances in Turkey*, Earth Science Informatics, 1889-1904, 15(3). <https://doi.org/10.1007/s12145-022-00843-2>.
- **Işık, M. S., Erol, S., Erol, B.** (2022). *Investigation of the Geoid Model Accuracy Improvement in Turkey*, Journal of Surveying Engineering, 148(3). [https://doi.org/10.1061/\(ASCE\)SU.1943-5428.0000397](https://doi.org/10.1061/(ASCE)SU.1943-5428.0000397).
- **Işık, M. S., Erol, B., Çevikalp, M. R., Erol, S.** (2021). An Investigation on the Geoid-Quasigeoid Separation with the Case Study in Colorado, U.S., IAG Scientific Assembly 2021, July 2021.
- **Işık, M. S., Erol, B., Sakil, F. F., Çevikalp, M. R., Erol, S.** (2021). Gravimetric Geoid Modelling Using the Least Squares Modification of Hotine Integral in Turkey, IAG Scientific Assembly 2021, July 2021.
- **Işık, M. S., Erol, B., Erol, S., Sakil, F. F.** (2021). *High-Resolution Geoid Modeling Using Least Squares Modification of Stokes and Hotine Formulas in Colorado*, Journal of Geodesy, vol. 95, 49, <https://doi.org/10.1007/s00190-021-01501-z>.

- **Işık, M. S., Erol, B., Erol, S., Sakil, F. F.** (2019). High-Resolution Geoid Modeling Experiment Using GRAV-D Data Over Colorado. In International Geodesy and Geophysics Union General Assembly 2019 (IUGG2019), 08-18 July, Montreal, Canada.

OTHER PUBLICATIONS AND PRESENTATIONS:

- Özturk, O., Işık, M. S., Sariturk, B., Şeker, D. Z. (2022). *Generation of Istanbul Road Data Set using Google Map API for Deep Learning-Based Segmentation*, International Journal of Remote Sensing, 43(8), <https://doi.org/10.1080/01431161.2022.2068989>.
- Wang, Y. M., Sánchez, L., Ågren, J., Huang, J., Forsberg, R., Abd-Elmotaal, H. A., Ahlgren, K., Barzaghi, R., Bašić, T., Carrion, D., Claessens, S., Erol, B., Erol, S., Filmer, M., Grigoriadis, V. N., Işık, M. S., Jiang, T., Koç, Ö., Krcmaric, J., ... Zingerle, P. (2021). *Colorado geoid computation experiment – Overview and summary*, Journal of Geodesy, vol. 95, 127, <https://doi.org/10.1007/s00190-021-01567-9>.
- Işık, M. S., Özbeý, V., Erol, S., Tarı, E. (2021). *GNSSPy: Python Toolkit for GNSS Data*, IEEE International Geoscience and Remote Sensing Symposium IGARSS, 2021, pp. 8550-8553, <https://doi.org/10.1109/IGARSS47720.2021.9553880>.
- Erol, B., Işık, M. S., Erol, S. (2020). *Global ve Bölgesel (Yüksek Çöziünlükli) Sayısal Yükseklik Modellerinin Doğruluk Analizi Üzerine Bir İnceleme*, Afyon Kocatepe Üniversitesi Fen Ve Mühendislik Bilimleri Dergisi, 20 (4), 598-612, <https://doi.org/10.35414/akufemubid.746252>.
- Işık, M. S., Özbeý, V., Bayır, E., Yüksel, Y., Erol, S., Tarı, E. (2020). Python Toolkit for GNSS Data: GNSSPy. Presented at the 2020 EGU General Assembly European Geoscience Union (EGU2020), 04-08 April, Vienna, Austria.
- Erol, B., Işık, M. S., Erol, S. (2020). *Assessment of gridded gravity anomalies for precise geoid modeling in Turkey*, Journal of Surveying Engineering, 146(3), [https://doi.org/10.1061/\(ASCE\) SU.1943-5428.0000317](https://doi.org/10.1061/(ASCE) SU.1943-5428.0000317).
- Erol, B., Işık, M. S., Erol, S. (2020). *An Assessment of the GOCE High-Level Processing Facility (HPF) Released Global Geopotential Models with Regional Test Results in Turkey*, Remote Sensing, 12(3):586, <https://doi.org/10.3390/rs12030586>.
- Sánchez L., Ågren J., Huang J., Wang Y.M., Mäkinen J., Denker H., Ihde J., Abd-Elmotaal H., Ahlgren K., Amos M., Barzaghi R., Bašić T., Blitzkow D., Carrion D., Claessens S., Erol B., Erol S., Filmer M., Forsberg R., Grigoriadis V.N., Işık, M. S., Jiang T., Li X., Liu Q., Matos A.C.O.C., Matsuo K., Novák P., Pail R., Pitoňák M., Roman R., Schmid M., Sideris M., Varga M., Vergos G.S., Véronneau M., Willberg M., Zhang V., Zingerle P. (2019). Advances in the realisation of the International Height Reference System. GGOS Days 2019 in SIRGAS 2019 Symposium, Nov 11 -14, Rio de Janeiro, Brazil.

- **Özbey, V., Işık, M. S.** (2019). Python Toolkit for GNSS Data: GNSSPy. In International Geodesy and Geophysics Union General Assembly 2019 (IUGG2019), 08-18 July, Montreal, Canada.
- **Sakil, F. F., Erol, S., Işık, M. S., Erol, B.** (2019). A Comparison of Least Squares Modification of Stokes and Hotine Formulas with Case Study Results from Colorado Geoid Modeling. In International Geodesy and Geophysics Union General Assembly 2019 (IUGG2019), 08-18 July, Montreal, Canada.
- **Koç, Ö., Erol, S., Işık, M. S., Erol, B.** (2019). Contribution of Cryosat-2 SAR/SARin Data to Local Vertical Datum Validation and Height System Unification in Turkey. In International Geodesy and Geophysics Union General Assembly 2019 (IUGG2019), 08-18 July, Montreal, Canada.
- **Sánchez L., Ågren J., Huang J., Wang Y.M., Mäkinen J., Denker H., Ihde J., Abd-Elmotaal H., Ahlgren K., Amos M., Barzaghi R., Bašić T., Blitzkow D., Carrion D., Claessens S., Erol B., Erol S., Filmer M., Forsberg R., Grigoriadis V.N., Işık, M. S., Jiang T., Li X., Liu Q., Matos A.C.O.C., Matsuo K., Novák P., Pail R., Pitoňák M., Roman D., Schmid M., Sideris M., Varga M., Vergos G.S., Véronneau M., Willberg M., Zhang C., Zingerle P.** (2019). IHRF2019: the first realisation of the International Height Reference System. In International Geodesy and Geophysics Union General Assembly 2019 (IUGG2019), 08-18 July, Montreal, Canada.
- **Erol, B., Işık, M. S., Erol, S.** (2018). Methodology Assessment of High Resolution Geoid Modeling Using The GRAV-D Data Over Colorado. In International Symposium on Gravity, Geoid and Height Systems 2018 (GGHS2018), 17-21 September, Copenhagen, Denmark.
- **Erol, S., Erol, B., Işık, M. S.** (2018). Data Quality Assessments for High-frequency Geoid Modeling in Turkey. In International Symposium on Gravity, Geoid and Height Systems 2018 (GGHS2018), 17-21 September, Copenhagen, Denmark.
- **Koç, Ö., Erol, S., Işık, M. S., Erol, B.** (2018). Validation of Mediterranean Sea MSS and Marine Geoid using Recent Global and Regional Models, Local Tide Gauge and Coastal Altimetry Products. In International Symposium on Gravity, Geoid and Height Systems 2018(GGHS2018), 17-21 September, Copenhagen, Denmark.
- **Kuçak, A., Erol, S., Özogel, E., Işık, M. S., Erol, B.** (2018). On the Use of DEM by Unmanned Aerial Vehicle and Airborne LIDAR Data in Local Geoid Model Determination and Validation. In XXVIII International Symposium on “Modern Technologies, Education and Professional Practice in Geodesy And Related Fields”, Sofia, Bulgaria.
- **Erol, S., Köz, İ., Gür, Y.Ö., Işık, M. S., Erol, B.** (2018). An Overview the 2017 July 20 Mw 6.6 Bodrum–Kos Earthquake by Means of Geodetic and Geophysical Data Analyses. In XXVIII International Symposium on “Modern Technologies,

Education and Professional Practice in Geodesy And Related Fields”, Sofia, Bulgaria.

- **Vergos, G., Erol, B., Natsiopoulos, D. A., Grigoriadis, V. N., Işık, M. S., Tziavos, I. A.** (2018). *Preliminary results of GOCE-based height system unification between Greece and Turkey over marine and land areas*, Acta Geodaetica et Geophysica, 53(1), 61-79. <https://doi.org/10.1007/s40328-017-0204-x>.
- **Erol, B., Erol, S., Işık, M. S.** (2017). *Vertical Reference System and Geoid Modeling Studies in Turkey*, XXVII International Symposium on Modern Technologies, Education and Professional Practice in Geodesy and Related Fields, 09-10 Kasım, Sofia, Bulgaria.
- **Işık, M. S., Erol, B., Erol, S.** (2017). *Analysis on the Quality of High-Resolution Global Digital Terrain Models (DTM) Using GPS/leveling Data in Turkey*, International Symposium on GIS Applications in Geography and Geosciences (ISGGG2017), 18-21 October, Çanakkale, Turkey.
- **Işık, M. S., Erol, S., Erol, B.** (2017). *Comparison of Geostatistical Kriging and Least Squares Collocation in Gravity Field Data Interpolation*, International Symposium on GIS Applications in Geography and Geosciences (ISGGG2017), 18-21 October, Çanakkale, Turkey.
- **Özen, B., Işık, M. S., Erol, B.** (2017). *Web-based Geoid Calculation Tool for Practical Height Transformation in Turkey*, International Symposium on GIS Applications in Geography and Geosciences (ISGGG2017), 18-21 October, Çanakkale, Turkey.
- **Erol, B., İnce, E. S., Abbak, R. A., Erol, S., Işık, M. S., Feizabadi, M.** (2016). *GOCE Uydu Verileri İle Hesaplanan Global Jeopotansiyel Modellerin Yersel Veriler İle Doğruluklarının Değerlendirilmesi*, Türkiye Ulusal Jeodezi Komisyonu Toplantısı (TUJK2016), 3-4 Kasım, İstanbul, Türkiye.
- **Işık, M. S., Erol, B.** (2016). *GOCE Uydu Verileri İle Hesaplanan Global Jeopotansiyel Modellerin Yersel Veriler İle Doğruluklarının Değerlendirilmesi*, Türkiye Ulusal Jeodezi Komisyonu Toplantısı (TUJK2016), 3-4 Kasım, İstanbul, Türkiye.
- **Vergos, G., Erol, B., Natsiopoulos, D. A., Grigoriadis, V. N., Işık, M. S., Tziavos, I. A.** (2016). *GOCE-based Comparison and Unification of the Greek and Turkish Height Systems with special emphasis on the Aegean Sea and the Terrestrial-border Territories*. Presented at the International Symposium on Gravity, Geoid and Height Systems 2016 , Session 5 - “Vertical Datum unification and practical realizations”, 19-23 September, Thessaloniki, Greece.
- **Erol, S., Erol, B., Işık, M. S.** (2016). *Wavelet Analysis and Reconstruction of GOCE/ GRACE Geopotential Models Using GPS/leveling Data in Turkey*. Presented at the International Symposium on Gravity, Geoid and Height Systems 2016 , Session-1 “Future gravity field mission concepts and performance”, 19-23 September, Thessaloniki, Greece.

- **Işık, M. S., İnce, E. S., Erol, B.** (2016). *An Investigation on the Improvement of Regional Geoid Model in Turkey with Contribution of Methodology and Recent Satellite Missions Data*. Presented at the International Symposium on Gravity, Geoid and Height Systems 2016 , Session-1 “Future gravity field mission concepts and performance”, 19-23 September, Thessaloniki, Greece.
- **Erol, S., Erol, B., Işık, M. S.** (2016, canceled). *Assessment and Improvement of GOCE based Global Geopotential Models Using Wavelet Decomposition*. Presented at 41st COSPAR Scientific Assembly, Istanbul, Turkey.
- **Işık, M. S., Erol, B.** (2016). *Geoid Determination Using GOCE-Based Models in Turkey*. Presented at the 2016 EGU General Assembly, Session Session G4.2 - Satellite Gravimetry: Data Analysis, Results and Future Concepts, 17-22 April, Vienna, Austria.
- **Vergos, G., Erol, B., Natsiopoulos, D. A., Grigoriadis, V. N., Işık, M. S., Tziavos, I. A.** (2016). *GOCE-based height system unification between Greece and Turkey. First considerations over marine and land areas*. Presented at the 2016 EGU General Assembly, Session Session G4.2 - Satellite Gravimetry: Data Analysis, Results and Future Concepts, 17-22 April, Vienna, Austria.
- **Erol, S., Işık, M. S., Erol, B.** (2016). *Assessments on GOCE-based Gravity Field Model Comparisons with Terrestrial Data Using Wavelet Decomposition and Spectral Enhancement Approaches*. Presented at the 2016 EGU General Assembly, Session Session G4.2 - Satellite Gravimetry: Data Analysis, Results and Future Concepts, 17-22 April, Vienna, Austria.
- **Işık, M. S., Erol, B.** (2015). *Geoid Modelling in Turkey Using Remove-Compute-Restore and Least Squares Modification of Stokes' Integral Methods*, 26th International Union of Geodesy and Geophysics (IUGG) General Assembly, 22 June - 02 July, Prague, Czech Republic.
- **Feizabadi, M., Işık, M. S., İpbüker, C.** (2015). *Geomatik Mühendisliği Uygulamalarında Dönüşüm Yöntemleri*, 15. Harita Bilimsel ve Teknik Kurultayı, 25-28 Mart 2015, Ankara, Türkiye.
- **Işık, M. S., Erol, B.** (2014). *Comparison of Remove-Compute-Restore and KTH Method for Gravimetric Geoid Determination in the Northwest of Turkey*, XXIV International Symposium on Modern Technologies, Education and Professional Practice in Geodesy and Related Fields, November 6th-7th, Sofia, Bulgaria.
- **Işık, M. S., Şenyıldız, Z., Sunar, F.** (2014). *Çok Zamanlı Uydu Verilerinin Tarımsal Haritalamada Kullanımı: Altınova Devlet Üretme Çiftliği*, 5. Uzaktan Algılama-CBS Sempozyumu (UZAL-CBS), 14-17 Ekim, İstanbul, Türkiye.